EFFECT OF SUBSTITUENTS ON THE PHOTOPHYSICAL PROPERTIES AND NONLINEAR OPTICAL PROPERTIES OF ASYMMETRICAL ZINC(II) PHTHALOCYANINE WHEN CONJUGATED TO SEMICONDUCTOR QUANTUM DOTS

A thesis submitted in fulfilment of the requirement for the degree of

Master of Science

Of

Rhodes University

By

Sithi Mgidlana

January 2019

Acknowledgements

Distinguished Professor Tebello Nyokong, my incredible supervisor for allowing me the space I needed to work and remarkable support throughout this thesis. It is such an honour to share scientific knowledge and research ideas with her.

Dr Britton, my co-supervisor for his availability and constructive comments.

Dr Mack, for helping with laser which decisively affect the outcome and presentation of this thesis.

S22 lab members

Dr Oluwole, the first person to teach me what scientific research is, always ready to help and his notable human qualities. Thank you for your valuable advice and support throughout this thesis.

Drs, Sekhosana, Babu and Managa thank you all for your assistance.

S22, many thanks for help and encouragement

Funding

1. National Research Foundation (NRF) through DST/NRF South African Research Chairs Initiative for Professor of Medicinal Chemistry and Nanotechnology.
2. Dr Desmond E. Goddard bursary.

Abstract

Various characterization techniques have been used to characterize the synthesized asymmetrical zinc phthalocyanines (ZnPc) derivatives. Techniques include Ultraviolet-visible (UV-vis) spectrophotometry, matrix assisted laser desorption time of flight mass spectrometry (MALD-TOF MS), proton nuclear magnetic resonance (^{1}H-NMR), elemental analysis and Fourier-transform infra-red spectroscopy (FT-IR). The complexes are covalently linked to core/shell and core/shell/shell semiconductor quantum dots (SQDs) via amide bond formation. Photophysical properties of complexes improved in the presence of semiconductor quantum dots (SQDs). SQDs contain cadmium/telluride (CdTe) as core, coated in the first shell with zinc selenide (ZnSe) or zinc sulfide (ZnS) and with zinc oxide (ZnO) in second shell. The photophysical properties of the phthalocyanine (Pc) complexes and their conjugates with SQDs are investigated in solution. Triplet quantum yields of complexes improved in the presence of semiconductor quantum dots.

The optical limiting behaviour of the Pc complexes and conjugates are assessed using the open aperture Z–scan technique at laser excitation wavelength of 532 nm with 10 ns pulse. Pcs complexes showed good nonlinear optical response with higher nonlinear absorption coefficient. The conjugates afforded higher nonlinear absorption coefficient than Pc complexes alone.

Table of contents

ABBREVIATIONS

Abs – absorbance

DBU – 1,8-diazabicyclo-[5.4.0]-undec-7-ene

DCC – dicyclohexylcarbodiimide

DLS – Dynamic light scattering

DMF – dimethyl formamide

DMSO – dimethyl sulfoxide

EDX - Energy dispersive X-ray

ESA – excited state absorption

FRET – Förster resonance energy transfer

FT-IR – Fourier transform infra-red

FCA – free-carrier absorption

HOMO – highest occupied molecular orbital

^{1}H-NMR – proton nuclear magnetic resonance

isc – intersystem crossing

LUMO – lowest unoccupied molecular orbital

MS – mass spectroscopy

MALDI – matrix-assisted laser desorption ionization

MPcs – metallophthalocyanines

NIR – near infra-red

Nd-YAG – neodymium-doped yttrium aluminium garnet

NLA – nonlinear absorption

NLO – nonlinear optics

NLR – nonlinear refraction

NLS – nonlinear scattering

List of Abbreviations

NP - nanoparticle

OL – optical limiting

PACT – photodynamic antimicrobial chemotherapy

PDT – photodynamic therapy

PL – photoluminescence

Pcs – phthalocyanines

SQDs – semiconductor quantum dots

RSA – reverse saturable absorption

TCSPC – time correlated single photon counting

THF – tetrahydrofuran

TOF – time-of-flight

TEM – transmission electron microscopy

UV-vis – ultraviolet-visible

VR – vibrational relaxation

XRD – x-ray diffraction

List of Symbols

A – absorbance

F – area under fluorescence curve

N_A – Avogadro constant

w_o – beam waist

r – center-to-center distance

ΔA_T – change in absorbance in the triplet state

β_{eff} – effective nonlinear absorption coefficient

L_{eff} – effective path length

Eff – efficiency of energy transfer

σ_{ex} – excited state absorption cross section

S_1 – first excited singlet state

T_1 – first excited triplet state

τ_F – fluorescence lifetime

Φ_F – fluorescence quantum yield

υ – frequency of light

S_o – ground singlet state

I_o – input irradiance

τ_{isc} – intersystem crossing period

τ – lifetime

I_{lim} – limiting threshold intensity

α – linear absorbance

k - Magnitude of absorption cross-sections ratio

β – nonlinear absorption coefficient

S_n – nth excited singlet state

T_n – nth excited triplet state

List of Symbols

I_{oo} – on-focus peak input irradiance

I_{out} – output intensity

l – pathlength (thickness of sample holder)

ϵ_o – permittivity of free space

h – Planck's constant

z_o – Rayleigh length

n – refractive index

z – sample position

$[\chi^{(3)}]$ – third-order susceptibility

τ_T – triplet lifetime

Φ_T – triplet quantum yield

λ – wavelength

Chapter 1 : Introduction

The thesis presents the synthesis of phthalocyanines, multishell semiconductor quantum dots (SQDs) and their conjugates for applications in nonlinear optics (NLO).

Chapter 1 Introduction

1.1 Nonlinear optics

Nonlinear optics (NLO) is increasingly investigated for development of materials that can be used in many areas including information technology, optical communication, optical computing, data storage and optical switching **[1-5]**. There is a need for protection of optical sensors including human eye from hazardous sources of intense laser. Hence, an investigation on organic materials for NLO applications is on the increase.

A device designed to keep the power, irradiance, energy or fluence transmitted by an optical system below some specified maximum value is known as an optical limiter (OL) **[6]**. Mechanisms involved in optical limiting behaviour of NLO absorbers include nonlinear absorption (NLA), nonlinear refraction (NR) and nonlinear scattering (NLS) **[7]**. **Fig. 1.1** shows the NLA behaviour that occurs when incident light strongly interacts with a molecule or material. This is mainly based on reverse saturable absorption (RSA), **Fig. 1.2**. Various material including inorganic **[8]**, organic **[9]** and biological **[10]** materials have been previously investigated for the development of materials that can protect optical sensors from damage resulting from a device at high power intensity. Reports have proven that organic materials can outperform other NLO materials **[11,12]**.

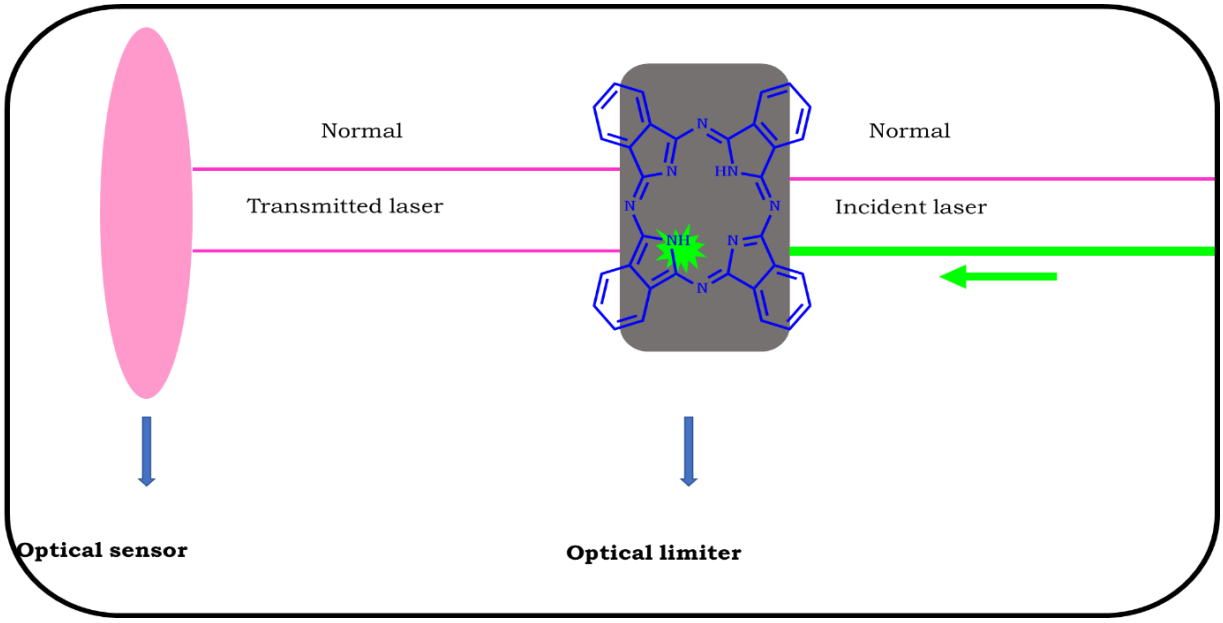

Fig. 1.1: *Representation of a phthalocyanine as an optical limiter.*

Organic molecules have attracted intensive research due to the fact that these materials are readily available at low costs, efficient and flexible; allowing for structural modification to afford efficient NLO behaviour. The family of organic materials that often afford good NLO performance are the π-electron conjugated systems such as phthalocyanines, which are the subject of this thesis **[13-15]**. Phthalocyanines remain one of the choice molecules for NLO applications due to their remarkable physicochemical properties **[16]**.

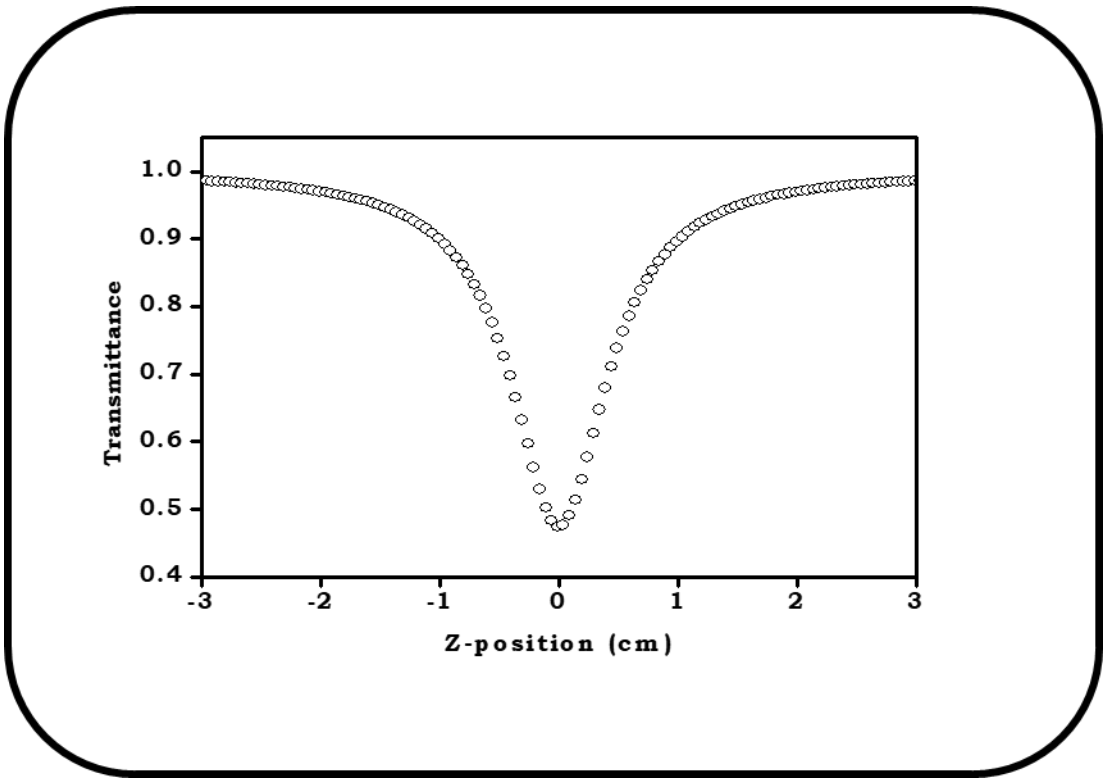

***Fig. 1.2**: Z-scan profile showing reverse saturable absorption of a molecule **[unpublished work]**.*

1.2 Phthalocyanines

Phthalocyanines (Pcs), are macroheterocyclic complexes consisting of the 18 π-electron system with four azoporphyrin ring (Scheme 1.1). The symmetry of Pcs D_{2h} increases (to D_{4h}) when a metal ion (M) is incorporated into the Pc cavity, forming metallophthacyanine (MPc). MPcs have a distinctive strong absorption in the visible region known as Q-band and broader absorption at 350 nm called B-band comprising of two overlapping bands. **Fig 1.3** shows a typical ground state electronic absorption spectrum of metallophthalocyanine. Gouterman **[17]** proposed a four-orbital model that gives an ideal picture of electronic transitions that occur between the lowest unoccupied molecular orbitals (LUMO) and the highest occupied molecular

orbitals (HOMO) of MPcs, **Fig. 1.3** (inset). The narrow symmetrical Q band of an MPc is due to electronic transitions π (a_{1u}) → $\pi^*(e_g)$ and is influenced by nature of the peripheral and non-peripheral substituent. Two transitions, a_{2u} → e_g and b_{2u} → e_g, respectively account for the B_1 and B_2, components of the broad B band.

Due to unique optical and electronic properties, MPcs have found applications in nonlinear optics **[18]**, photodyanamic therapy (PDT) **[19]**, photoantimicrobaterial chemotherapy **[20]**, photocatalysis **[21]**, gas sensors **[22]**, solar cells **[23]**, and electrochromic devices **[24]**.

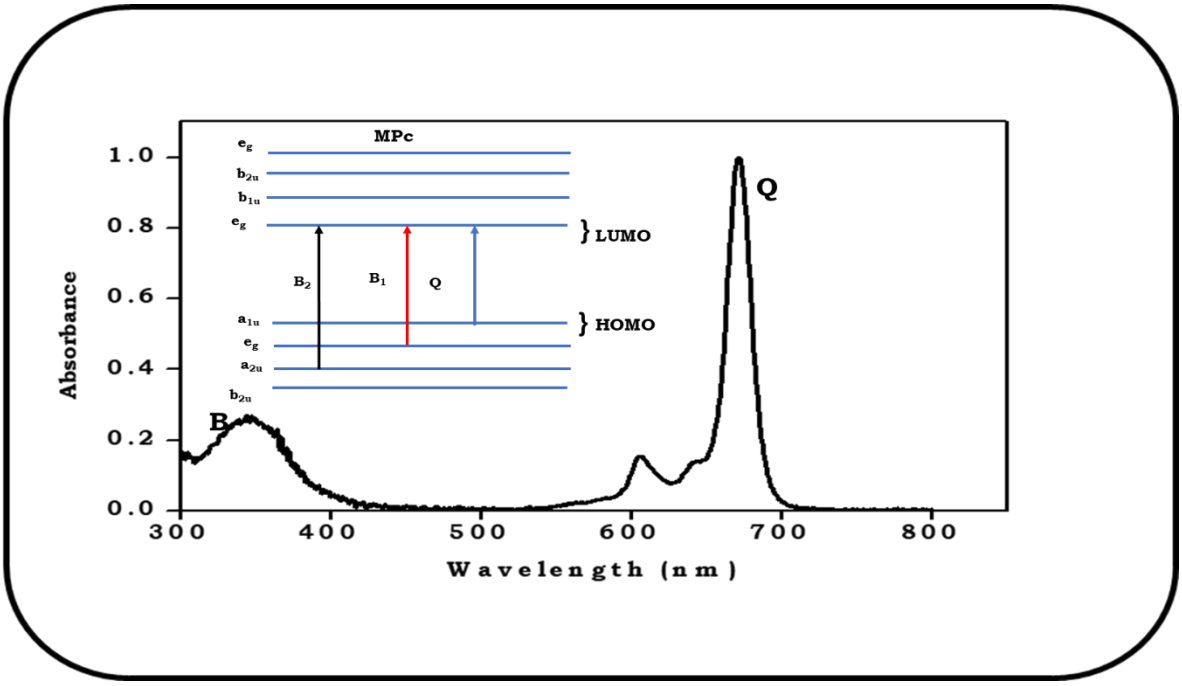

***Fig. 1.3**: Typical ground state absorption spectra of a metallophthalocyanine* **[unpublished work]**.

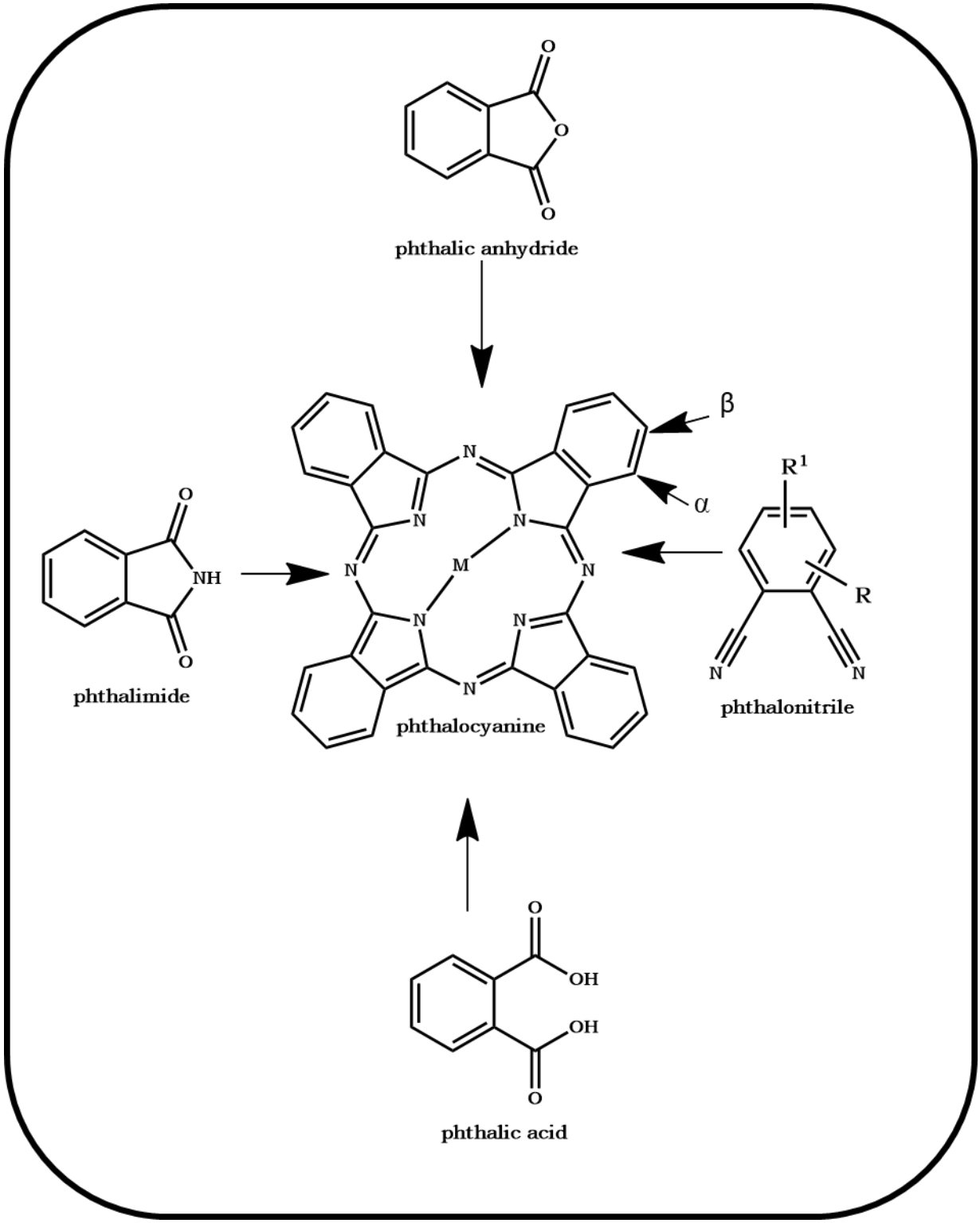

***Scheme 1.1**: The simplest approaches for the syntheses of symmetrical phthalocyanines (R^1- β, R - α).*

1.2.1 Synthesis of Symmetrical and Asymmetrical Phthalocyanine

Synthesis of symmetrical metallophthalocyanines predominantly involve cyclotetramerization reactions with precursors such as phthalimide **[25]** phthalic anhydride **[26]**, and phthalic acid **[27]** (Scheme 1.1), to mention a few. The use of phthalonitriles is considered as the simplest approach (Scheme 1.1) which often affords high yields and less side products. For synthesis of substituted Pcs, 3-nitrophthalonitriles or 4-nitrophthalonitriles are usually employed to synthesize precursors containing desired substituents (R, R^1), Scheme 1.1. The substituted phthalonitriles are cyclised in the presence or absence of metal salt (M) and an alcoholic solvent such as 1-pentanol at high temperatures. Phthalocyanine can be substituted at α (non-peripheral) or β (peripheral) positions (or both) from substituted phthalonitriles for preparation or for a suitable application (Scheme 1.1).

Design and synthesis of asymmetrical Pcs have recently been a centre of focus amongst phthalocyanine researchers. Asymmetric synthesis can be achieved by using different methods such as subphthalocyanine ring expansion route **[28-30]**, statistical mixed condensation route **[28,31,32]** and polymeric–support based route **[28,33,34]**. However, the most utilized protocol for A_3B Pcs is statistical mixed condensation, with two non-identical phthalonitriles reacting in the presence or absence of metal salt, Scheme 1.2. A mixture of six different products are obtained and chromatography is usually used to isolate the target molecule. In this work a number of AAAB (A_3B) phthalocyanine complexes were synthesized.

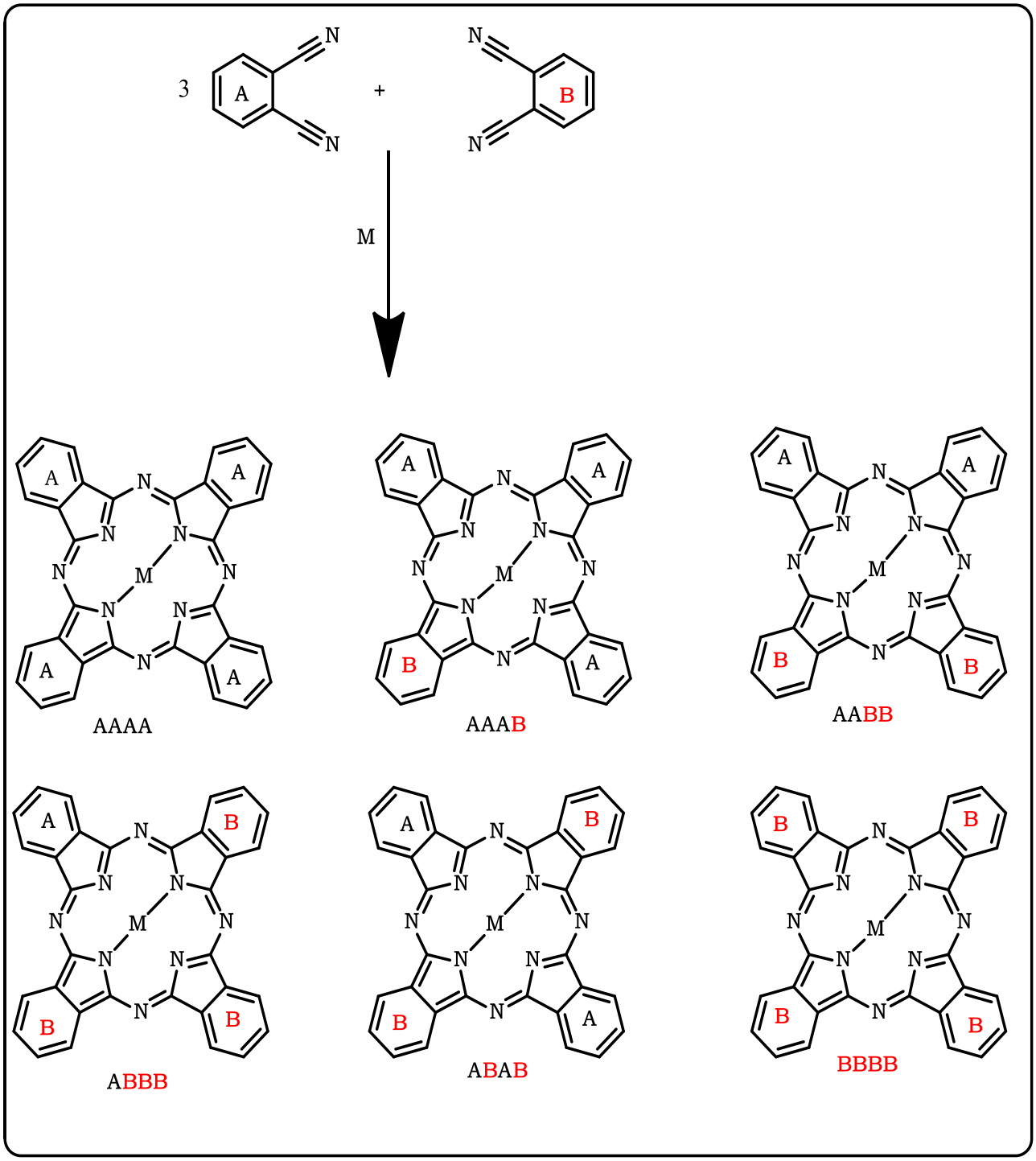

***Scheme 1.2**: Synthetic route to asymmetric phthalocyanine (**M**= central metal)*

1.2.2 Metallophthalocyanines as nonlinear optical material

Pcs are promising materials for development of nonlinear optical devices such as optical switches, and limiters **[35,36]** due to their conjugated π-electron ring system. The prerequisite for good optical limiter is to exhibit third order nonlinear susceptibility properties. Third order nonlinear susceptibility studies of many organic material including phthalocyanine (Pcs) have been previously conducted **[37-42]**.

NLO behaviour have been previously studied for phthalocyanines, but mainly for symmetrical Pcs **[43-46]**. However, it has been recently reported that asymmetrical Pcs show improved photophysical and NLO behaviour **[47-50]** due to their increased dipole moments which contribute to fast NLO response and afford specific binding to other molecules in comparison to their symmetrical analogues. Similarly, diamagnetic metals such as zinc are known to play indispensable role in optical limiting property of Pcs due to their ability to contribute towards the high population of the triplet state through rapid intersystem crossing. Hence, this thesis reports on asymmetrical Pcs with Zn(II) as central metal.

1.2.3 Photophysical properties of metallophthalocyanines

A Jablonski diagram (**Fig. 1.4**) provides a representation of the energy changes which Pcs undergo upon excitation. In the diagram, the S_o and S_1 represent the ground and singlet excited states of the Pcs, respectively. The transition from $S_o \rightarrow S_1$ populates the excited singlet state; while $S_1 \rightarrow T_1$ on the other hand is due to intersystem crossing (isc) to populate the triplet state, followed by triplet-triplet absorption indicated by $T_1 \rightarrow T_n$. Strong intersystem

crossing and triplet-triplet absorption often afford strong nonlinear absorption which is very important for NLO.

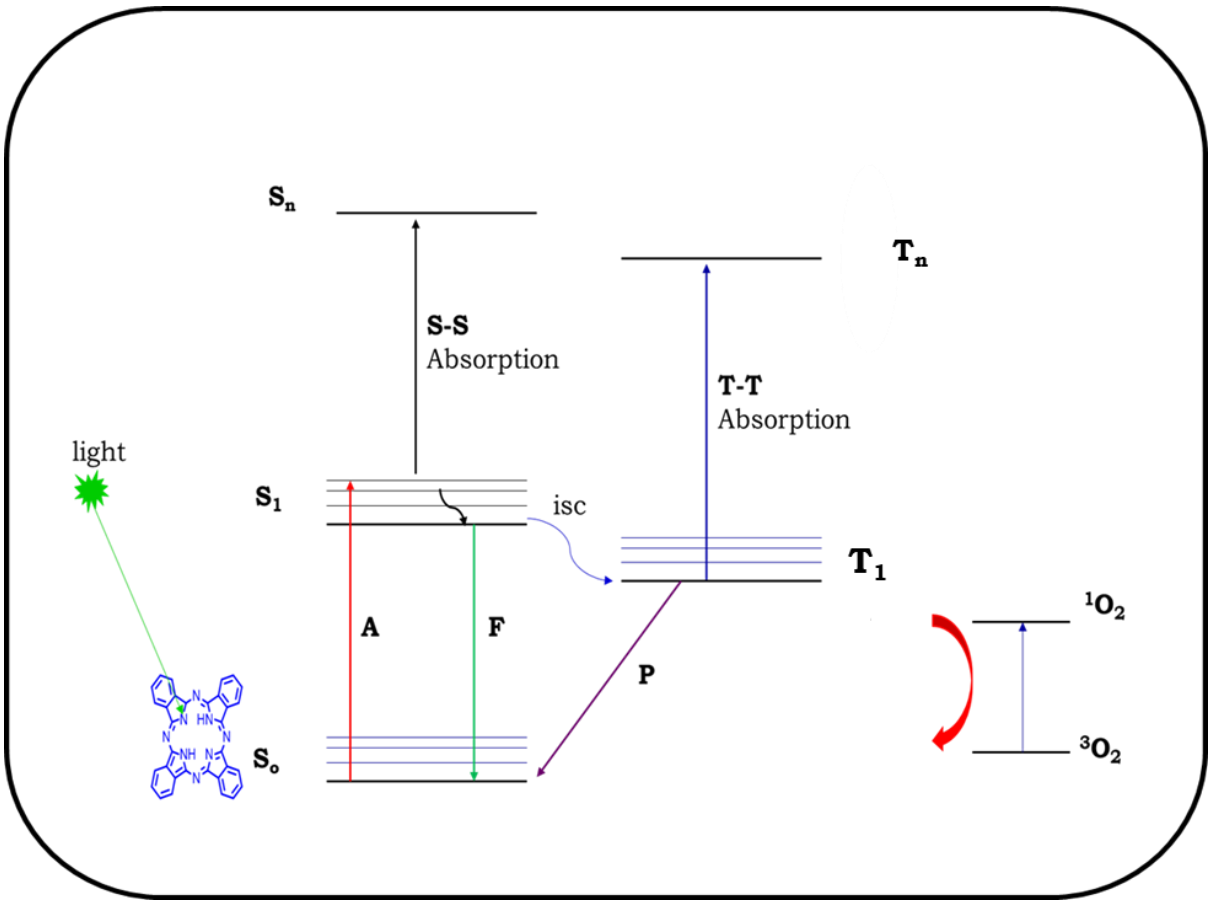

Fig. 1.4: *Basic Jablonski diagram.*

Photophysical properties of metallophthalocyanine (physical changes associated with MPcs when it interacts with photons) involve estimation of the following parameters: fluorescence quantum yield (Φ_F) **[51-53]** and fluorescence lifetime (τ_F) **[54,55]**, Foster resonance energy transfer (FRET), triplet quantum yield (Φ_T) and triplet lifetimes (τ_T). Comparative methods are employed in determining fluorescence quantum yield (Φ_F), equation 1.1 **[56,57]**

$$\Phi_F = \Phi_F^{std} \frac{F\ A_{std}\, n^2}{F_{std} A\, n_{std}^2} \qquad 1.1$$

where Φ_F^{std} is fluorescence quantum yield of the standard. When exciting at wavelengths where Pcs absorb, unsubstituted ZnPc in dimethylsulfoxide (DMSO) is used as a standard (Φ_F^{std} =0.2) **[57,58]**, and where semiconductor quantum dots (SQDs) absorb, quinine sulphate in sulfuric acid is used (Φ_F^{std}=0.52) **[59]**. A, n, F are absorbance at the excitation wavelength, refractive index of solvent and integrated fluorescence emission intensity, respectively. 'Std' represent standard.

The $\pi^* \leftarrow \pi$ transition energy of MPc (acceptor) lies below the energy of SQDs (donor), hence intramolecular energy transfer is expected from the excited donor to the acceptor.

Fluorescence quantum yield of SQDs in the presence of MPc, ($\Phi_{F(SQDs)}^{Conjugate}$) may be determined using equation 1.2 **[60]**.

$$\Phi_{F(SQDs)}^{Conjugate} = \Phi_{F(SQDs)} \frac{F_{F(SQDs)}^{Conjugate}}{F_{(SQDs)}} \qquad 1.2$$

where $\Phi_{F(SQDs)}$ is the fluorescence quantum yield of the SQDs alone and is used as the standard, $F_{(SQDs)}$ is the integrated fluorescence intensity of the SQDs alone and $F_{F(SQDs)}^{Conjugate}$ is the integrated fluorescence intensity of the SQDs when coordinated to Pc derivatives.

Fluorescence lifetimes for complexes and conjugates were obtained from Time Correlated Single Photon Counting (TCSPC) amongst other techniques.

In the presence of semiconductor quantum dots (SQDs) Forster resonance transfer (FRET) is possible from SQDs (donor) to Pc (acceptor) **[61-63]**. FRET efficiencies were determined using equation 1.3 **[64-66]**:

$$Eff = 1 - \frac{\tau_{F(GQDs)}^{conjugate}}{\tau_{F(GQDs)}} \qquad 1.3$$

where $\tau_{F(GQDs)}$ are fluorescence lifetimes of the SQDs alone and ($\tau_{F(GQDs)}^{conjugate}$) the fluorescence lifetimes of the SQDs in the conjugates.

Triplet quantum yield values were determined using comparative methods and equations 1.4-1.6 **[67-72]**

$$\Phi_T = \Phi_T^{std} \frac{\Delta A_T \varepsilon_T^{std}}{\Delta A_T^{std} \varepsilon_T} \quad 1.4$$

$$\varepsilon_T = \varepsilon_S \frac{\Delta A_T}{\Delta A_s} \quad 1.5$$

$$\varepsilon_T^{std} = \frac{\Delta A_T^{std}}{\Delta A_S^{std}} \quad 1.6$$

where Φ_T^{std}, ΔA_T^{std}, ε_T^{std} are triplet quantum yield of standard (Φ_T =0.65, ZnPc in DMSO) **[67,69]**, changes in the triplet state absorption and molar extinction co-efficient of the ZnPc standard, respectively.

Triplet lifetimes of species (measure of the length of time spent in the excited triplet state) are determined by fitting exponential data of the triplet decay curves using origin Pro. 8.0 program.

1.3 Semiconductor quantum dots

Nanoparticles are materials which have size (diameter) ranges of 1 to 100 nm. The difference in size and shape of nanoparticles alters their chemical and physical properties. Among many nanoparticles (NPs) such as silica, graphene, and quantum dots to mention just a few, semiconductor quantum dots (SQDs) remain one of the most interesting NPs with diverse applicability as will be discussed below.

SQDs are photostable, high fluorescent nanocrystals with sizes ranging from 2-20 nm in diameter. Their properties can be manipulated to suit specific applications by changing their sizes and surface. SQDs have broad absorption and narrow emission as shown in **Fig. 1.5**, and have been reported to show usefulness in drug delivery **[73]**, biomedical imaging **[74]**, fluorescence sensing **[75]** and photodynamic therapy **[76]**. The broad absorption spectra of SQDs is attributed to discrete energy levels they occupy when excited by photon. Smaller SQDs exhibit blue shifted absorption due to a large band gap, the opposite is observed for larger SQDs **[77]** which are known for their large bathochromic shifts.

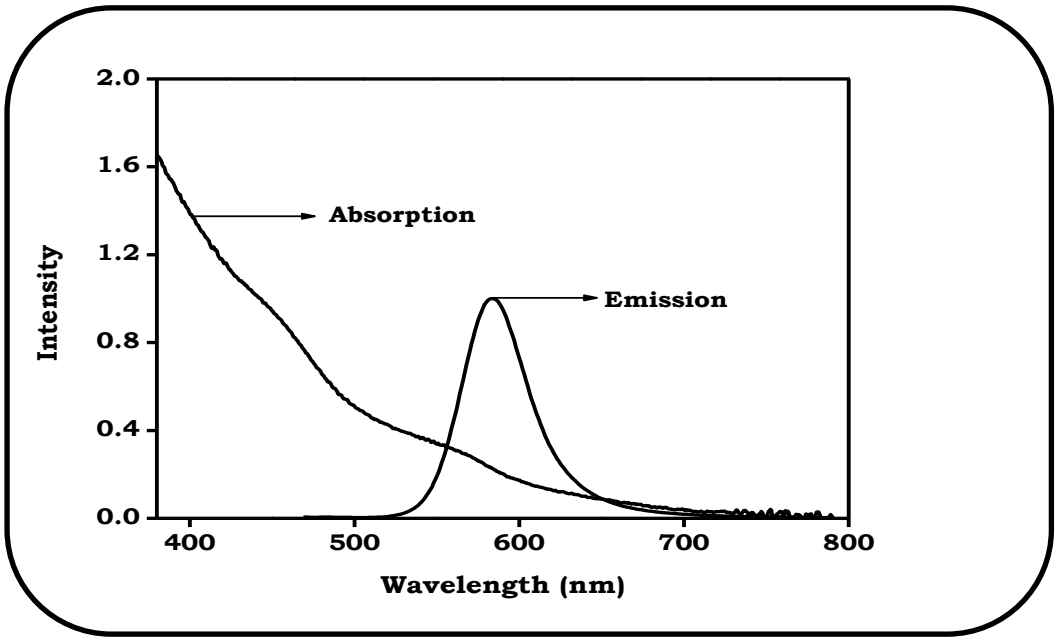

***Fig. 1.5**: Broad absorption and narrow emission spectra of SQDs **[unpublished work]**.*

SQDs can be designed in the form of binary or ternary metal composition such as CdTe (binary) and CdTeSe (ternary). Additionally, SQDs can be made as core, core/shell and core/shell/shell depending on their desired applications,

Fig. 1.6. This work focuses on core/shell and core/shell/shell containing cadmium telleride (CdTe) as core, coated with zinc selenide (ZnSe) or zinc sulfide (ZnS) to form CdTe/ZnSe or CdTe/ZnS and further coated with zinc oxide (ZnO) to obtain CdTe/ZnSe/ZnO or CdTe/ZnS/ZnO **[78,79]**. Glutathione (GSH) functionalized CdTe/ZnSe (SQD1), CdTe/ZnS (SQD2), CdTe/ZnSe/ZnO (SQD1/ZnO) and CdTe/ZnS/ZnO (SQD2/ZnO) SQDs are employed (**Fig. 1.7**). CdTe quantum dots are chosen as core due to their ability to exhibit high nonlinear absorption coefficient **[80]**. On the other hand, NLO behaviour of ZnSe in crystal form and when incorporated into a polymer has been investigated **[81,82]**. Hence, SQDs containing CdTe are employed to enhance the NLO behaviour of Pcs by synergistic effect.

The presence of shells is known to enhance photoluminescence and stability of core SQDs **[83,84]**. Also during synthesis, thiol containing capping agents have been used to stabilize, improve solubility and allow for linking to other molecules **[85-88]**.

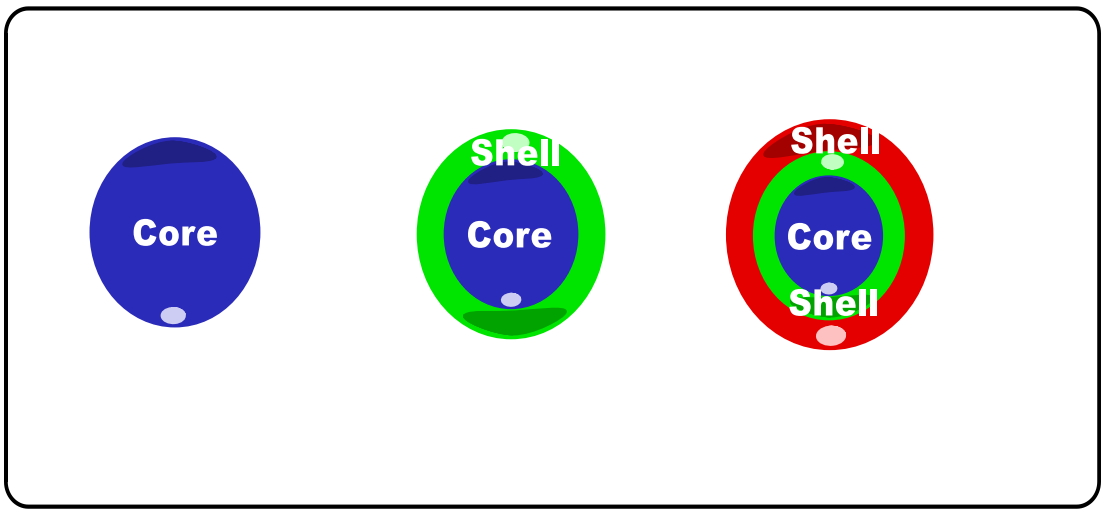

***Fig. 1.6**: Representative structure of bare semiconductor quantum dots (SQDs)*

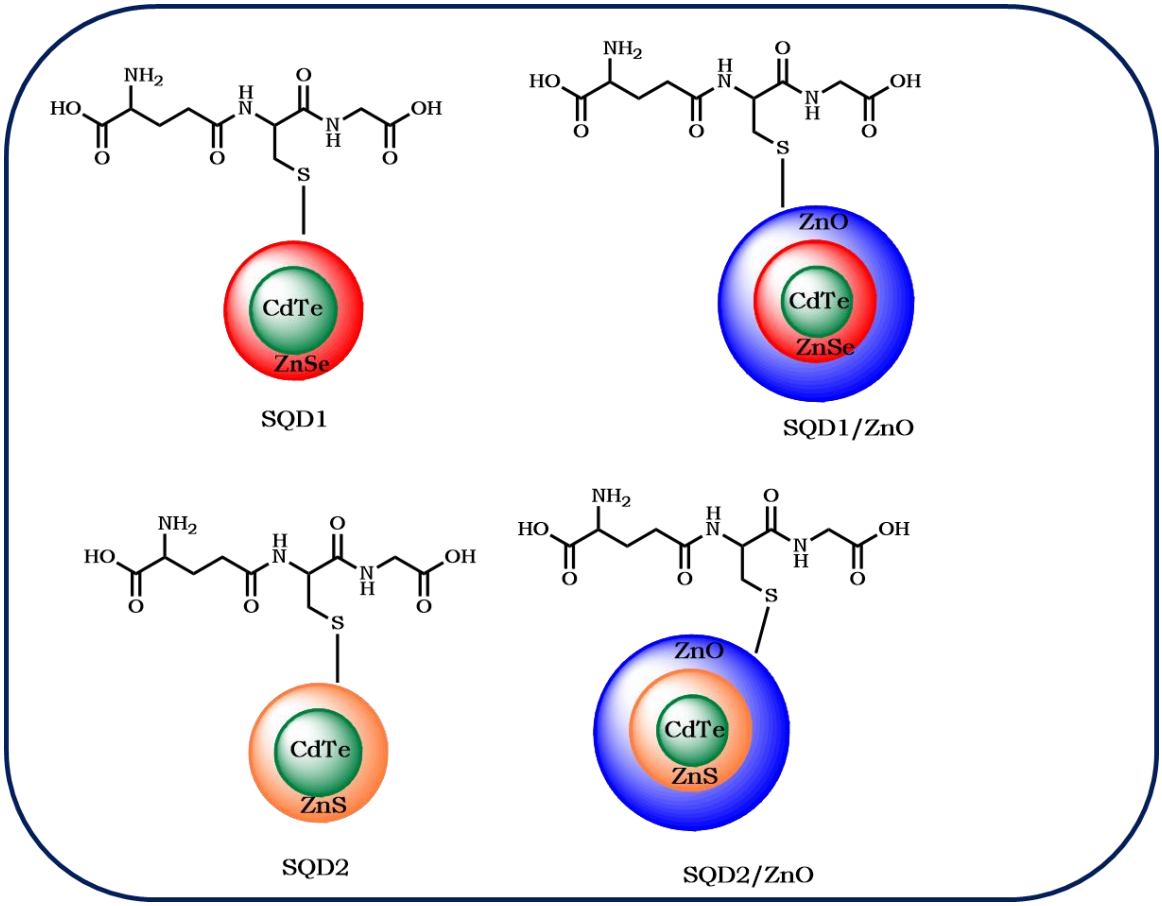

Fig. 1.7 *Semiconductor quantum dots employed in this thesis.*

There are two main synthetic routes for fabrication of SQDs, namely; organometallic and hydrothermal routes. Hydrothermal method is preferred over organometallic due to disadvantages associated with organometallic preparation of SQDs such as harsh synthetic conditions, toxic reagents, low fluorescence behavior upon phase transfer and toxic solvents while water requires mild conditions, hence hydrothermal method is employed in this work.

1.4 Phthalocyanine-Semiconductor conjugates

Phthalocyanines and semiconductor quantum dots show NLO behaviour with strong nonlinear optical absorption and the focus of this thesis is on covalently linkage of phthalocyanines to SQDs (Pc-SQDs). Pcs have been covalently conjugated to quantum dots for applications in fluorescence sensing **[89]**, in photodynamic antimicro chemotherapy **[90]**, in PDT **[91]**, and for photophysical studies **[92]**. **Table 1.1** shows Pcs that were conjugated to quantum dots for NLO **[37,43,93-97]**. The table shows that there are limited reports on investigation of NLO properties of asymmetrical Pc-SQDs. Hence, evaluation of NLO response of novel asymmetrical Pcs when conjugated to SQDs is main subject of this thesis.

Table 1.1 Phthalocyanines which have been used with quantum dots in nonlinear optics.

Phthalocyanaine	Bond	SQDs	Ref.
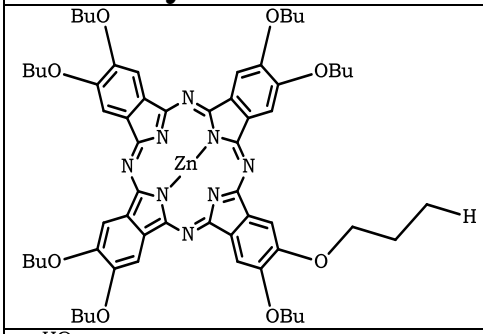	Mixed		[93]
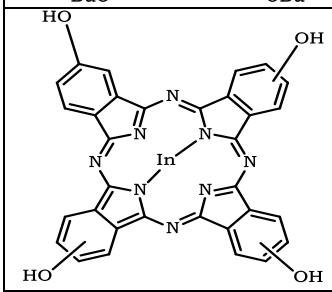	Mixed	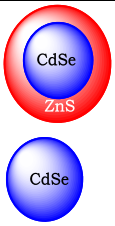	[43]
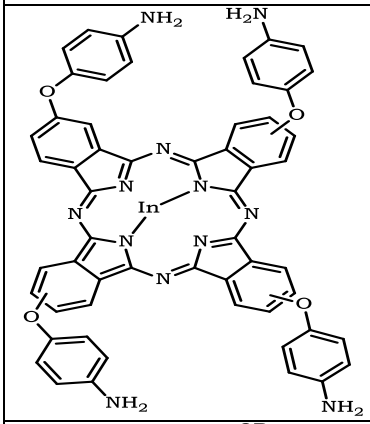	Amide	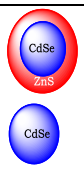	[43]
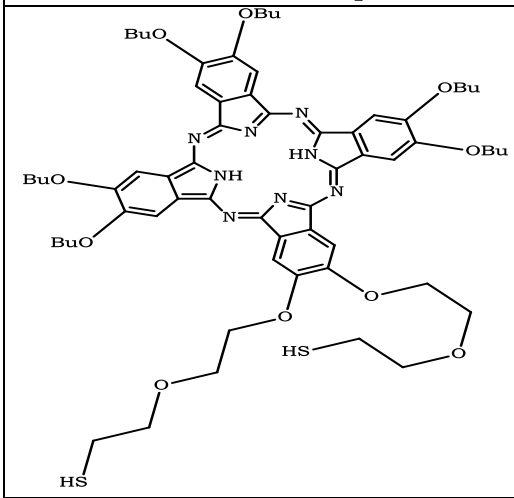	S-CdSe		[94]

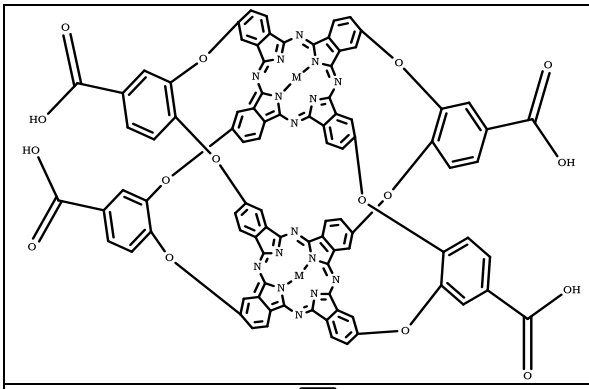	Amide	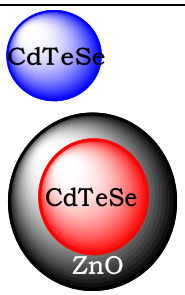	**[37]**
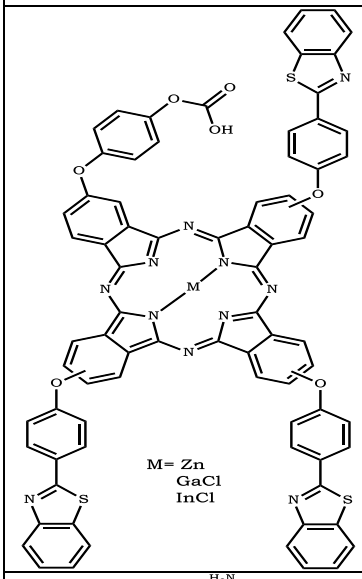	Amide		**[95]**
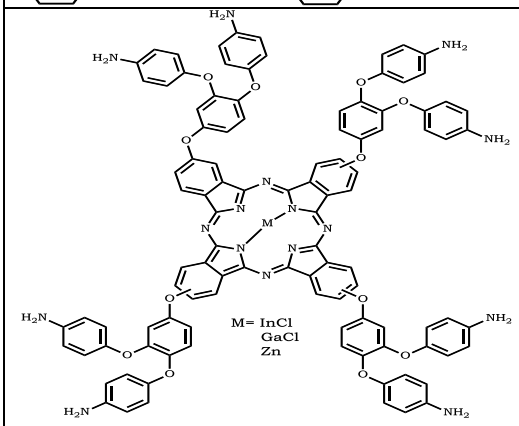	Amide		**[96]**
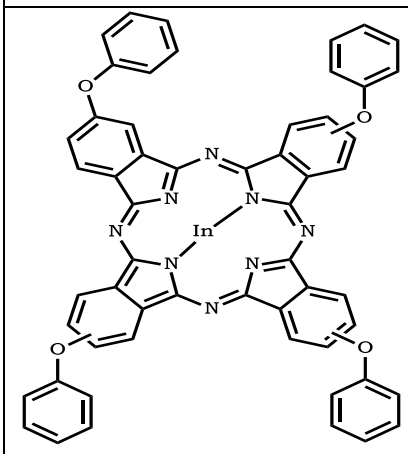	Mixed		**[97]**

Again, some NLO studies of these combined systems **(Table 1.1)** have been performed in mixture, however in this work the focus is on NLO properties of phthalocyanines when covalently linked to SQDs.

1.5 Phthalocyanines employed in this work

Pcs employed (**Table 1.2**) in this work consist of (phenoxy)propanoic acid (**1**), carboxyphenoxy (**2**), (oxy)phenoxy acetic acid (**3**), benzothiazole (**4**), pyridiloxy (**5**) and hydroxyphenylalanine (**6**) on β position. The syntheses of complexes **1**, **[98]**, **2 [99]** and **3** [**100]** have been reported in the literature. Complexes **4-6** are synthesized for the first time in this work.

NLO properties of 4-hydroxyphenylalanine have been studied in crystal form **[101,102]**, thus evaluation of NLO properties of 4–hydroxyphenylalanine substituted phthalocyanine (**6**) are investigated in this work. Complexes **1**-**3** and **6** will be compared for the nature of COOH group and the effects of conjugation to core/shell and core/shell/shell semiconductor quantum dots. Pcs having one functional group are preferred for covalent linkage for restrained formation of conjugates. Complexes (**1**-**3**, **5** and **6**) will be covalently linked (amide bonds) to glutathione (GSH) functionalized SQDs through the carboxylic moiety of the MPc and the amino group of the GSH. Complex **4**, on the other hand will be linked to SQDs via amide bond but using the COOH group of GSH-SQDs and amino group of the complex. The covalent linkage of complexes to SQDs is expected to promote enhanced photophysical properties resulting from spin orbit coupling **[103-105]**, thus fostering rapid intersystem crossing (isc) to the triplet state. SQDs are expected to contribute to NLO behaviour of MPc through free-carrier absorption (FCA) mechanism

[106]. All Pcs contain Zn central metal to enhance triplet state population and NLO and contain (COOH or NH_2) for linking to SQDs by amide bond. Complexes **1**-**3** were conjugated to SQD1 and SQD1/ZnO while **4**-**6** were conjugated to SQD2/ZnO.

Table 1.2: MPcs alone and when covalently linked to semiconductor quantum dots (SQDs).

Complexes	**SQDs**	**NLO Studies**
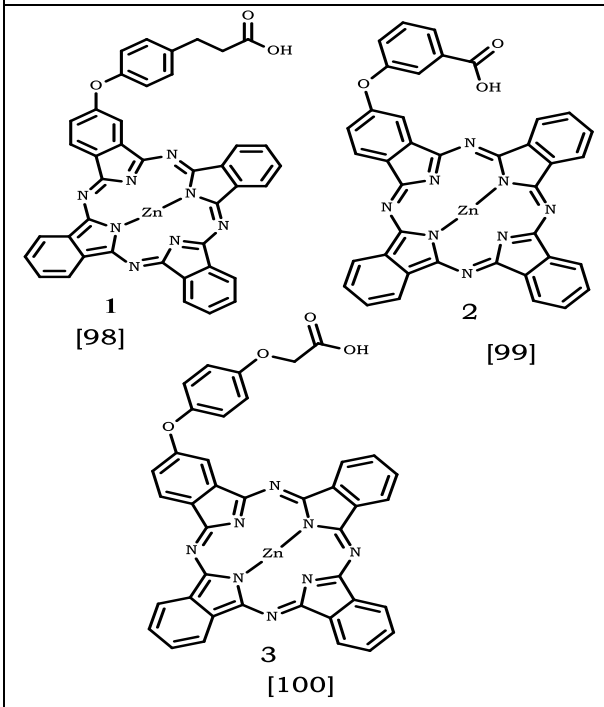 1 [98] 2 [99] 3 [100]	SQD1 and SQD1/ZnO (all GSH capped)	Φ_F, τ_F , Φ_T, τ_T β_{eff}, $I_m[\chi^{(3)}]$, I_{lim}, k
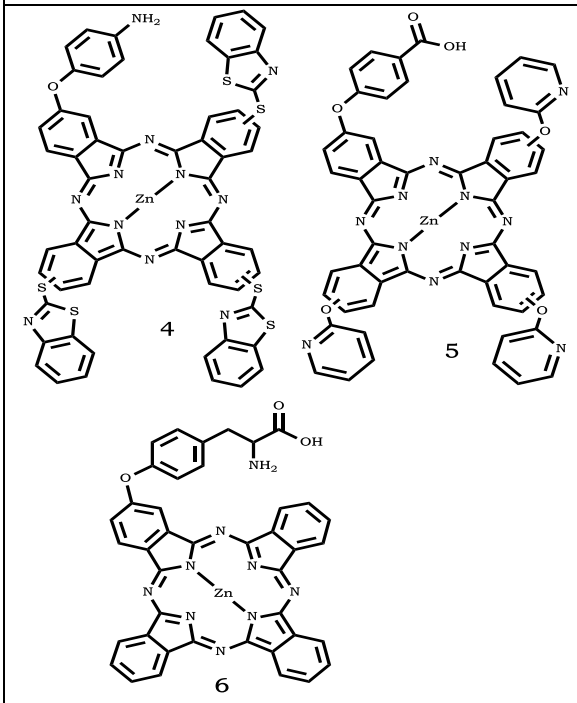 4 5 6	SQD2 and SQD2/ZnO (all GSH capped)	Φ_F, τ_F , Φ_T, τ_T β_{eff}, $I_m[\chi^{(3)}]$, I_{lim}, k

1.6 Determination of NLO parameters

The open aperture Z-scan technique was used in this work for the determination of the NLO parameters. The technique provides nonlinear absorption and nonlinear refraction behaviour of the samples.

Z-san technique originated as a useful technique in nonlinear optics due to its simplicity and high sensitivity **[107]**. Z-scan consists of a beam splitter, lenses and photodetectors, as shown in **Fig 1.8**. Nonlinear optical response of a material using Z-scan involves movement of a sample. Precise results of Z-scan measurements depend on the quality of the beam and laser stability. Thus, to maintain stability, the laser beam is divided into two parts viz reflected beam and transmitted beam. The beam splitter directs the reflected beam towards photo-detector 1 (D1) while the transmitted beam gets relayed before reaching the sample in the form of signal through the lens and enters photodetector 2 (D2). Detecting reference (reflected beam) by D2 makes it easier for one to observe the stability of the laser as fluctuation of laser energy can directly impact on results.

Z-scan experiment data are often analyzed using the method described by Sheik-Bahae *et al*, equation 1.7 and 1.8 **[107]**:

$$T_{(Z)} = \frac{1}{1+\beta_{eff}L_{eff}(I_{00}/(1+(z/z_0)^2))} \qquad 1.7$$

$$l_{eff} = \frac{1-e^{-\alpha l}}{\alpha} \qquad 1.8$$

where $T_{(Z)}$ is the normalized transmittance of the sample, I_{00} is the intensity of the light on focus, β_{eff} is the two-photon nonlinear absorption coefficient, z_0 is the Rayleigh length, z is the sample position with respect to input intensity,

L_{eff} is the effective length for two photon absorption, α is the linear absorption and l is the path length of the sample.

The sensitivity and how fast the material respond to the induced perturbation by laser pulses is known as third-order susceptibility $I_m[\chi^{(3)}]$) equation 1.9 **[108]**

$$I_m[\chi^{(3)}] = \frac{n^2 \varepsilon_0 c \lambda \beta_{eff}}{2\pi} \quad 1.9$$

where n and c are the linear refractive index (n = 1.479 for DMSO), and speed of light, respectively ε_o is the permittivity of free space and λ is the wavelength of the laser.

The ground state absorption cross-section is obtained from absorption spectroscopy using equation.1.10

$$\delta_{0=}{}^{\alpha}/_{N_0} \quad 1.10$$

where α is the linear absorption and N_0 is the number of molecules per cm^3.

The magnitude of absorption cross-sections ratio (k) for the conjugates is obtained from the ratios (δ_{ex}/δ_o). Excited state absorption cross–section (δ_{ex}) is obtained by fitting experimental data set from Z-scan into excited state absorption, equations 1.11 and 1.12 **[109,110]**:

$$\frac{T}{T_{linear}} = \frac{\ln(1+q)}{q} \quad 1.11$$

$$q = \frac{\alpha}{2h\nu}\delta_{ex} I_o L_{eff} \quad 1.12$$

Where T, T_{linear} h, ν, λ, I_o, is nonlinear transmittance, linear transmittance, Planck's constant, frequency of the laser, wavelength and the total fluence on-axis, respectively.

The final parameter is limiting threshold (I_{lim}), describing the values input fluence at which the transmittance is reduced by 50% of the linear transmittance value **[111]**.

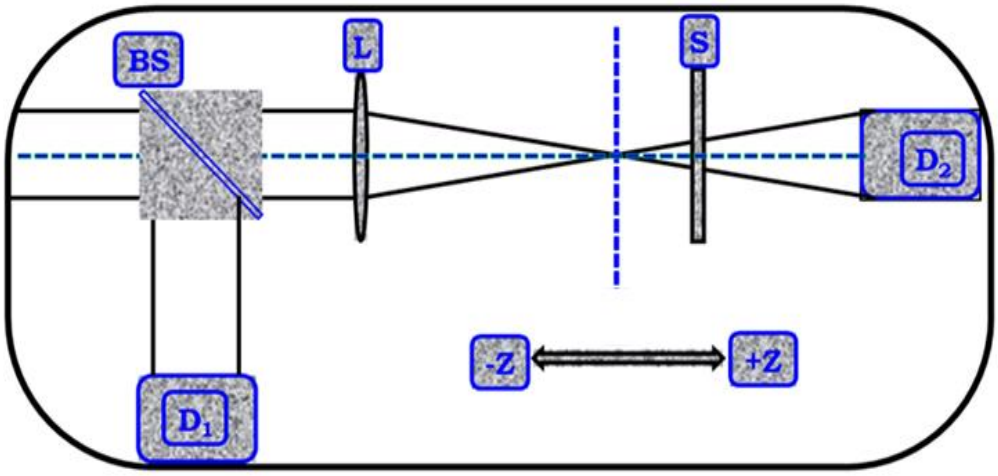

***Fig. 1.8**: Schematic illustration of open aperture Z–scan set–up. BS = Beam splitter, L = Lens, D1 and D2 = Photodetectors, Z = Z – Position, and S = Sample.*

1.7 Summary of aims of this Thesis

The aims of this thesis are listed as follows:

I. Synthesis of asymmetrical phthalocyanine with amino and carboxylic functional groups.

II. Synthesis of glutathione capped semiconductor quantum dots

III. Covalent linkage of asymmetrical phthalocyanine (Pcs) to glutathione capped semiconductor quantum dots (SQDs) via amide bond

IV. Characterization of asymmetrical Pcs, SQDs and nanoconjugates

V. Investigation of photophysical properties of Pcs in the presence and absence of SQDs

VI. Evaluation of nonlinear optical properties of Pcs and nanoconjugates using Z-scan technique.

Chapter 2: Experimental

Chapter 2 Experimental

2.1 Equipment

1. Fourier transform infra-red (FT-IR) spectra were recorded on a Bruker® ALPHA FT-IR spectrometer with universal attenuated total reflectance (ATR) sampling accessory.
2. Ultraviolet-visible (UV-vis) absorption spectra were acquired on a Shimadzu UV–2550 spectrophotometer.
3. Mass spectra data were acquired on a Bruker Auto FLEX III Smart beam TOF/TOF mass spectrometer operated in positive ion mode using α-cyano-4-hydrocinnamic acid as a matrix.
4. Proton nuclear magnetic resonance (^{1}H-NMR) spectra were recorded on a Bruker AMX Advance 600 MHz NMR spectrometer using tetramethyl silane (TMS) as an internal reference.
5. The elemental compositions (CHN) of complexes **4**, **5** and (CHNS) **6** were measured on a Vario-Elementar Microcube ELIII elemental analyzer.
6. X-ray powder diffraction (XRD) patterns were measured on a Bruker D8 Discover equipped with a Lynx Eye detector (proportional counter), using Cu Kα radiation (l = 1.5405 A°, nickel filter) as described before in the literature **[88].**
7. The morphologies of the semiconductor quantum dots (SQDs) and their nanoconjugates were assessed using transmission electron microscope (TEM) ZEISS LIBRA model 120 operated at 90 kV.
8. Energy dispersive X-ray spectrometer (INCA PENTA FET coupled with VAGA TESCAM operated at 20 kV) was used to qualitatively determine the elemental compositions of the SQDs and the nanoconjugates with complexes.

9. The triplet state quantum yields and lifetimes of the samples were obtained by laser flash photolysis system consisting of a LP980 spectrometer with a PMT-LP detector and an ICCD camera (Andor DH320T-25F03). The signal from the PMT detector was recorded on a Tektronix TDS3012C digital storage oscilloscope. The excitation pulses were produced using a tunable laser system consisting of a Nd:YAG laser (355 nm, 135 mJ/4–6 ns) pumping an optical parametric oscillator (OPO, 30 mJ/3–5 ns) with a wavelength range of 420–2300 nm (NT-342B, Ekspla). The solution was deaerated with argon for 30 minutes.

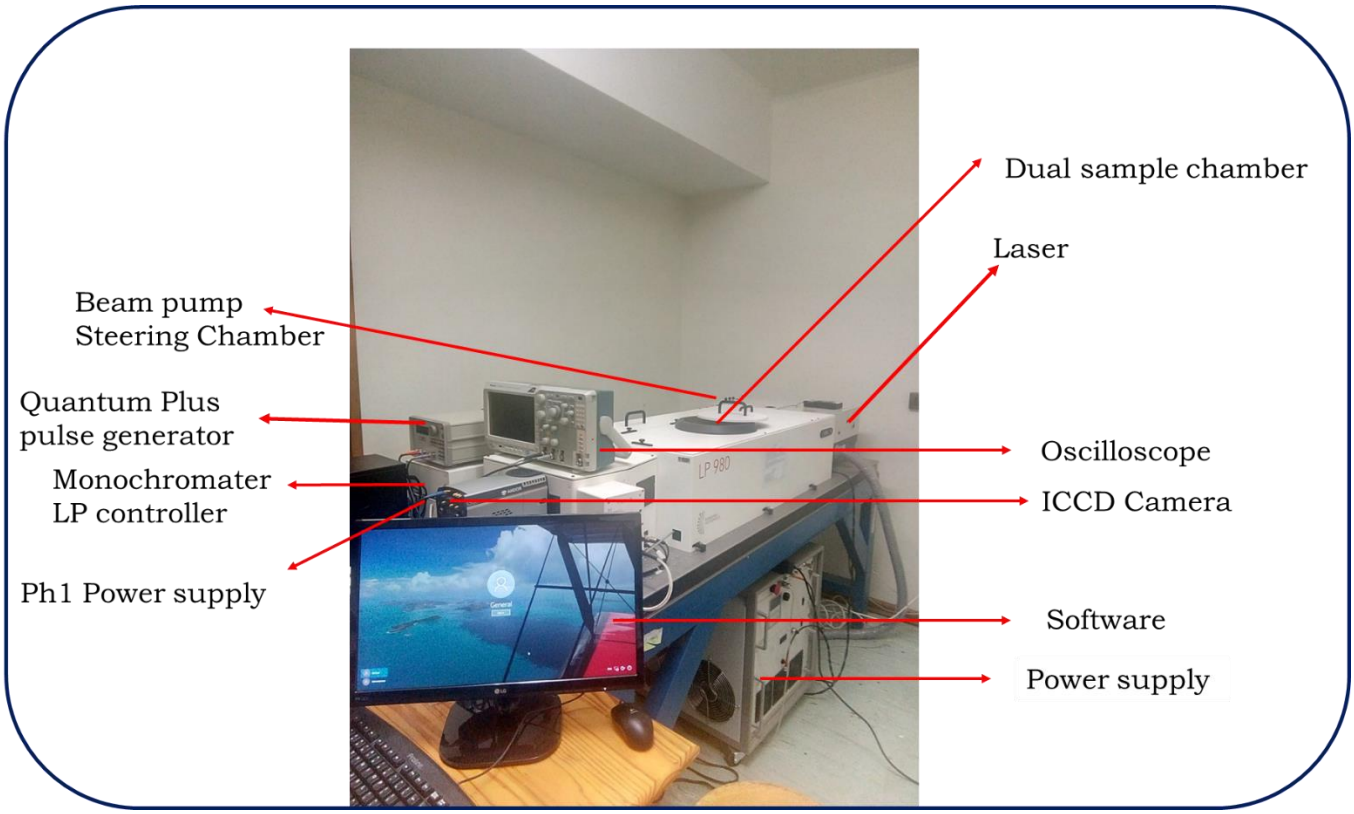

Fig. 2.1: *Laser flash photolysis system.*

10. Fluorescence lifetimes were measured using a time correlated single photon counting setup (TCSPC) (FluoTime 300, Picoquant GmbH) with diode laser (LDH-P-670 or LDH-P-485, Picoquant® GmbH, 20 MHz repetition rate, 44 ps pulse width) [112], Fig. 2.2.

11. Fluorescence excitation and emission spectra were obtained on a Varian Eclipse® spectrofluorometer using a 360 - 1100 nm filter, absorbance at the excitation wavelength was adjusted to ~ 0.05 to ensure good statistics **[112]**.

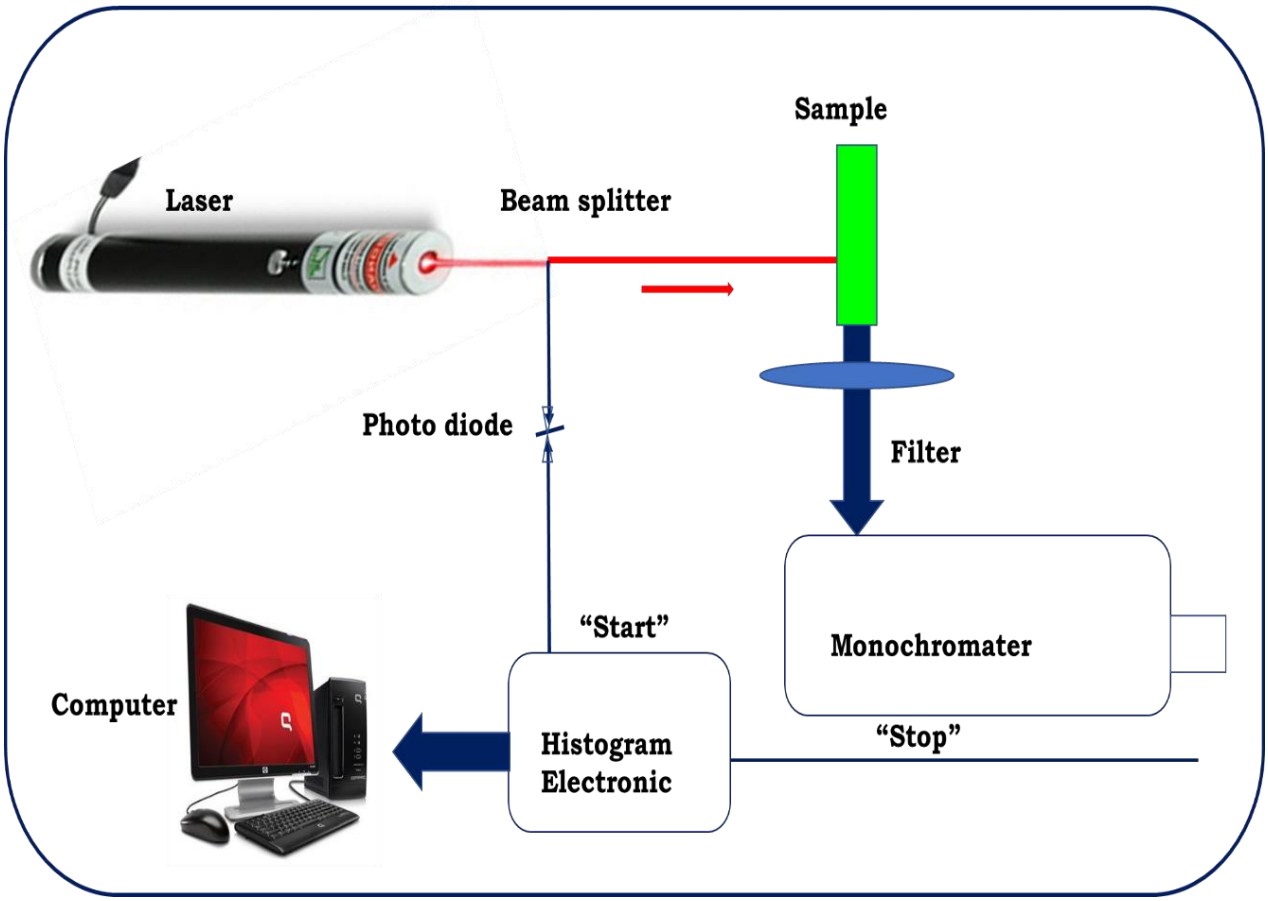

***Fig. 2.2**: Representation of the time correlated single photon counting (TCSPC) set-up.*

12. Optical nonlinearities of the Pc complexes and their conjugates with SQDs were studied using a Z-scan set–up as described in the literature using a frequency-doubled Nd:YAG laser (Quanta-Ray, 1.5 J/10 ns fwhm pulse duration) as the excitation source **[45]**.

2.2 Materials

Zinc acetate dihydrate, *N,N'*-dicyclohexylcarbodiimide (DCC), dimethyl sulfoxide (DMSO), unsubstituted zinc phthalocyanine (ZnPc), 1-pentanol, 1,8-diazabicyclo[5.4.0]undec-7-ene (DBU), phthalonitrile (**12**), and silica gel were obtained from Sigma Aldrich®. Ultra–pure water was obtained from a Milli–Q Water System (Millipore Corp, Bedford, MA, USA). Methanol, tetrahydrofuran (THF), absolute ethanol and dimethyl formamide (DMF) were obtained from SAARCHEM®. The following compounds were synthesized as reported in literature: 4-(benzo[d]thiazol-2-ylthio)phthalonitrile (**7**) **[46]**, 4-aminophenoxyphthalonitrile (**8**) **[85]**, dicyano phenoxy)benzoic acid (**9**) **[113]**, 3-(3,4- 4-(2-pyridinyloxy)phthalonitrile (**10**) **[45]**, 4–hydroxyphenylalanine (tyrosine) phthalonitrile (**11**) **[114]**, **(Table 2.1**) . The syntheses of glutathione (GSH) capped CdTe/ZnSe-GSH (SQD1) **[91]**, CdTe/ZnSe/ZnO-GSH (SQD1/ZnO) **[91]**, CdTe/ZnS (SQD2) **[88]** have been reported. Complexes **1 [98]**, **2 [99]** and **3 [100]** were synthesized as previously reported elsewhere in literature.

Table 2.1: Precursors employed in this work

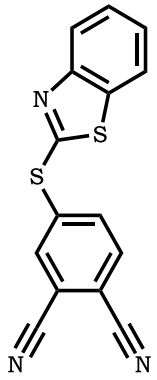 7 [46]	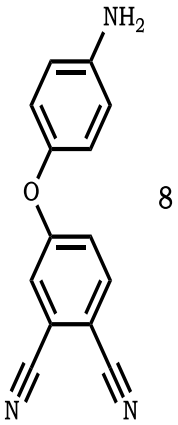 8 [85]	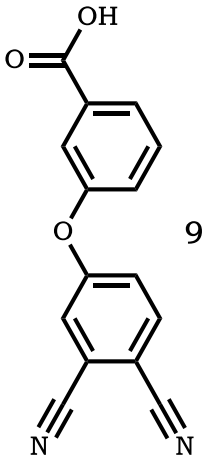 9 [113]	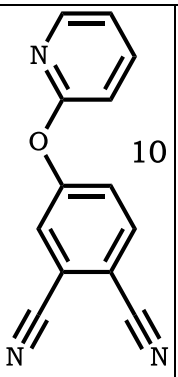 10 [45]	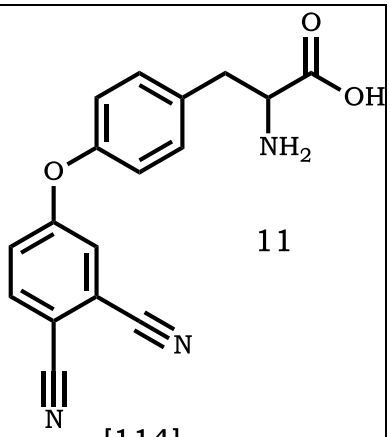 11 [114]

2.3 Synthesis of asymmetrical zinc phthalocyanine derivatives

2.3.1 Zn(II) aminophenoxy-tris(benzothiazole) phthalocyanine (4) (Scheme 3.1)

The synthesis of complex **4** was as follows: compounds **8** (0.80 g, 3.40 mmol) and **7** (2.99 g, 10.21 mmol) were transferred into a round bottom flask containing zinc acetate dihydrate (0.63 g, 2.87 mmol) and 5 ml of 1-pentanol. Catalytic amount of DBU (0.50 ml, 11 mmol) was added to the flask and the reaction mixture was refluxed in the presence of nitrogen flow at 140 ˚C for 6 h with constant stirring. The obtained crude product was precipitated out of solution with methanol. The purification and isolation of the A_3B target ligand was obtained by silica packed column with gradient eluents of tetrahydrofuran and methanol.

Yield: 39%. UV-Vis in DMSO λ_{max}/nm (logε) 690 (5.28), 617 (4.15), 348 (4.50). IR [ν_{max}/cm^{-1}]: NH_2 (3413), Ar-CH(1240), S-C (780). ^{1}H-NMR (600 MHz in DMSO–d_6) δ(ppm): 9.40 (6H, m, benzothiazole-H), 8.15-8.28 (6H, m benzothiazole) 7.25-8.1 (12H, m, Pc macrocycle-H), 6.40-6.93(4H, m, Ar-H), 5.72 (2H, d, amine-H). *Anal. Calcd for $C_{59}H_{30}N_{12}OS_6$: C, 60.02; H, 2.56; N, 14.42; S, 16.26; Found: C,60.36; H, 2.33; N, 14.44; S, 17.13*. MALDI-TOF-MS: (m/z) Calcd 1180.3 Found 1179.3 $[M - H]^-$

2.3.2 Zn(II) 3-carboxyphenoxy-tris(pyridin-2-yloxy) phthalocyanine (5) (Scheme 3.2)

Complex **5** was synthesized as described for **4** except for the use of compounds **9** (0.50 g and 1.89 mmol) and **10** (1.26 g, 5.68 mmol) instead of **7** and **8**. All the other reagents and quantities were the same. Reaction conditions and purification procedure was as described for complex **4**.

Yield = 31%. UV-Vis in DMSO λ_{max}/nm (log ε) 678 (4.95), 608 (4.02), 340 (4.32). IR [ν_{max} /cm^{-1}]: 3060 (OH), 2924(N=C),1653 (C=O) (780). ^{1}H NMR (600 MHz in DMSO–d6) δ (ppm): 9.40(1H, s, Carboxylic acid–OH), 8.0-8.5(4H, m, Ar-H), 7.83-7.96 (12H, m, pyridloxyl-H), 7.00-7.60, 6.25-6.75 (12H, m, Pc macrocycle-H). Anal. Calcd. for $C_{54}H_{29}N_{11}O_6$: C, 64.13; H, 3.23; N, 15.240; Found: C,63.91; H, 4.29; N,15.99 MALDI-TOF-MS: m/z Calcd 992.7, Found 993.2 $[M + H]^+$

2.3.3 Zn(II) amino-carboxyethylphenoxy phthalocyanine (6) phthalocyanine (Scheme 3.3)

Complex **6** was synthesized as described for **4** except for the use of compounds **11** (1.0 g, 3.26 mmol) and 1,2-dicyanobenzene (1.3 g, 9.77 mmol) instead of **7** and **8**. All the other reagents and quantities were the same. Reaction conditions and purification procedure was as described for complex **4**.

Yield = 25%. UV-Vis in DMSO $\lambda_{max/}$nm (log ε) 677 (5.41), 608 (4.08), 343 (4.15).IR [ν_{max}/cm^{-1}]:3706 (NH_2), 2971 (OH), 2868 (C-H), 1716 (C=O), 1056(C-O). H^1 NMR (600 MHz in DMSO – d_6). δ(ppm) 9.44 (1H, s, Carboxylic acid–OH), 8.27 (2H, d, amine–H), 7.83-7.95 (15H, m, Pc macrocycle-H), 6.63-6.87

(4H, m, phenyl-H) 3.50 (3H, m, alkyl-H): . Anal. Calcd for $C_{41}H_{25}N_9O_3$ Zn: C, 63.53 ; H, 3.35; N, 14.05; Found: C,63.29 ;H, 2.83; N,13.73. MALDI-TOF-MS: m/z Calcd 755.7 Found 756.86 $[M + H]^+$.

2.3.4 GSH-CdTe/ZnS/ZnO (SQD2/ZnO) (Scheme 3.4)

The synthesis of GSH functionalized CdTe/ZnS/ZnO (SQD2/ZnO) was performed as described in the literature **[88]** with modifications. Briefly, zinc acetate (0.45 g, 6.92 mmol) was dissolved in 40 mL ultrapure millipore water. The resulting Zn solution was added into the refluxing core/shell (CdTe/ZnS-GSH) SQDs (SQD2) under open air and allowed to stir for 45 min to form core/shell/shell (CdTe/ZnS/ZnO-GSH) SQDs (SQD2/ZnO). The resulting mixture was precipitated with methanol and finally purified with ethanol and it was air – dried in enclosed fume hood.

2.3.5 Covalent coupling of complexes 1-3, 5,6 with SQDs (Scheme 3.5)

Complexes **1** to **3**, **5**,**6** (0.0162 mmol each) were each dissolved in dry DMF (2 mL), then DCC (0.015, 0.073 mmol) was added to activate the carboxylic moiety of the Pcs. The mixtures were stirred for 48 h at ambient temperature. Thereafter, SQDs (0.02 g each) were added and the mixtures were allowed to stir for further 48 h to afford the amide bond formation between the QDs and the MPc complexes. The products were isolated out of solution using ethanol and successively purified with methanol and air dried in enclosed fume hood. The conjugates are denoted as:**1**–SQD1, **1**– SQD1/ZnO, **2**–SQD1, **2**–SQD1/ZnO, **3**–SQD1 and **3**– SQD1/ZnO, **5**-SQD2, **5**-SQD2/ZnO, **6**-SQD2, and **6**-SQD2/ZnO.

2.3.6 Covalent coupling of complexes 4 with the SQDs (Scheme 3.6)

The amide bond conjugates of **4** with SQD2 or SQD2/ZnO were formed by the activated –COOH group of the latter and the amine moiety of the former as follows: DCC (0.015 g, 0.073 mmol) was transferred into a flask containing SQDs (0.02 g in 2 ml of a mixture of water/DMF (1:1)) to activate the –COOH moiety of the SQDs. The solution was left stirring for 48 h and afterwards, complex **4** (0.012g, 0.0102 mmol) was added to the –COOH activated SQDs and the mixture was allowed to stir for further 48 h to afford **4**–SQD2, **4**–SQD2/ZnO.

Publications

Publications

The forthcoming chapters discuss results that have been published or accepted in peer-reviewed journals. The articles are listed below

1. ***Sithi Mgidlana***, David O. Oluwole, Tebello Nyokong, Effects of the carboxylic acid substituents on the photophysical and nonlinear optical properties of asymmetrical Zn(II) phthalocyanines–quantum dots conjugates. Inorganic and Nano-metal chemistry, in press.
2. ***Sithi Mgidlana***, David O. Oluwole, Tebello Nyokong, Fabrication of efficient nonlinear optical absorber using Zn phthalocyanine–semiconductor quantum dots conjugates. Polyhedron, 159 (2019) 102-115.

Chapter 3: Synthesis & Characterization

Chapter 3 Syntheses and Characterization

3.1 Synthesis

3.1.1 Phthalocyanines (Pcs)

In the following subsections, the synthesis of complexes **1** to **3** will not be considered since they are known complexes **[98-100]**. Complexes **4**–**6** are new, hence they will be discussed.

The syntheses of low symmetry complexes **4**–**6** is achieved by a statistical cross condensation reaction of two different phthalonitriles (Schemes 3.1–3.3). Complex **4** is prepared from cross condensation of 4-(benzo[d]thiazol-2-ylthio)phthalonitrile **(7)** and 4-aminophenoxyphthalonitrile **(8)** in the presence of zinc metal salt, refluxing pentanol and catalytic amount of DBU for 6h. 3-(3,4-Dicyanophenoxy)benzoic acid **(9)** and 4-(pyridin-2-yloxy)phthalonitrile **(10)**; are used for **5** and 4–hydroxyphenylalanine)phthalonitrile **(11)** and dicyanobenzene (**12**) are used for **6**.

This method usually results in the formation of a mixture of products which requires column chromatography for separation to obtain the target A_3B complex. Extensive purification and isolation of the target complex is obtained using silica–packed column chromatography with gradient eluents of methanol in tetrahydrofuran resulting in low yield.

The complexes are successfully characterized by spectroscopic techniques such as UV-Vis, MALDI-TOF MS, FTIR, and elemental analyses and ^{1}H NMR spectroscopies (**Figs.** A1, A2, A3 appendix). ^{1}H NMR spectrum of complex **4** shows a singlet which integrated into 2 protons as a result of an amine moiety at 5.72 ppm and 12 protons at 7.25-8.10 ppm for Pc macrocycle. Signals appearing at 9.40 ppm and 8.15-8.28 ppm corresponding to benzothiazole aromatic ring.

Complex **5** show singlet of carboxylic acid at 9.40 ppm, the Pc aromatic ring and pyridloxyl substituent give 12 protons at 6.25-6.75 ppm and 7.83-7.96 ppm, respectively.

Singlet of carboxylic acid for complex **6** appears at 9.44 ppm and a signal appearing at 3.50 ppm is a result of alkyl protons while 8.27 ppm account for doublet from 2 protons of the amine. Aromatic protons of the phenyl ring appear at 6.63-6.87 ppm and the signal at 7.83-7.95 ppm account for protons of the Pc ring.

There is a disappearance of the –CN vibrational band at ~ 2230 cm^{-1} of the phthalonitriles confirming the formation of complexes **4** to **6**.

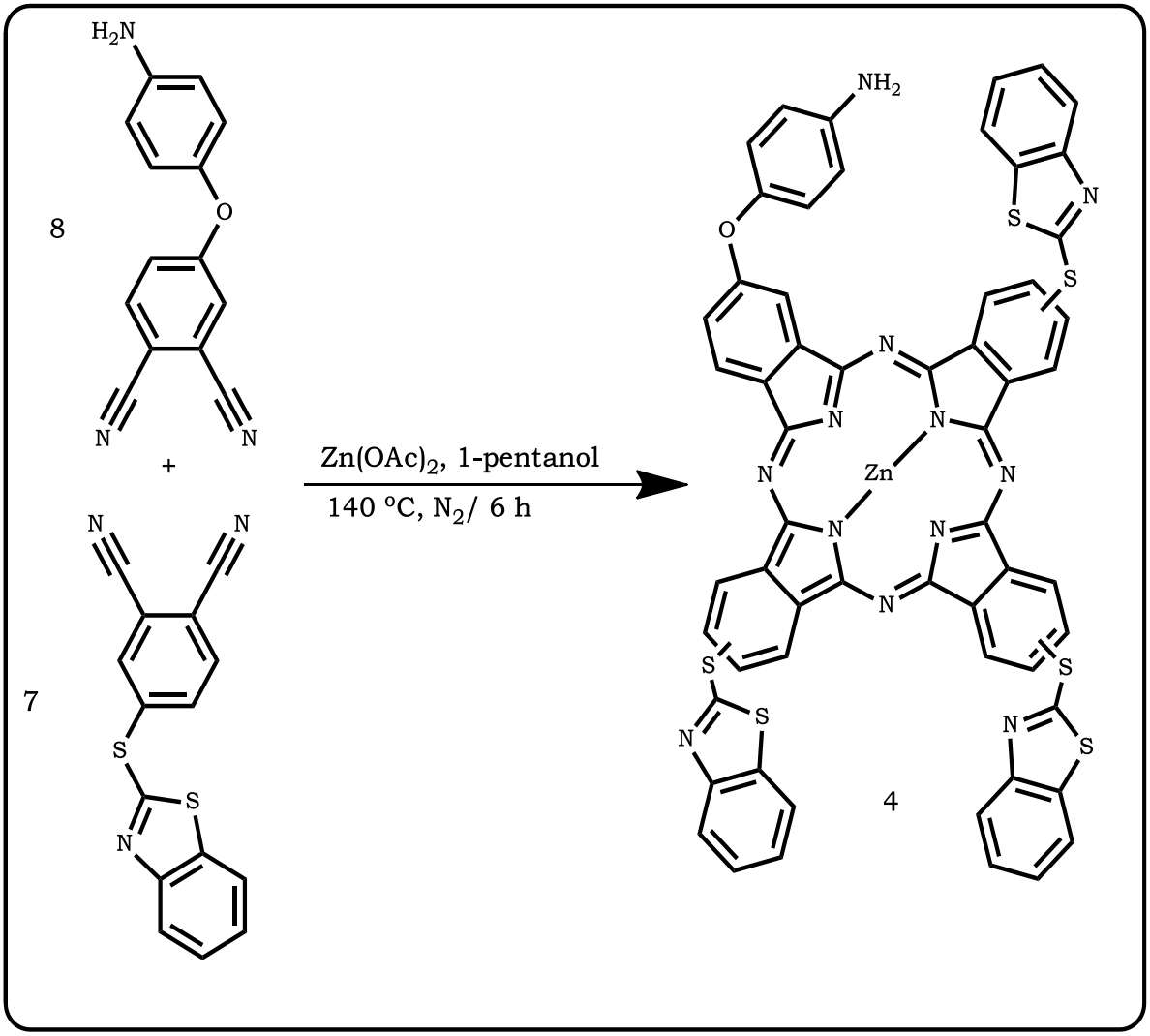

***Scheme 3.1**: Synthetic pathway for Zn(II) mono aminophenoxytris(benzothiazol-2-ylthio) phthalocyanine (**4**).*

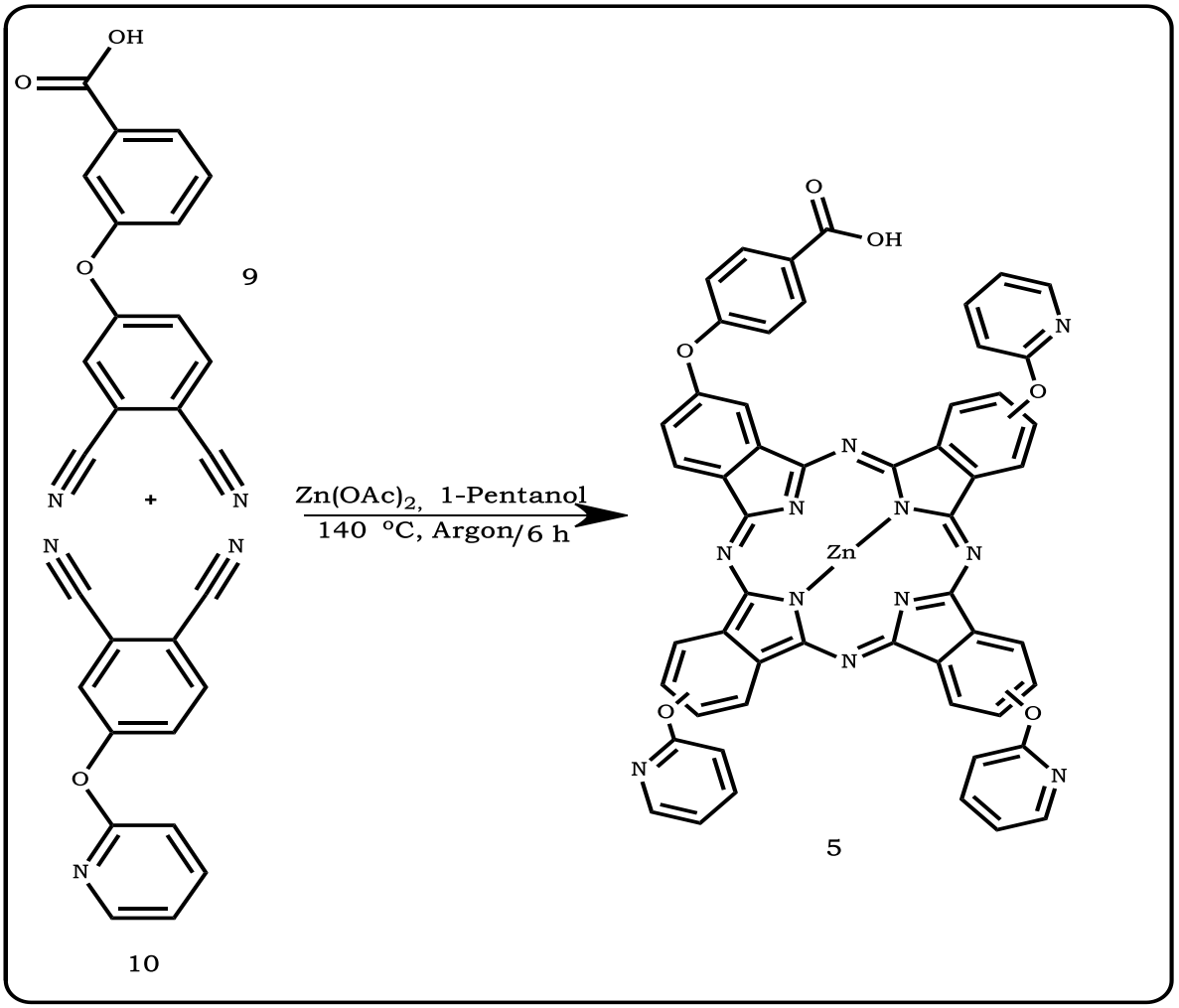

***Scheme 3.2**: Synthetic route for Zn(II) mono 3-carboxyphenoxy tris(pyridin-2-yloxy) phthalocyanine (**5**).*

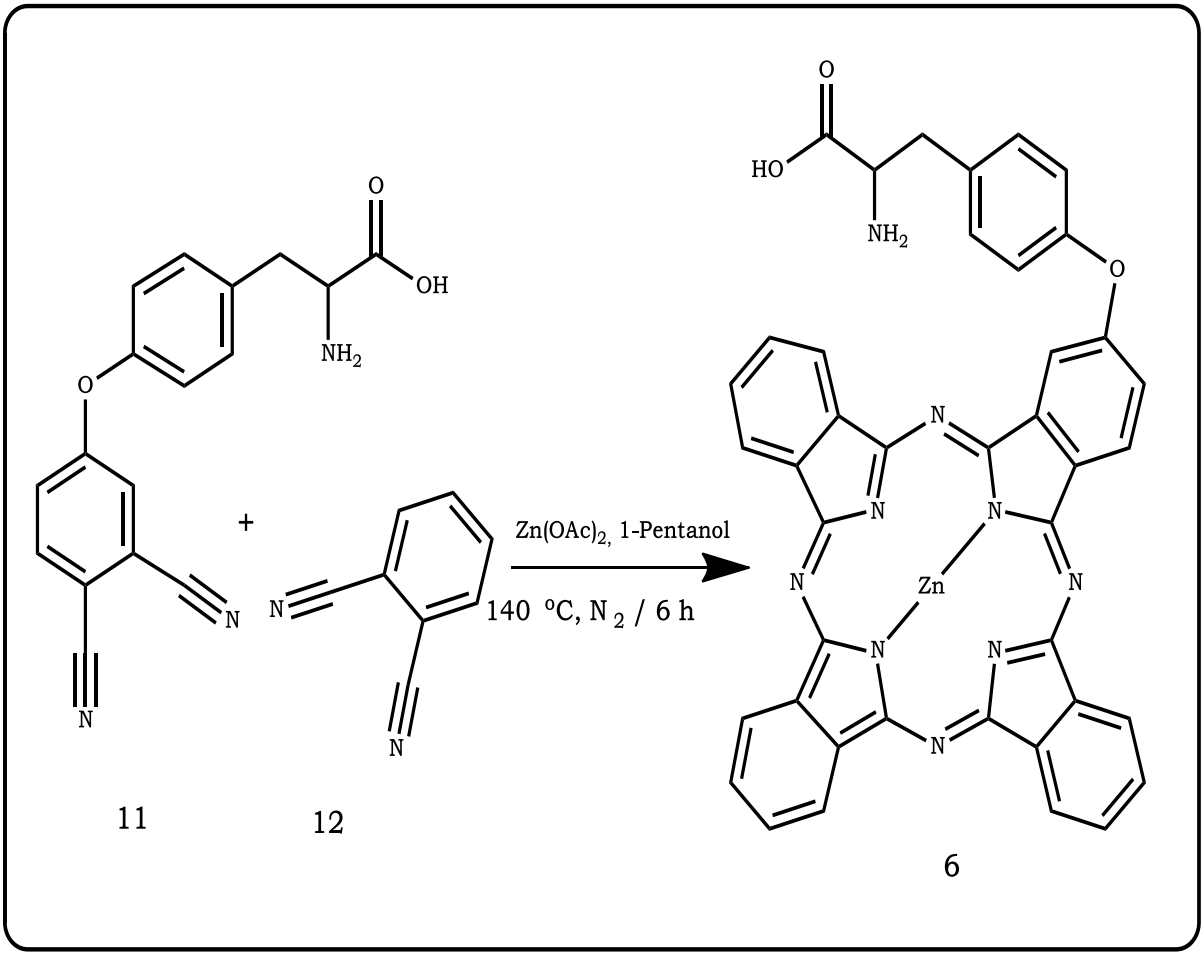

Scheme 3.3 *Synthetic pathway for Zn(II) mono amino-carboxyethylphenoxy phthalocyanine (**6**)*

3.1.2 Covalent linkage of Complexes 1-6 with SQDs

SQD2/ZnO semiconductor quantum dots are new, hence discussed here. **Scheme 3.4** shows the synthesis of SQD2/ZnO, prepared from SQD2 using Zn acetate. All SQDs have CdTe as core. When ZnSe is used as the first shell, SQDs denoted as SQD1, and when ZnS is used as the first shell denoted as SQD2. Core/shell SQDs are then coated with ZnO as second shell and these are denoted with ZnO.

Dicyclohexylcarbodiimide (DCC) was used to activate carboxylic acid functional groups of the complexes **1-3** and **5**, **6** for coupling with GSH functionalized SQDs (**Scheme 3.5**) using **5** as an example) while **4** is conjugated to SQDs through activation of the carboxylic acid of the GSH functionalized SQDs **(Scheme 3.6).**

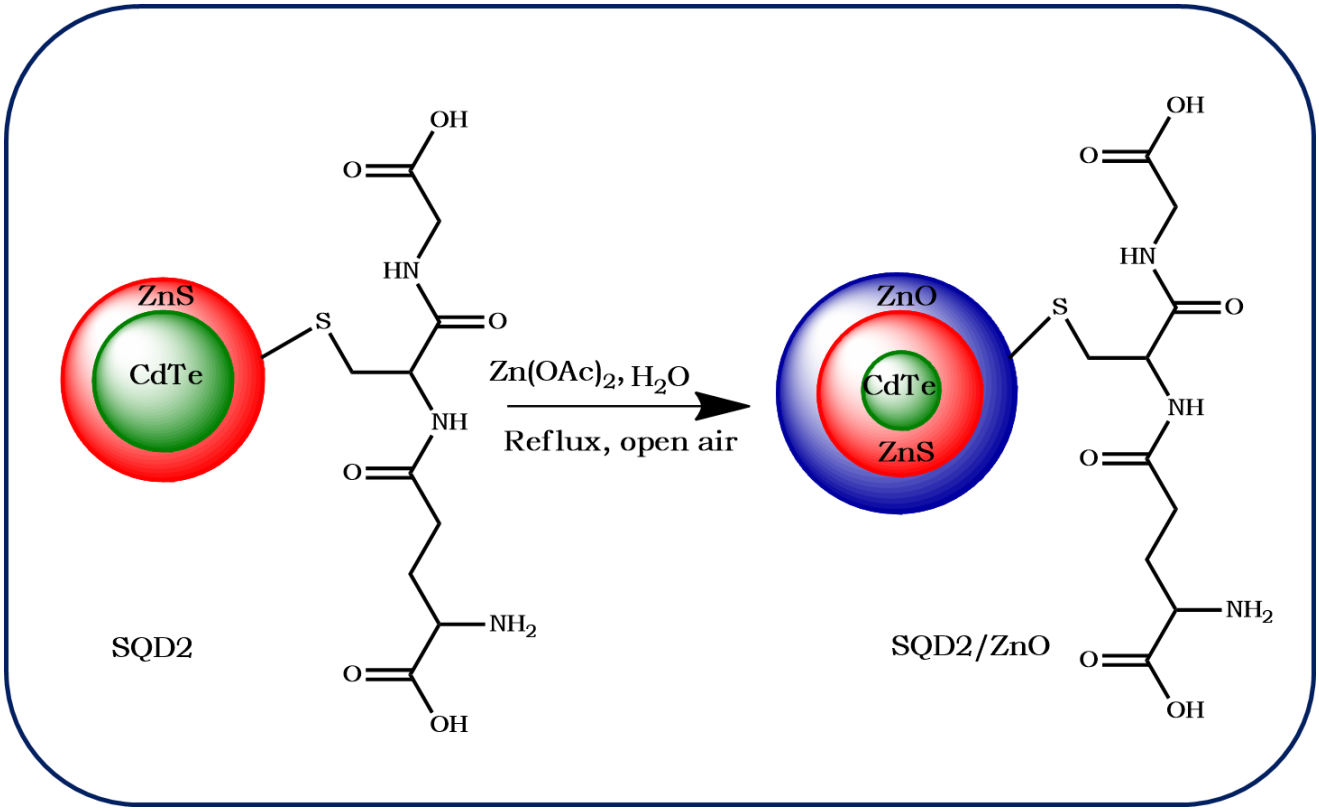

Scheme 3.4 *: Synthetic pathway for glutathione capped CdTe/ZnS/ZnO (SQD2/ZnO)*

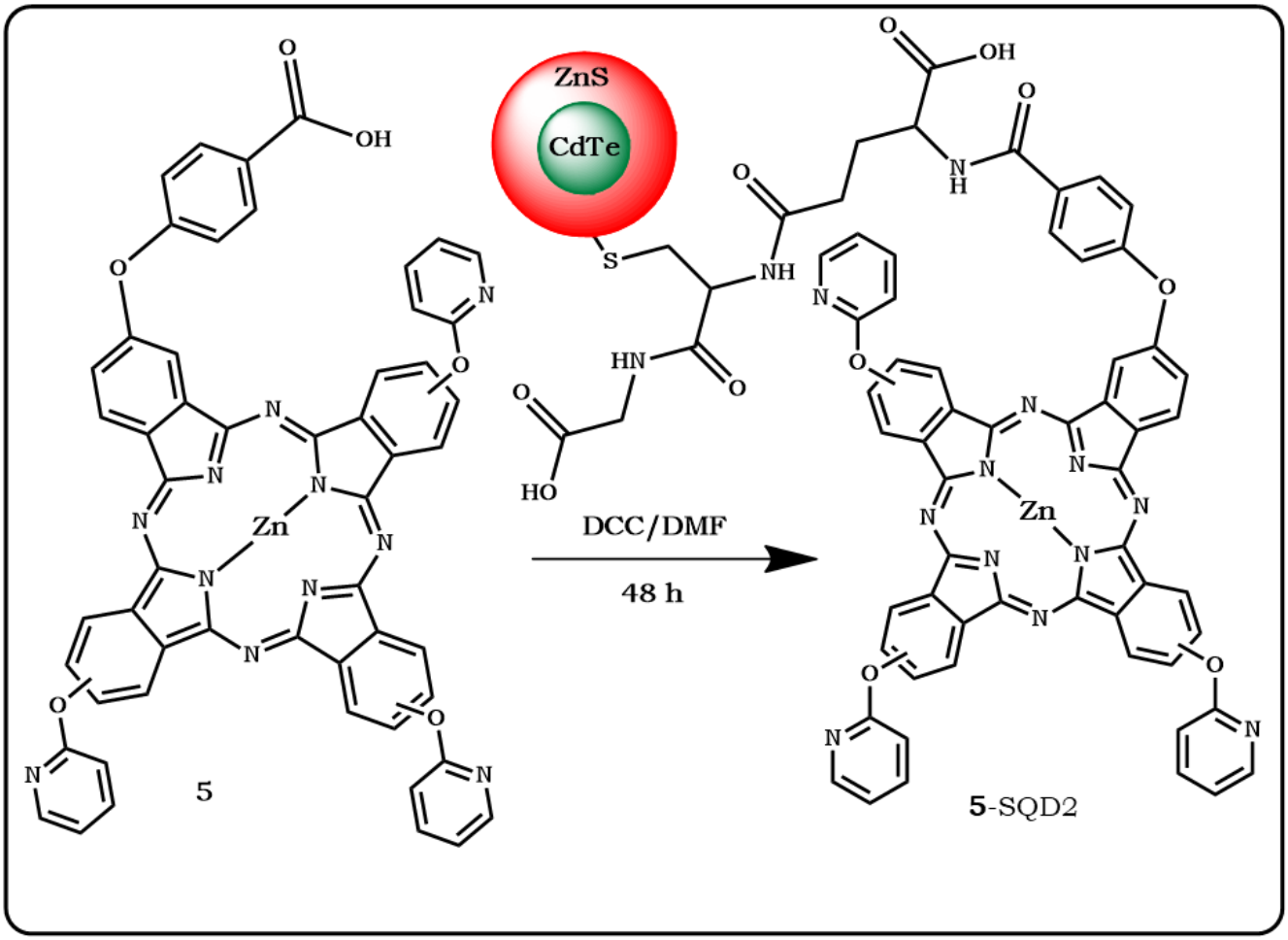

Scheme 3.5 *: Scheme for covalent coupling of* ***5*** *to SQD2 as an example.*

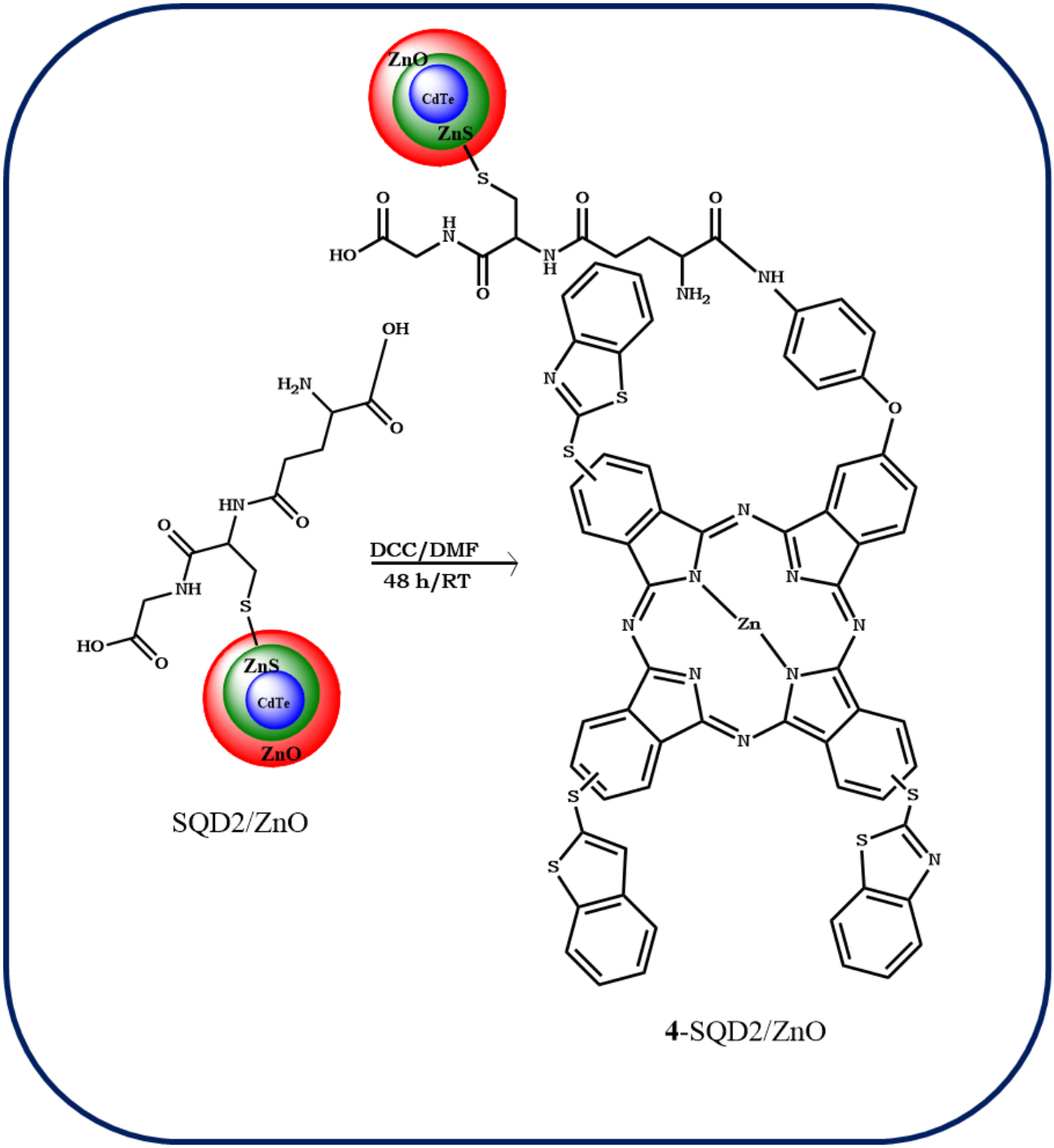

***Scheme 3.6**: Scheme for covalent coupling of **4** to SQD2/ZnO as an example.*

3.2 UV-visible absorption spectra

Fig 3.1(A) shows the ground state electronic absorption spectra of all the Pc complexes in dimethyl sulfoxide (DMSO). Complexes **1**-**3** exhibit narrow symmetrical Q bands, typical of monomeric Pc **Fig. 3.1 (A) [47]**. Complexes **4**-**6** show broadening in the vibrational band, typical of aggregation **[47]**. Aggregation in Pcs is evidenced by broadening or splitting of the Q-band with the low energy band being due to monomer and the high energy band due to aggregation. **Table 3.1** shows red shifted Q – band absorption for complex **4** due to the presence of electron donating sulphur groups in its molecular structure which is known to account for bathochromic shift of Q-band **[115]**. The SQDs show their broad absorption at ~460 nm and 550 nm for SQD2 and SQD2/ZnO, respectively as examples (**Fig. 3.1(B)**). The red shifted behaviour of SQD2/ZnO in comparison to SQD2 is typical of core/shell/shell SQDs compared to core/shell due to increase in size **[91]**.

Fig 3.1(C) shows the spectra of the conjugates (using and **2, 6**, **2**-SQD1 and **6**-SQD2/ZnO as examples). There are no significant shifts in the Q bands of complexes **1** to **6** following conjugation to SQDs, **Table 3.1**. The slight increase in the absorption below 600 nm is due to the absorption by SQDs, **Fig 3.1(C)**. There is no effect of core/shell or core/shell/shell on the spectra of Pc.

The loading of complexes **1**-**6** onto the SQDs is investigated following methods described in the literature **[116]**. This involves dissolving the same mass of the Pc alone and the conjugate in an equal volume of

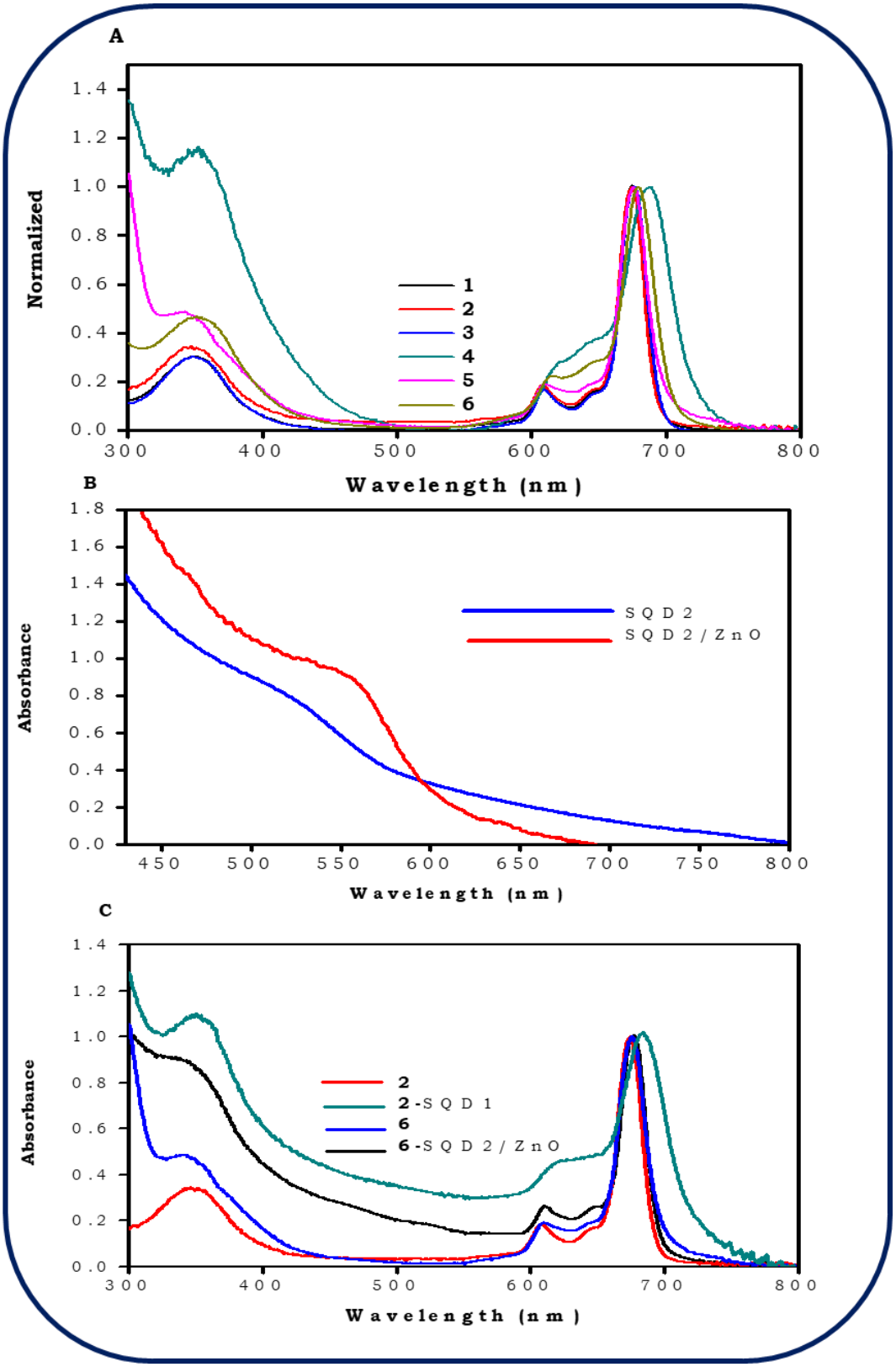

Fig. 3.1 *Electronic absorption, for complexes* ***1****-****6*** *(A), SQD2 and SQD2/ZnO (B) and complexes* ***2*** *and* ***6*** *alone and when conjugated to SQDs (using SQD1 and SQD2/ZnO as examples) (C).*

solvent and comparing the Q-band absorbance intensity of the Pc in the conjugate with that of the initial Pc before the conjugation. There is no significant difference (except for **2**-SQD) in loading between core/shell/shell and core/shell for SQD1 (ZnSe 1st shell). But for SQD2 (ZnS 1st shell) the core/shell/shell (SQD2/ZnO) have larger loading than core/shell. Thus larger loading is observed for large SQDs (to be discussed bellow).

3.3 FT-IR spectra

FT-IR technique was used to analyse functional groups of complexes, SQDs, and conjugates (complexes **3** and **5** as examples). Broad OH stretching appeared at 2971 cm^{-1} for **3** and 3060 cm^{-1} for **5** as a result of carboxylic acid, **Fig. 3.2**. The intense vibrational peak at 1200 cm^{-1} is attributed to the Ar–O–Ar for **3** and **5**.

Broad vibrational stretching at 3504 cm^{-1} is observed for SQDs, indicating the presence of NH_2 as a result of GSH used as bifunctional capping ligand, **Fig. 3.2** using SQD1 and SQD2 as examples. NH_2 vibrational stretching in SQDs disappear in the conjugates, indicating the successful formation of the amide bond between the SQDs and the Pc complexes. The shift of the carbonyl in **3** from 1710 cm^{-1} to 1648 cm^{-1} could indicate successful formation of the amide bond; **Fig**. **3.2(A)**. Similarly, for **5**, carbonyl peak which appears at 1718 cm^{-1} shifts to 1680 cm^{-1} after conjugation, forming the amide bond, **Fig**. **3**.**2(B)**.

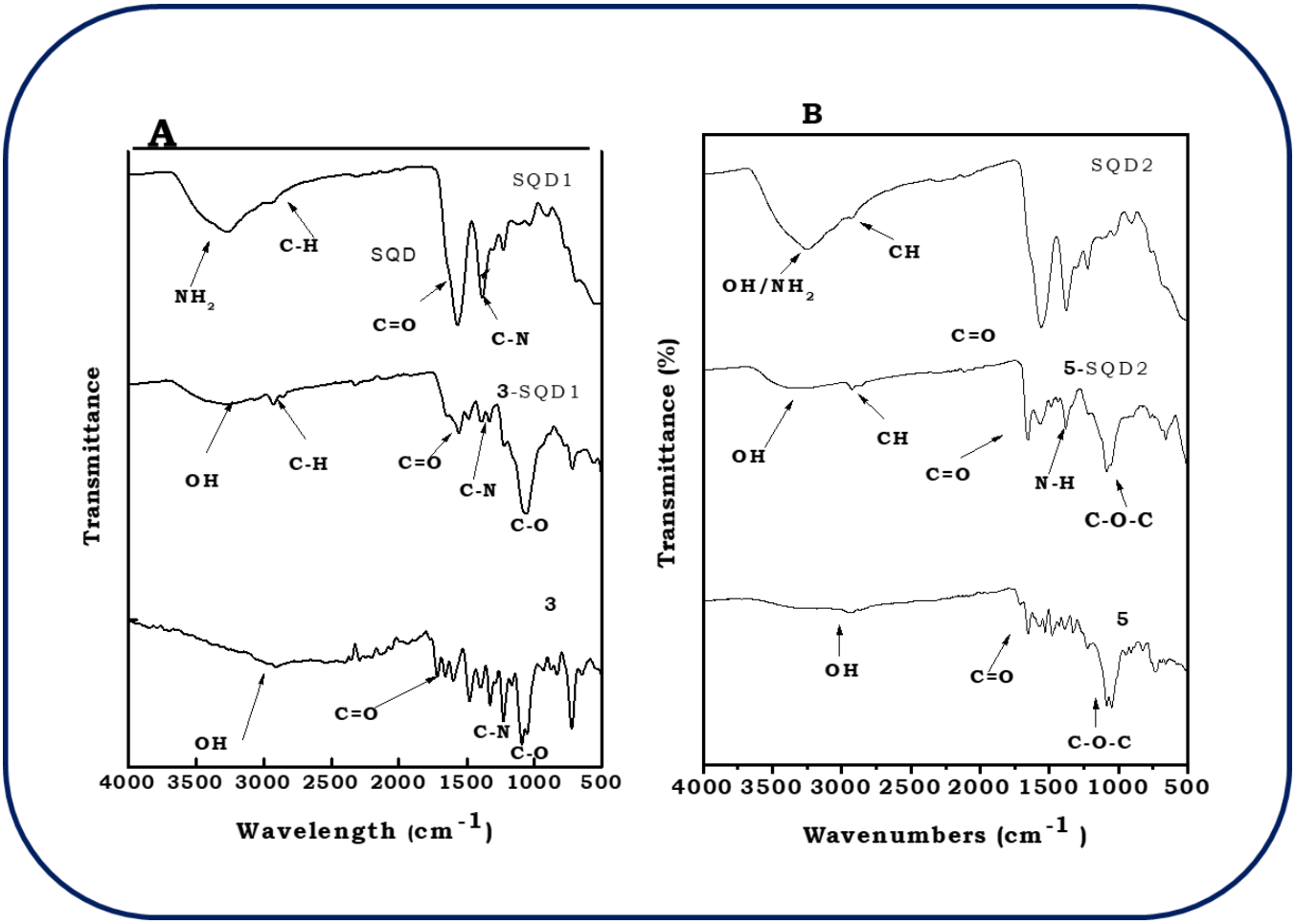

Fig. 3.2 *FT-IR spectra of SQD1,* ***3****-SQD1 and* ***3*** *(A) and SQD2,* ***5****-SQD2 and* ***5*** *alone (B) .*

3.4 XRD Patterns

The XRD patterns of Pc complexes (using complex **4** as an example in **Fig. 3.3**) contain a broad peak between 2θ = 17–25° for **4** alone, which is consistent with the amorphous nature of phthalocyanines **[117]**. In addition, there are some sharp peaks for complex **4** alone. Sharp XRD peaks are not unusual in phthalocyanines **[118]**. The 2θ values of the SQDs alone are in accordance with zinc blende crystal and cubic structure with three peak indexing to 111, 220, and 311 at 2θ= 26.3◦, 43.8◦, 51.9◦ (**Fig. 3.3**) which is consistent with the literature **[91]**. The conjugates show weak SQDs peaks.

Debye-Scherrer Equation (3.1) **[119]** was employed to estimate the sizes of the SQDs:

$$d = \frac{\kappa\lambda}{\beta cos\theta}$$

where λ is the wavelength of the X-ray source (1.5405 Å), k is an empirical constant equal to 0.9, β is the full width at half maximum of the diffraction peak and θ is the angular position. The sizes were 9.8 nm, 11.48 nm, 10.3, 13.74 nm for SQD1, SQD1/ZnO, SQD2 and SQD2/ZnO, respectively.

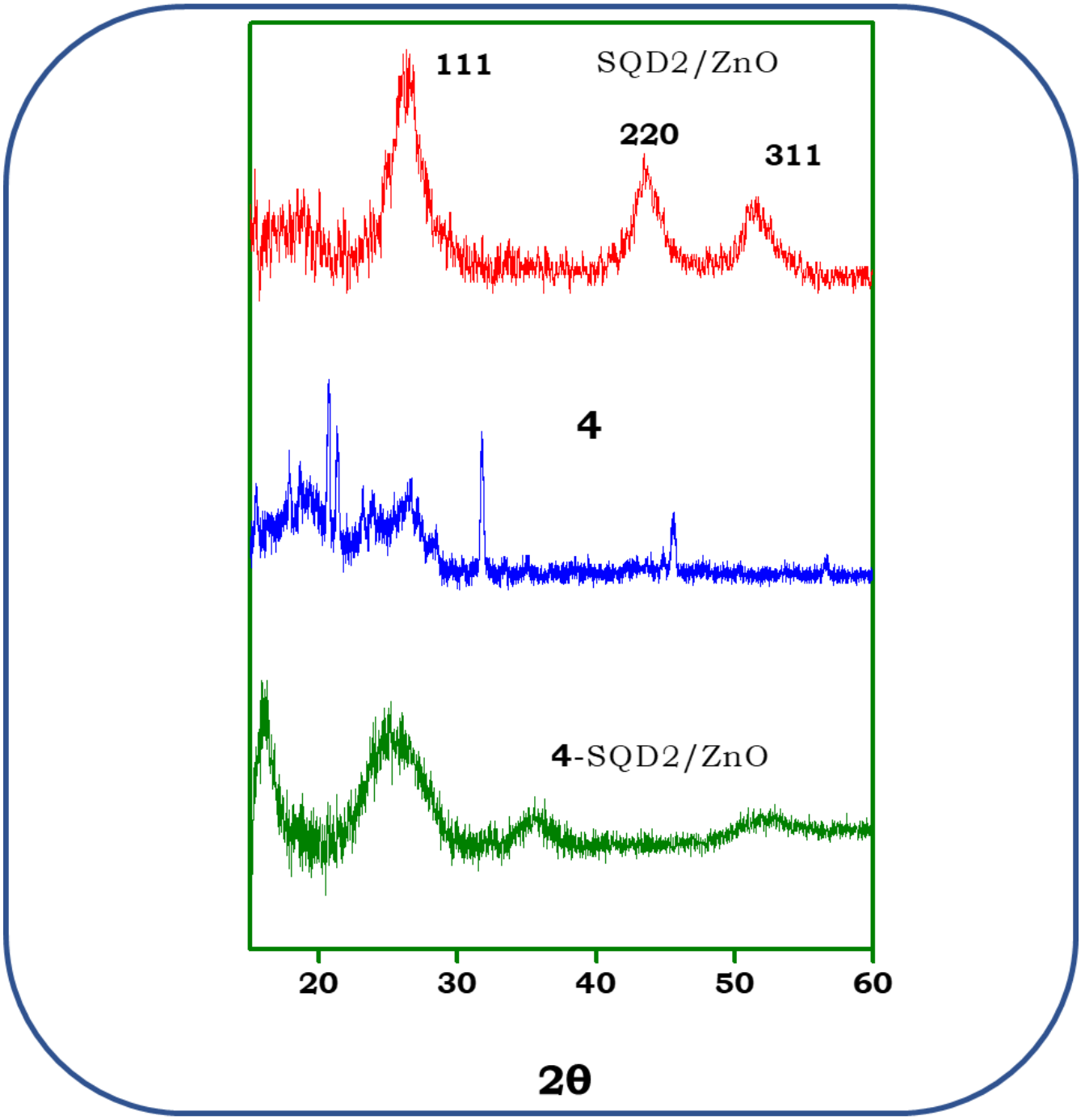

Fig. 3.3*: XRD plot showing diffraction patterns of complex* ***4****, SQD2/ZnO and conjugates.*

3.5 TEM images and EDX

TEM images (**Fig. 3.4**) revealed polydispersed and nanospherical semiconductor quantum dots. Following covalent linkage of the SQDs with Pcs, aggregation was observed which is typical of π–π stacking interaction of the Pc aromatic rings on the adjacent SQDs. Pc are known for π-π stacking **[120]**.

The elemental compositions of the complexes and nanoconjugates were qualitatively determined using an energy dispersive X-ray spectrometer (EDX) as shown in **Fig. 3.5**. The EDX spectra of complex **6** (as an example) showed the presence of C, N, O and Zn, which are the expected elements for Pcs. SQDs alone showed the expected atoms and additional peaks were observed upon conjugation.

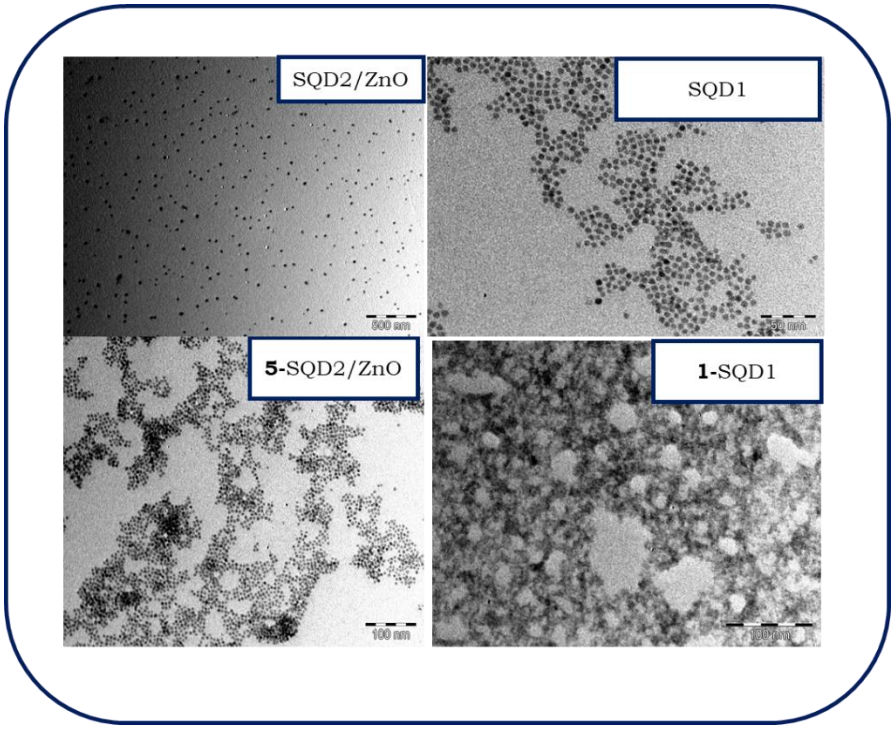

Fig. 3.4 *TEM images of SQD1, SQD2/ZnO and conjugates, using complex* ***1*** *and* ***5*** *as examples.*

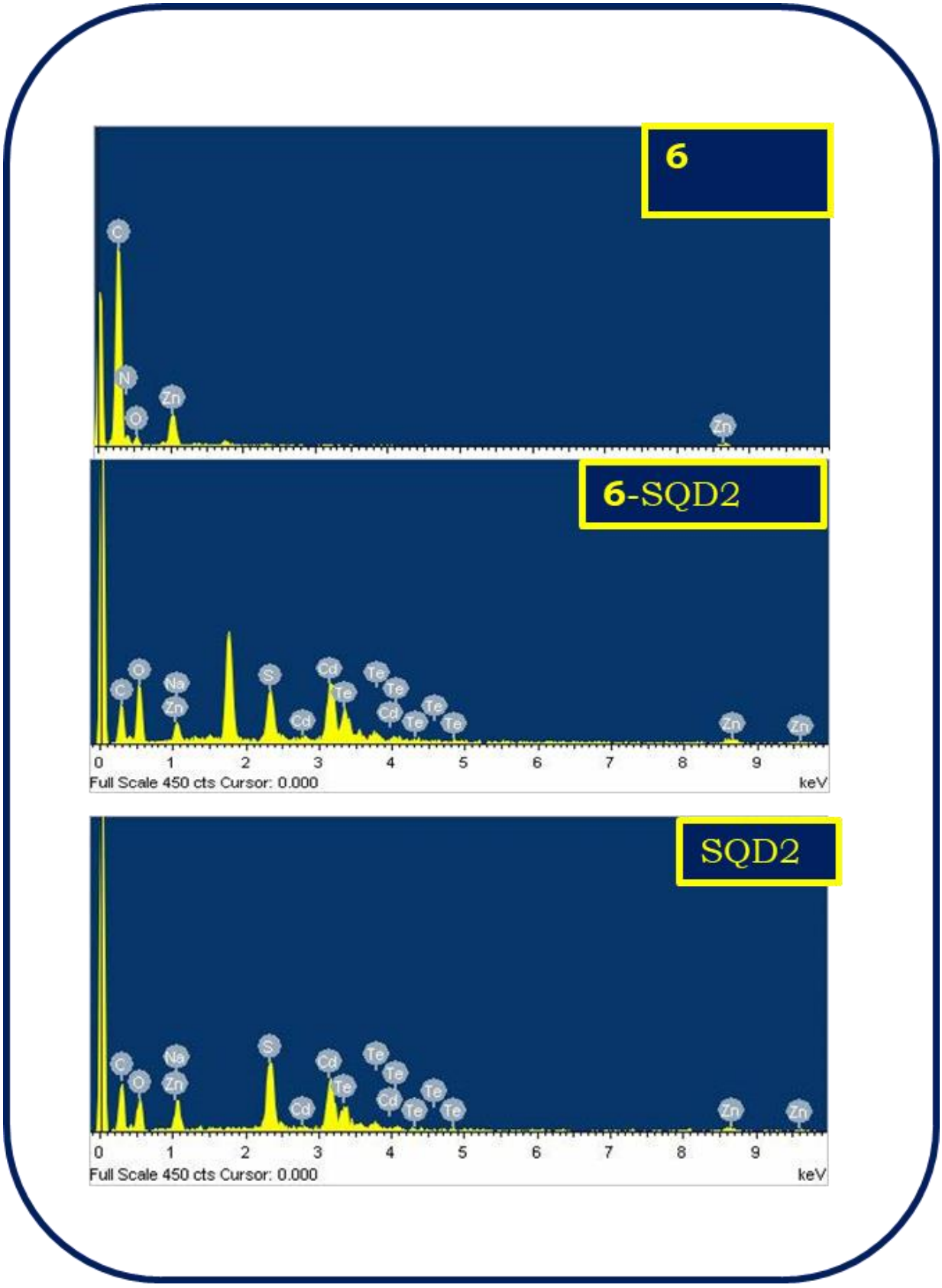

Fig. 3.5 *Representative EDX spectra for SQD2,* ***6****–SQD2 and* ***6*** *alone as examples.*

3.6 Dynamic Light Scattering

Dynamic light scattering (DLS) measurement of SQDs and conjugates were carried out in order to determine their sizes, **Fig. 3.6.** Generally, SQDs have small sizes ranging from 2 to 20 nm as reported in the literature **[121]**. The DLS sizes are 10.10 nm, 11.70 nm, 10.71 nm nm, 14.74 nm for SQD1, SQD1/ZnO, SQD2 and SQD2/ZnO, respectively **(Table 3.1)**. Following Pc conjugation to SQDs, the sizes of the conjugates were larger than the SQDs alone which could be attributed to aggregation, as previously stated, **Table 3.1**. **6-**SQD1 and **6-**SQD2, had the largest DLS size compared to the other samples due to the larger loading, **Table 3.1**. Except for **2**, core/shell-based conjugates had smaller size than core/shell/shell conjugates. This could be related to the high loading for shell than shell/shell and the reverse for **2**.

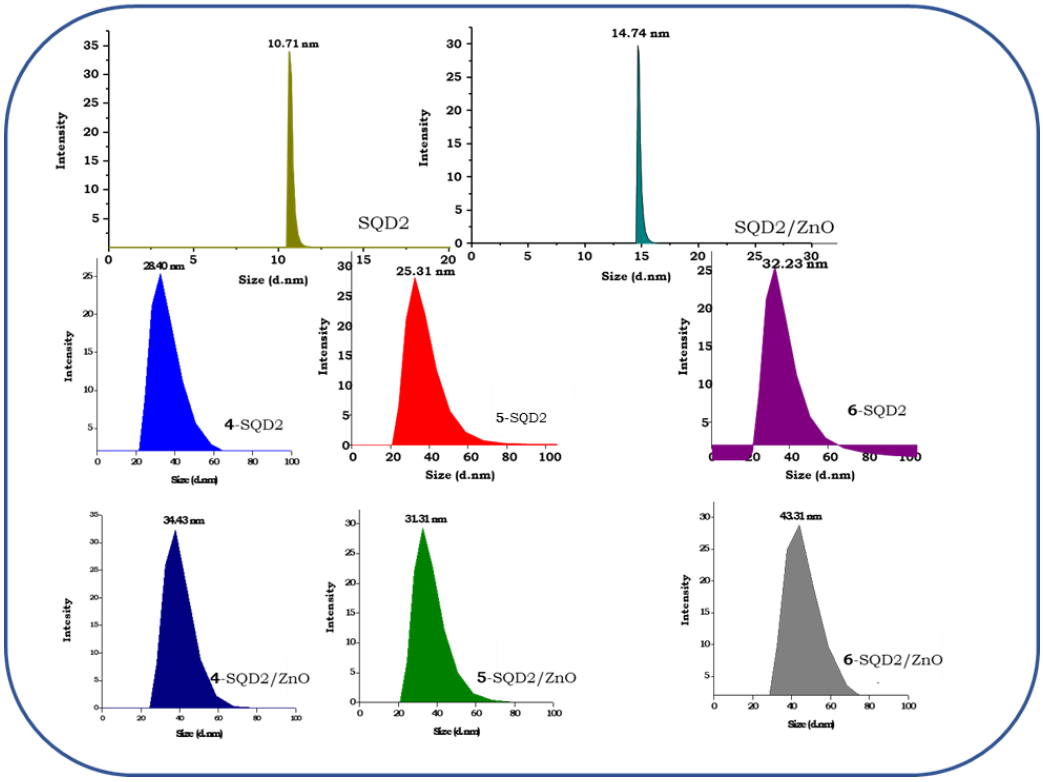

Fig. 3.6 *Dynamic light scattering of the SQDs and nanoconjugates, SQD2 and SQD2/ZnO used as examples.*

Table 3.1: Absorption, loading and DLS sizes of the samples.

Complexes and conjugates	***Abs (nm) in DMSO***	***Loading (μg/mg)***	***DLS size (nm)***
1	677	--	--
1-SQD1	676	6	15.7
1-SQD1/ZnO	676	5	17.0
2	674	--	--
2-SQD1	674	11	32.7
2-SQD1/ZnO	675	8	22.4
3	675	--	--
3-SQD1	676	4	14.0
3-SQD/ZnO	675	3	17.2
4	690	---	
4-SQD2	693	5	28.40
4-SQD2/ZnO	694	14	34.43
5	678	---	--
5-SQD2	680	4	25.31
5-SQD2/ZnO	680	7	31.31
6	677	---	--
6-SQD2	678	8	32.32
6-SQD/ZnO	685	22	43.31
SQD1	479	--	10.10
SQD1/ZnO	563	--	11.70
SQD2	460	--	10.71
SQD2/ZnO	550	--	14.74

Conclusion

The synthesis and characterization of novel Pcs are reported in this work. Successful conjugation of Pcs to glutathione capped quantum dots is confirmed using techniques FT-IR, EDX, XRD, DLS, TEM and UV-vis spectra.

Chapter 4: Photophysical properties

4.1 Photophysical properties

Photophysical studies of complexes **1-6** and their conjugates were evaluated in dimethyl sulfoxide. Firstly, it is presumed that triplet quantum yield of the complexes will be enhanced due to the lack of symmetry of the molecules arising from their increased molecular dipole moments **[48,49]**. Additionally, the complexes are designed with functionalities that can foster covalent linkage to semiconductor quantum dots (SQDs). The presence of SQDs in the conjugates is expected to deactivate the fluorescence behaviour of the complexes and improve triplet quantum yields due to the external heavy atom effect resulting from the heavy atoms in the SQDs components. The essential aim of having the SQDs in the conjugates is to increase triplet state quantum yield of Pcs, thus improving their NLO response.

4.1.1 Fluorescence Quantum yield (Φ_F) and lifetime.

The fluorescence quantum yield of the complexes and the SQDs were determined when alone (Equation 1.1) and SQDs in the composites (Equation 1.2), using unsubstituted ZnPc as standard in DMSO (Φ_F = 0.2 **[57]** for Pcs. When exciting where SQDs absorb, quinine sulphate in H_2SO_4 (Φ_F = 0.52) **[59]** was used as the standard (discussed in Chapter 1).

The Φ_F values for the Pc complexes alone range from 0.09 to 0.20 with **1** and **3** showing the highest (0.20) and **4** the least (0.09), **Table 4.1**. The low Φ_F value for complex **4** could be related to the fact that amino groups are known to quench the excited state of the phthalocyanines **[122]**. The conjugates afforded decreased Φ_F values implying quenching of the fluorescence of the Pcs by SQDs in the composites as compared to the values obtained for the Pc complexes alone. Lifetimes determined by time correlated single photon

counting (TCSPC), decay in **Fig. 4.1**. Conjugates afforded shortened fluorescence lifetimes compared to Pcs alone corresponding to their low Φ_F values **Table 4.1**. The decrease in Φ_F and lifetime values of the Pcs in the presence of SQDs is adduced to the heavy atom effect of the latter, which promotes rapid intersystem crossing to the excited triplet state of the former.

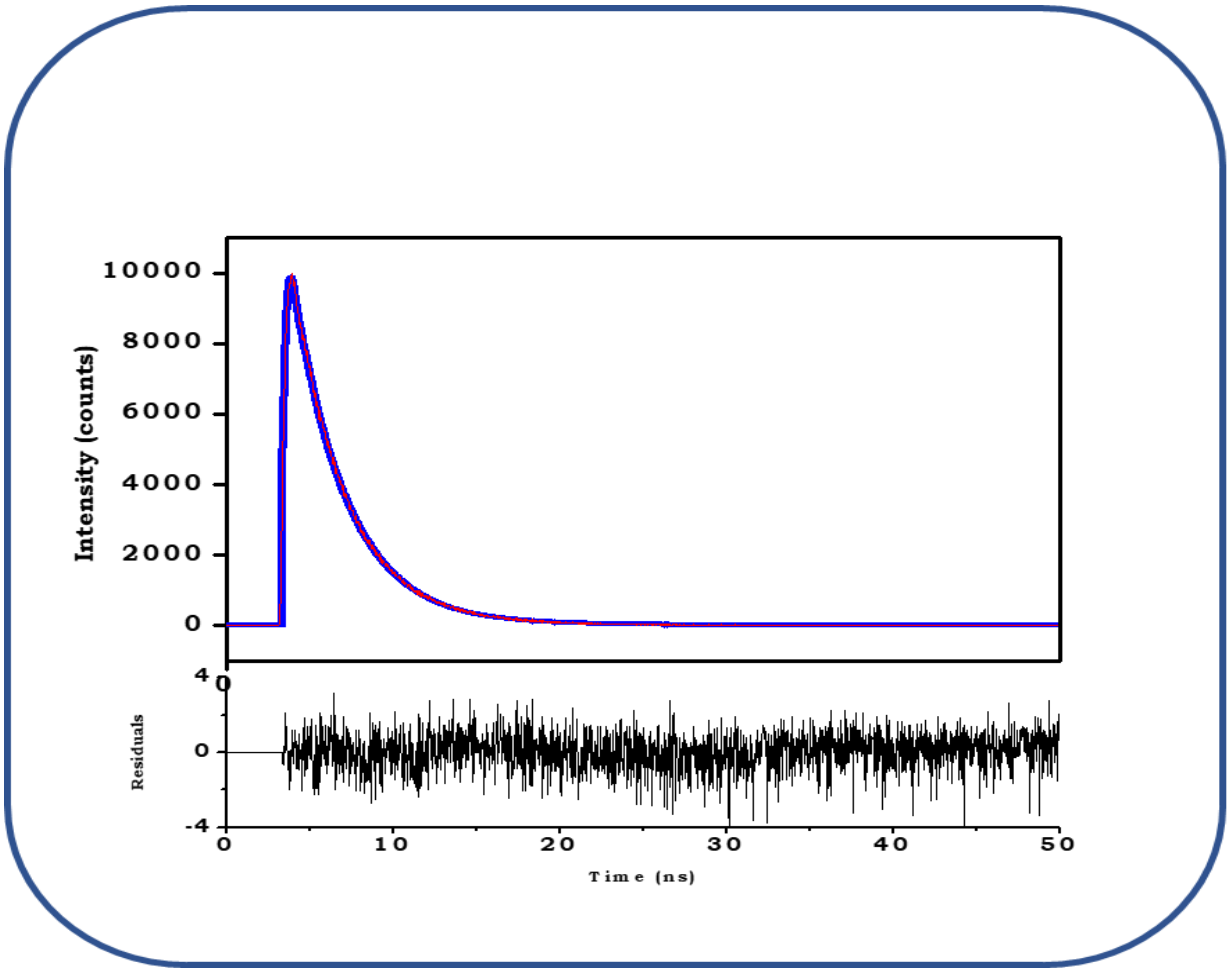

Fig. 4.1: *Fluorescence decay curve for complex* ***2*** *in DMSO with the fitting curve.*

Table 4.1: Photophysical properties of Pc complexes and their conjugates.

Complexes and conjugates	**Φ_F (Pc)[a]**	**τ_F (ns)[a]**	**Φ_T**	**τ_T (μs)**	**FRET eff**
1	0.20	3.21	0.67	231	--
1-SQD1	0.03 (0.02)	2.45 (0.16)	0.71	254	0.92
1-SQD1/ZnO	0.02 (0.04)	2.56 (0.09)	0.78	254	0.94
2	0.16	3.27	0.41	259	--
2-SQD1	0.03 (0.03)	2.65 (0.19)	0.86	281	0.90
2-SQD1/ZnO	0.02 (0.03)	2.16 (0.01)	0.61	275	0.91
3	0.20	3.16	0.48	271	--
3-SQD1	0.02 (0.02)	3.10 (0.27)	0.70	268	0.87
3-SQD1/ZnO	0.03 (0.02)	2.89 (0.02)	0.81	303	0.98
SQD1	(0.69)	(2.03)	--	--	--
SQD1/ZnO	(0.23)	(1.58)	--	--	--
4	0.09	4.55	0.67	203	**--**
4-SQD2	0.05 (0.01)	2.9 (1.07)	0.72	310	0.39
4-SQD2/ZnO	0.08 (0.001)	2.23 (1.08)	0.76	234	0.49
5	0.14	3.09	0.70	232	--
5-SQD2	0.07 (0.04)	2.81 (1.09)	0.86	319	0.30
5-SQD2/ZnO	0.02 (0.03)	2.73 (0.85)	0.87	220	0.60
6	0.12	2.86	0.69	208	--
6-SQD2	0.07 (0.03)	2.54 (0.52)	0.72	301	0.66

6-SQD2/ZnO	0.06 (0.04)	2.25 (0.47)	0.72	230	0.78
SQD2	(0.45)	(1.55)	--	--	--
SQD2/ZnO	(0.39)	(2.12)	--	--	--

[a]**values in brackets obtained when exciting where QDs absorb**

4.1.2 Förster resonance energy transfer (FRET)

Fig. 4.2 shows the mechanism of FRET, it involves energy transfer from SQDs (donor) to a MPc (acceptor). The energy transfer usually appears with decrease in the fluorescence emission intensity of the SQDs and the appearance of an induced fluorescence emission for MPcs.

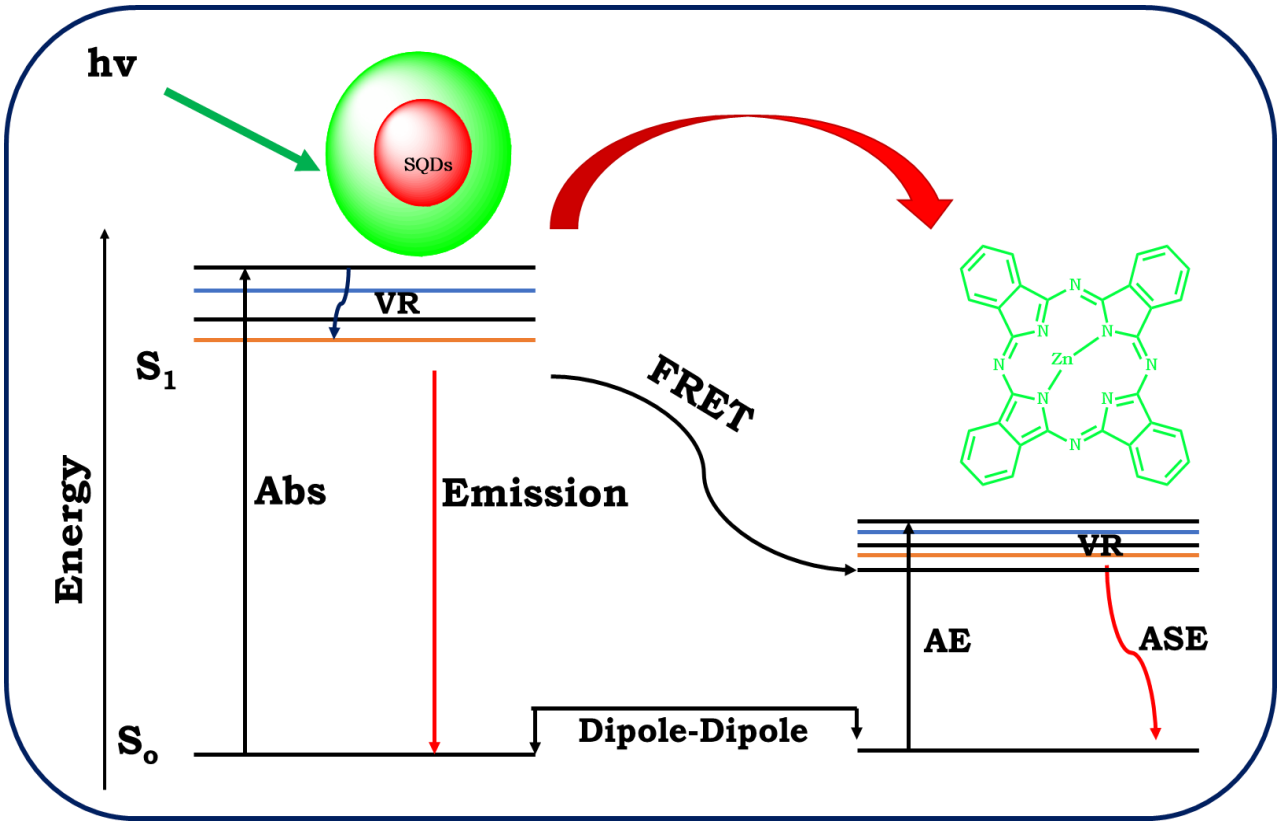

Fig. 4.2: *Energy transfer from SQDs to MPc (M = Zn).* ***Abs*** *= Absorption,* ***AE*** *= non-radiactive acceptor excitation,* ***ASE*** *= acceptor stimulated emission,* ***VR*** *= vibrational relaxation.*

When exiting where SQDs absorb, the observed decrease in Φ_F and lifetime values could be due to FRET and other processes which deactivate the excited states of the SQDs. For FRET to occur, there must be a spectral overlap between the emission spectra of the donor (in this case, SQDs) and the absorbance spectrum of the acceptor (Pc complexes), **Fig. 4.3** (complexes **1** and **6** used as examples). When the conjugates are excited at the wavelengths where the SQDs absorb and Pcs do not, decreased emission intensity of the SQDs is observed with enhancement of an emission peak of the Pcs, **Fig. 4.4**.

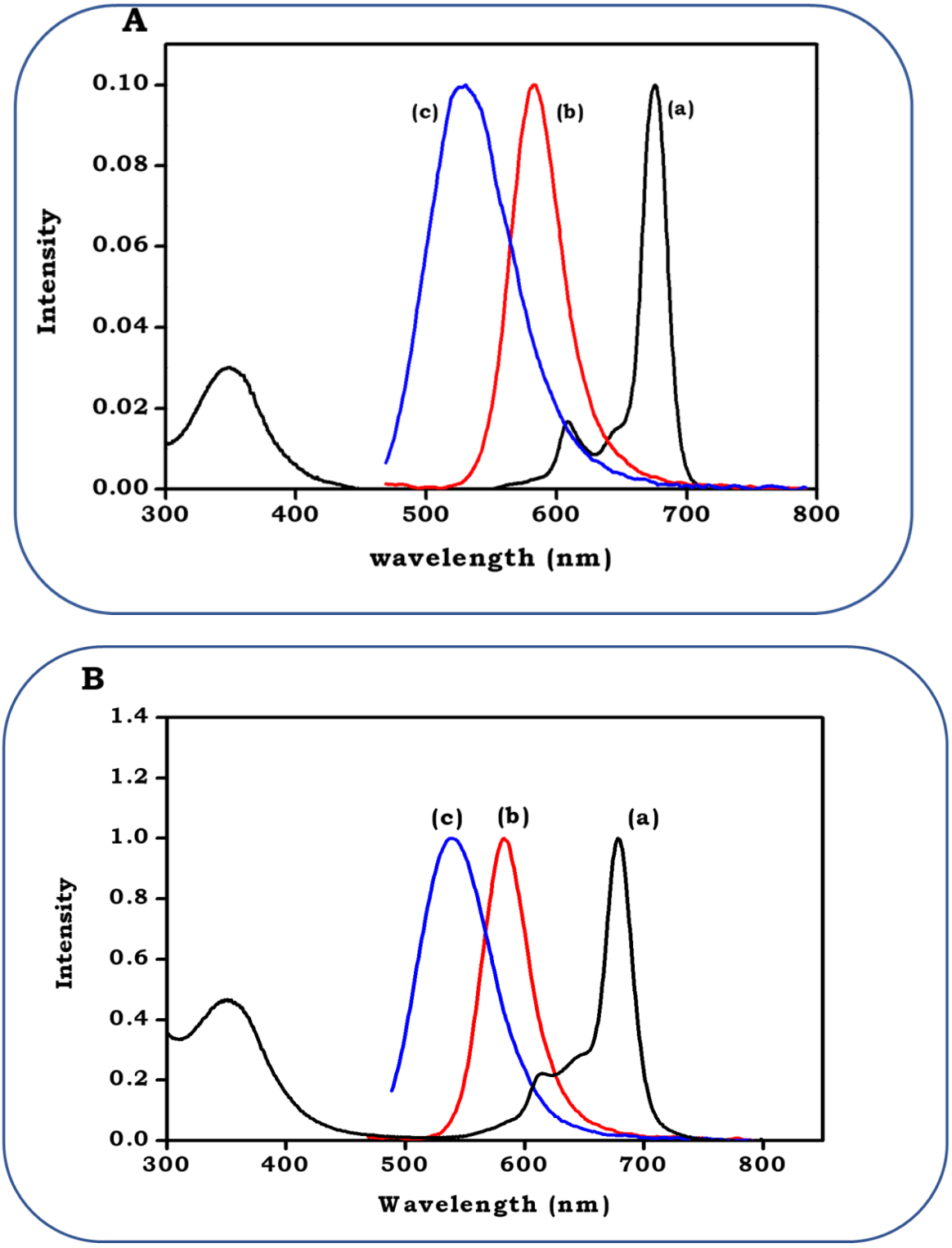

Fig. 4.3 (A) *(a) Absorption spectrum of* ***1*** *(a) overlaid with emission spectra of SQD1/ZnO (b) and SQD1 (c).* ***(B)*** *absorption spectrum of* ***6*** *(a) overlaid with emission spectra of SQD2/ZnO (b),* and *SQD2* (c).

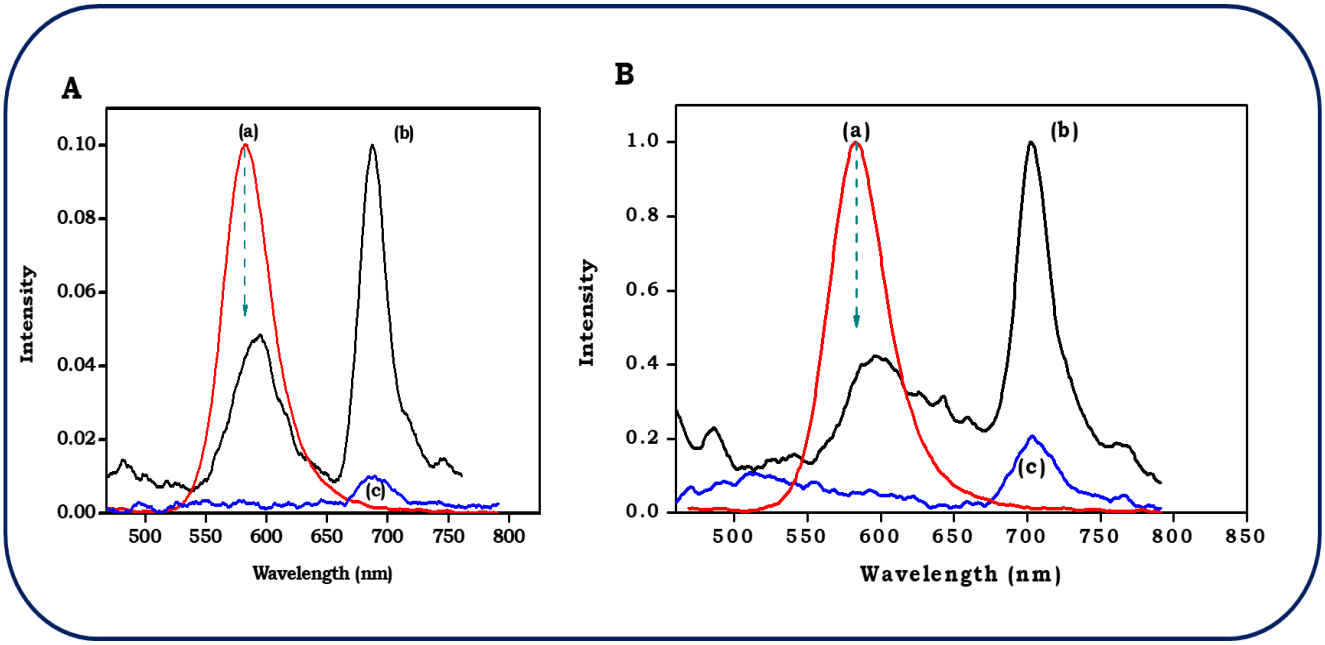

Fig. 4.4 (A) *Emission spectrum of SQD1/ZnO alone (a),* ***2****-SQD1/ZnO (b) and complex* ***2*** *alone (c).* ***(B)*** *Emission spectrum of SQD2 alone (a)* ***4****-SQD2 (b), and* ***4*** *alone (c) excitation wavelength = 430 nm.*

This phenomenon is adduced to intramolecular FRET, which is known to be responsible for the deactivation or quenching of the emission of SQDs leading to transfer of energy to the acceptor molecule (in this case, Pcs). Additionally, other factors like temperature could have contributed to the quenching of the SQDs emission besides the Pcs **[65,67]**. FRET efficiency (*Eff*) values are obtained using equation 1.3 (discussed in Chapter 1).

The FRET efficiency values of conjugates of Pcs and SQD1/ZnO and SQD1 were larger than those of Pcs and SQD2 and SQD2/ZnO, **Table 4.1**. This phenomenon is attributed to the closer emission spectral overlap of SQD1 (540 nm) and SQD1/ZnO (582 nm) with the Pcs absorption spectra as

compared to SQD2 (530 nm) and SQD2/ZnO (578 nm) due to red shifted signal of the former, **Fig. 4.3**.

4.1.3 Triplet Quantum yield and life time

Triplet quantum yields (Φ_T) are determined using comparative methods, equations discussed in chapter 1 (1.4-1.6) **[67-72]**

Fig. 4.5 shows the triplet decay curve for complex **6** as an example. The triplet decay curve obeys second order kinetics, which is typical of MPc complexes at high concentration used for triplet state studies **[123]**. The triplet quantum yield values of the Pc complexes (**1**, **4**-**6**) alone range from 0.67 to 0.70 with complex **5** showing the highest Φ_T values (0.70) and complex **1** and **4** accounted for the least Φ_T (0.67). It has been reported that alkyl substituents increase triplet state population **[124]**, hence the larger Φ_T value for complexes **1** and **6** compared to **2** and **3** could be due to the alkyl group separating the phenoxy ring from the COOH group, without the oxygen in the linker as is the case with complex **3**. The high triplet quantum yield of complexes **4** and **5** is due to extensive π-electron system and electron donating heteroatoms (nitrogen and sulfur), which prevent radiative deactivation of the singlet excited state.

In the presence of the semiconductor quantum dots, increase in the Φ_T values of the Pc complexes is attributed to the spin orbit coupling. As previously mentioned, heavy atoms are known to encourage high population of the excited triplet state by deactivation of the excited singlet state which favours

rapid intersystem crossing. The triplet quantum yields of the Pcs (**1** to **6**) increase in the presence of SQD1 and SQD2 due to the heavy atom effect. For SQD1, there is a larger increase in Φ_T value for **2**-SQD1 (0.86) as compared to **2**-SQD1/ZnO (0.61) most likely due to the larger loading in the former. The Φ_T values are larger for SQD1/ZnO compared to SQD1 containing conjugates except for **2**. This trend is in agreement with DLS sizes where the SQD1/ZnO containing conjugates were larger than the SQD1 conjugates for complexes **1** and **3** and not for **2**, suggesting that the size of the nanoconjugate affects its triplet state parameters.

There is no difference in the Φ_T values of **6**–SQD2 compared to **6**–SQD2/ZnO. The same applies to **5**–SQD2 compared to **5**–SQD2/ZnO and only a slight increase for **4**–SQD2 compared to **4**–SQD2/ZnO. Thus, there is no effect of the extra shell on the triplet quantum yield values for **5** and **6** conjugates containing ZnS. Increase in the Φ_T values is expected to result in the shortening of the triplet lifetime **[125]**. However, this is not always the case, in this study, increase in Φ_T values also afforded lengthening of the triplet lifetimes in most cases, due to the possible protection of the Pcs by the SQDs.

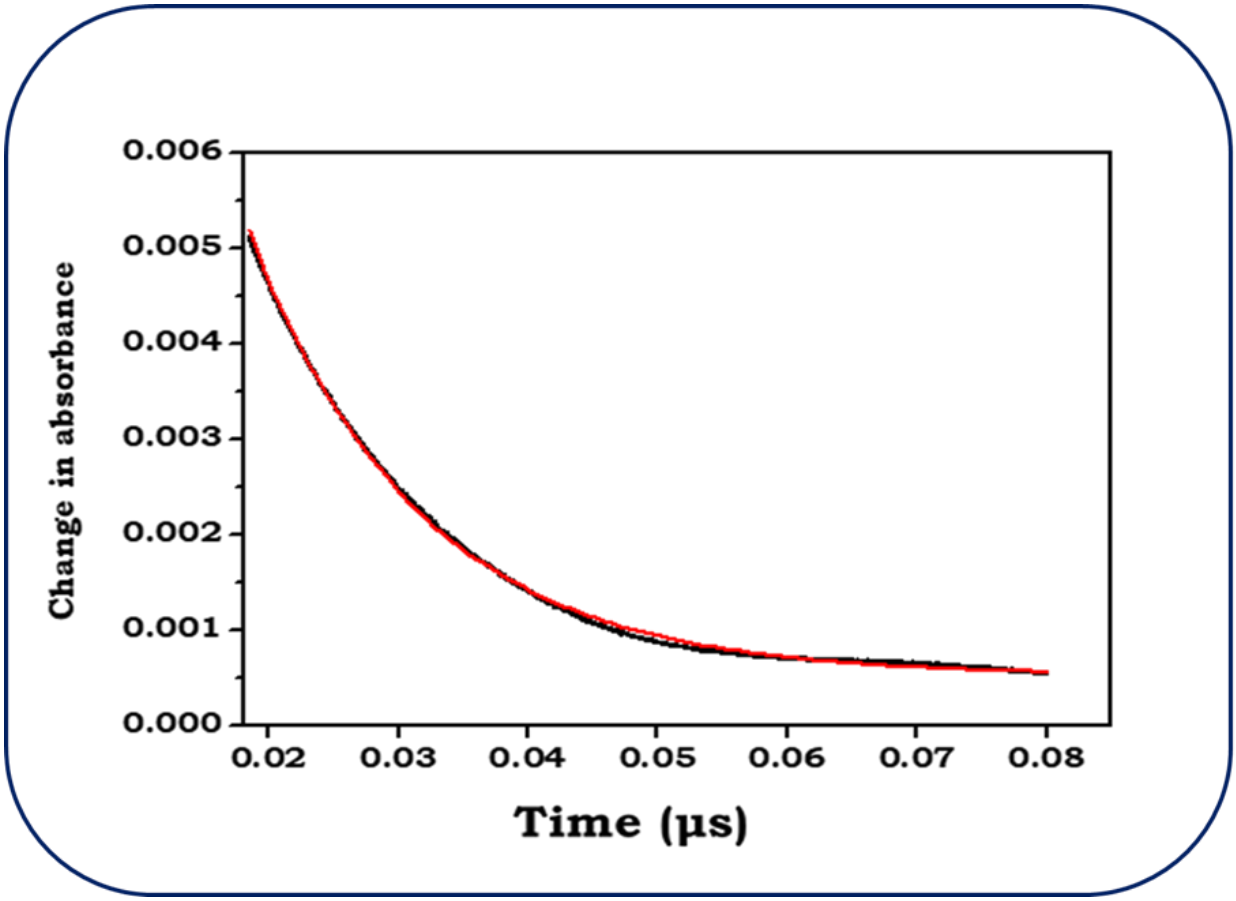

Fig. 4.5 *Triplet absorption decay curve for complex* ***6*** *in DMSO with the fitting curve.*

Conclusions

Photophysical properties of complexes alone and when conjugated to SQDs were studied. Increase in triplet quantum yield of complexes agree with decrease in fluorescence quantum yield. The triplet quantum yields of the Pcs increased in the presence of SQDs and decrease in fluorescence quantum yield was observed.

FRET efficiency was found to be higher for core/shell/shell than core/shell.

Chapter 5 : Nonlinear optical properties

Chapter 5 Nonlinear optical properties

5.1 Nonlinear optical parameters

Z-scan measures transmittance through sample as a function of incident laser intensity. Third order nonlinear susceptibility ($I_m[\chi^{(3)}]$), nonlinear absorption coefficient (β_{eff}), limiting threshold (I_{lim}), ratio of excited state to ground state absorption (k) of phthalocyanines alone and when linked to SQDs were obtained using the open aperture Z-scan technique. The β_{eff} values give an estimate of the degree of nonlinear absorptivity which depends on the population of molecules in the triplet state upon excitation and is evaluated in cm/GW using equations 1.7 and 1.8 (discussed in Chapter 1). Third order nonlinear susceptibility measures the degree of polarizability and fast response time of the molecule when light is applied on it and is measured in esu using equation 1.9 (discussed in Chapter 1). The absorption cross-section ratio (k) are obtained from using equations 1.10-1.12 (also discussed in Chapter 1). Limiting threshold (I_{lim}) describes the values input fluence at which the transmittance is reduced by 50% of the linear transmittance values **[126]**.

Complexes **1**-**6** and conjugated are investigated for NLO studies. The complexes exhibited the following important properties: reduced symmetry, extensive π-electron conjugation system and heavy atom effect on the SQDs. These properties are known to enhance NLO response.

5.2 Mechanism of NLO

Fig. 5.1 shows the five-energy model Jablonski diagram to describe the nonlinear optical dynamics in the studied complexes and the nanoconjugates. In this model, a molecule in the ground state is excited to the first excited singlet S_1 (δ_o) followed by transition from S_1 to higher excited singlet state S_n (δ_1). Since the lifetime S_n is very short, rapid relaxation occurs almost immediately from S_n to S_1 (τ_1) followed by intersystem crossing (isc) from S_1 to the first excited triplet T_1. The triplet state population will depend on the intersystem crossing rate and the triplet period. Since the triplet lifetime is longer than the intersystem crossing lifetime, there will be more crossovers through intersystem crossing to populate the triplet state. Subsequent absorption of laser radiation will result in further excitation of molecules from the T_1 state to a higher energy T_n state with excited state absorption cross section, δ_{ex}.

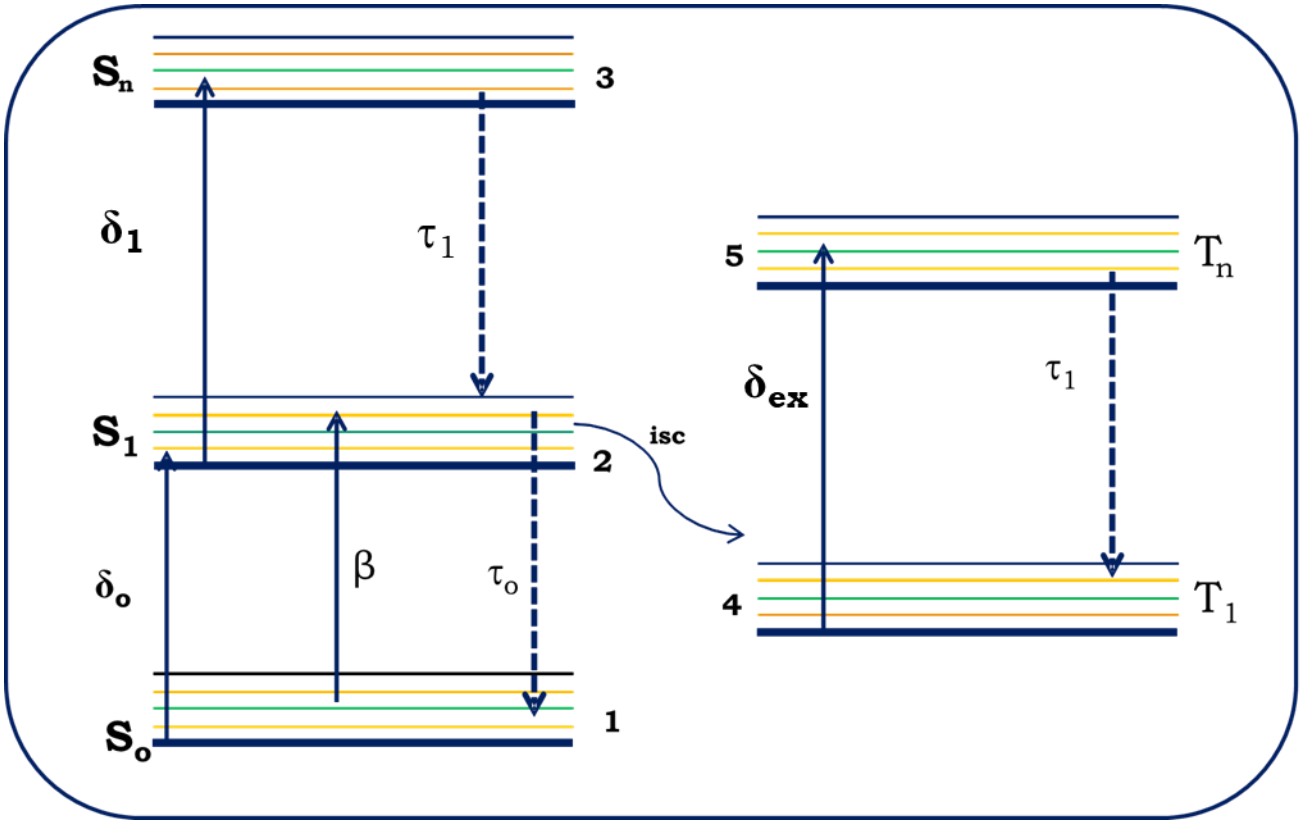

Fig. 5.1: *Five level energy diagrams explaining the dynamics of the excited state absorption in the Pc complexes, isc= intersystem crossing.*

5.3 Nonlinear optical studies of complexes 1-6 alone

NLO response of all the Pc complexes is studied in DMSO at the same absorbance (2 at the Q-band). The effect of substituents of Pcs on nonlinear properties are investigated.

5.3.1 Carboxylic acid Pcs

The effect of carboxylic acid (and no other substituents) on the NLO response of complexes is evaluated using complexes **1**, **2**, **3** and **6**. These complexes contain a single substituent on the peripheral position of the Pc. **Fig 5.2** shows Z-scan profiles of complexes **1, 2, 3** and **6**. Reverse saturable

absorption (RSA) is shown by the decrease in transmittance by more than 50% which is typical of phthalocyanines. For complexes **1-3** there is no significant difference in open aperture Z-scan curves **Fig 5.2 (A). Fig 5.2 (B)** shows a lower reduction in transmittance curve for complex **6** compared to **1-3**, (using **1** as an example). One would expect the decrease in transmittance to be the same for complexes **1** (Φ_T = 0.67) and **6** (Φ_T = 0.69) due to similar quantum yields, however it is not the case. This could be attributed to the shorter triplet lifetime for complex **6** (τ_T = 208 μs) compared to **1** (τ_T = 231 μs). As stated above complexes **1** and **6** have about same high triplet quantum yields but the latter larger β_{eff}, **Table 5.1** due to bioorganic nature on of the substituent (tyrosine) which contain both COOH and amino functional group. The similar trend is observed in k values (The ratio of excited state absorption (δ_{ex}) to ground state absorption cross-sections (δ_0)). $I_m[x^{(3)}]$ values are within the range (10^{-12} – 10^{-9}) reported for macrocycles like phthalocyanines **[127]**, which indicates that these complexes are good optical limiters.

The ability of a material to perform as better optical limiter is determined by lower I_{lim} value. The limiting threshold (I_{lim}) is defined as the input fluence at which the transmittance is 50% of the linear transmittance value **[126]**. **Fig. 5.3** shows plots of transmittance versus incident fluence obtained. I_{lim} is lowest for complex **3** at 0.83 compared to **1** at 0.92, **6** at 1.39 and **2** at 1.41, Table 5.1.

Table 5.1: Nonlinear optical parameters of complexes **1-6** and conjugates.

Samples	β_{eff} **(cm.GW^{-1})**	$I_m[\chi(3)]$**(esu)**	I_{lim}**(J·cm^{-2})**	**k(δ_{ex} / δ_o)**	δ_o**x10^{-19}**	δ_{ex}**×10^{-19}**	Φ_T
1	14.0	1.20×10^{-11}	0.92	1.06	8.28	8.78	0.67
1-SQD1	17.5	1.50×10^{-11}	0.77	1.15	8.28	9.52	0.71
1-SQD1/ZnO	18.0	1.54×10^{-11}	0.60	1.42	8.28	11.76	0.78
2	12.2	1.03×10^{-11}	1.41	0.89	8.75	7.79	0.41
2-SQD1	15.5	1.33×10^{-11}	0.55	1.10	8.75	9.63	0.86
2-SQD1/ZnO	15.0	1.29×10^{-11}	0.77	1.12	8.75	9.80	0.61
3	12.6	1.05×10^{-11}	0.83	1.02	4.35	4.44	0.48
3-SQD1	24.0	2.06×10^{-11}	0.53	2.59	4.35	11.27	0.70
3-SQD1/ZnO	24.0	2.06×10^{-11}	0.56	2.53	4.35	11.01	0.81
4	48.0	6.04×10^{-11}	1.23	1.34	6.33	8.40×10^{-19}	0.67
4-SQD2	70.0	5.90×10^{-11}	0.39	1.99	6.33	1.26×10^{-18}	0.72
4-SQD2/ZnO	74.0	6.25×10^{-11}	0.38	2.08	6.33	1.32×10^{-18}	0.76
5	78.1	6.66×10^{-11}	0.55	6.08	2.96	1.80×10^{-18}	0.70
5-SQD2	80.0	6.75×10^{-11}	0.28	6.42	2.96	1.90×10^{-18}	0.86
5-SQD2/ZnO	80.8	7.07×10^{-11}	0.27	6.69	2.96	1.98×10^{-18}	0.87
6	42.2	3.56×10^{-11}	1.39	1.15	8.54	9.6×10^{-19}	0.69
6-SQD2	52.2	4.04×10^{-11}	0.48	1.76	8.54	1.5×10^{-18}	0.72
6-SQD12/ZnO	71.2	4.69×10^{-11}	0.44	2.11	8.54	1.80×10^{-18}	0.72

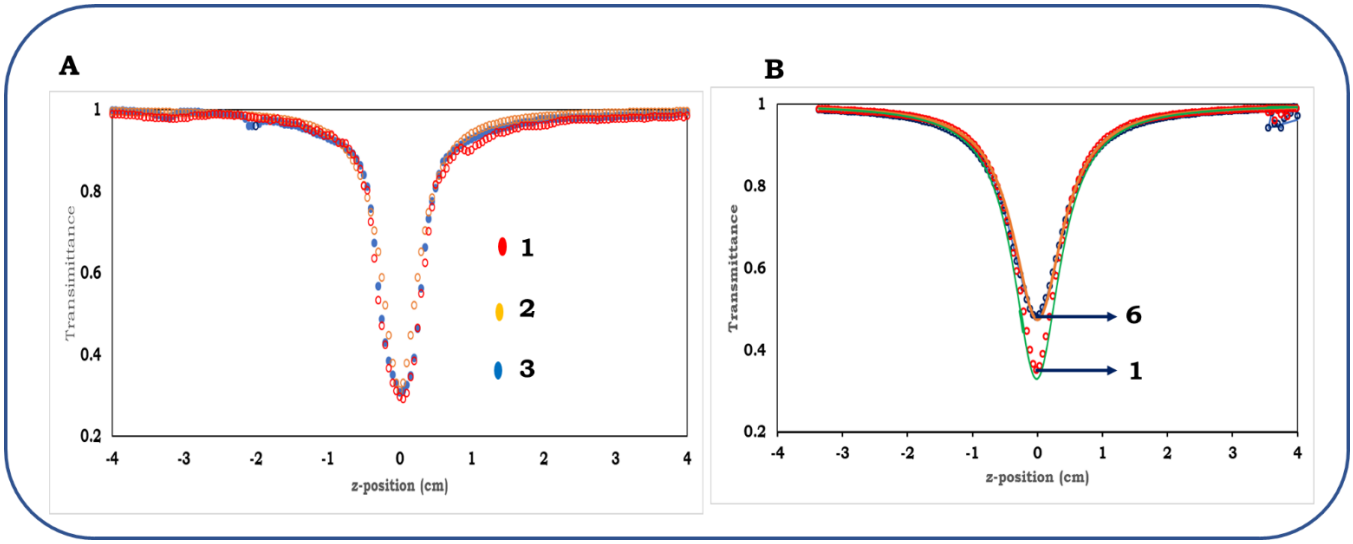

Fig. 5.2: *Open aperture Z-scan signature of complexes* ***1***-***3*** *(A), and* ***6*** *and* ***1*** ***(B)*** *in DMSO at λ = 532 nm.*

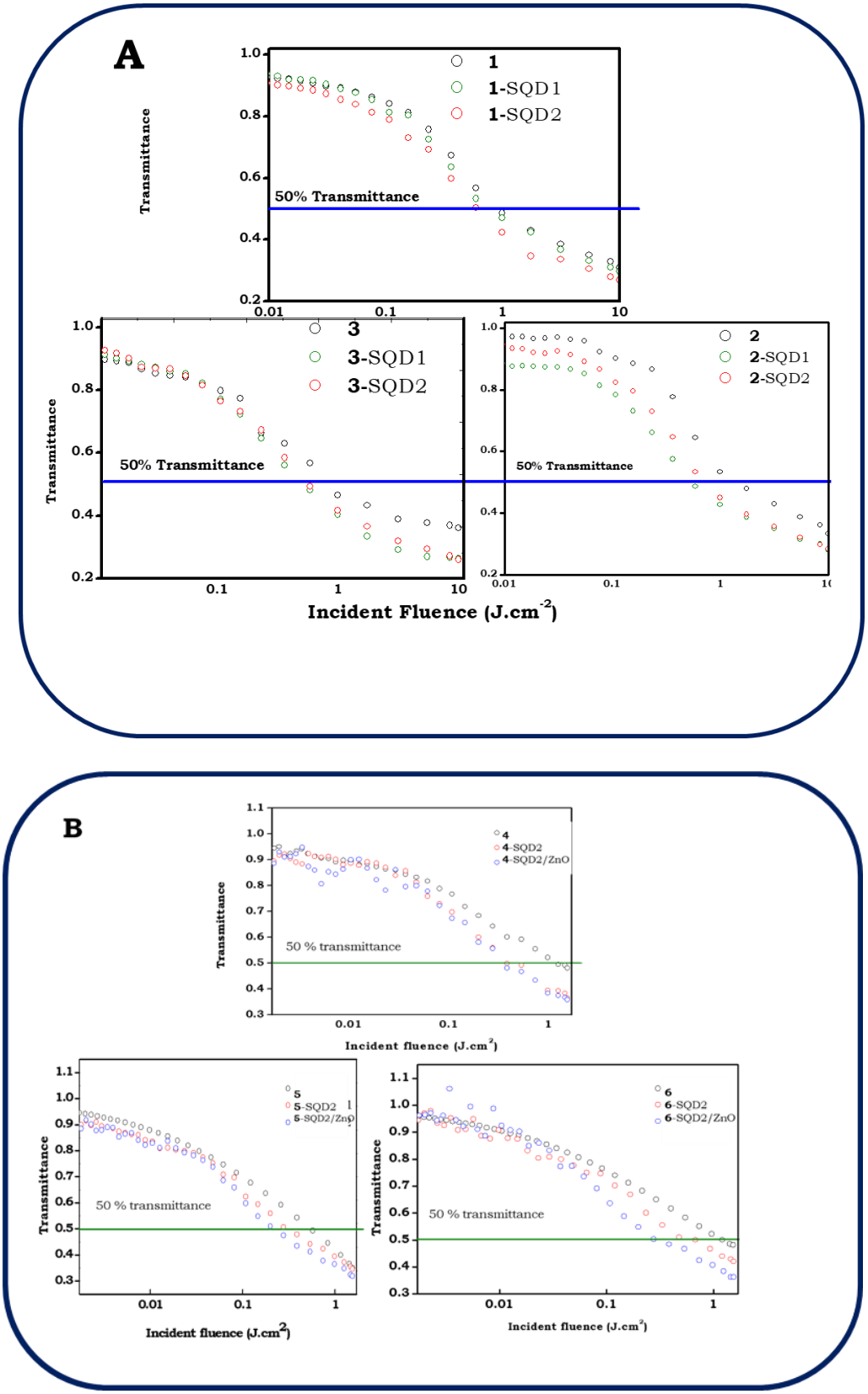

Fig. 5.3: *Transmittance versus incident fluence for complexes* ***1-6*** *and their nanoconjugates with SQDs*

5.3.2 NLO properties of complexes 4 & 5

Table 5.1 shows complex **5** recorded a fast NLO response with $I_m[\chi^{(3)}]$ 6.66×10^{-11} esu value and strong nonlinear absorption coefficient (β_{eff}) of 78.1 cm/GW due to higher triplet quantum for compared to **4**. Z-scan profiles of Pcs in **Fig. 5.4** follow the same trend. Absorption cross-sections ratio (k) for **5** is 6.08 compared to 1.34 for complex **4**. High k values result from large area occupied by the molecule in the excited state upon excitation.

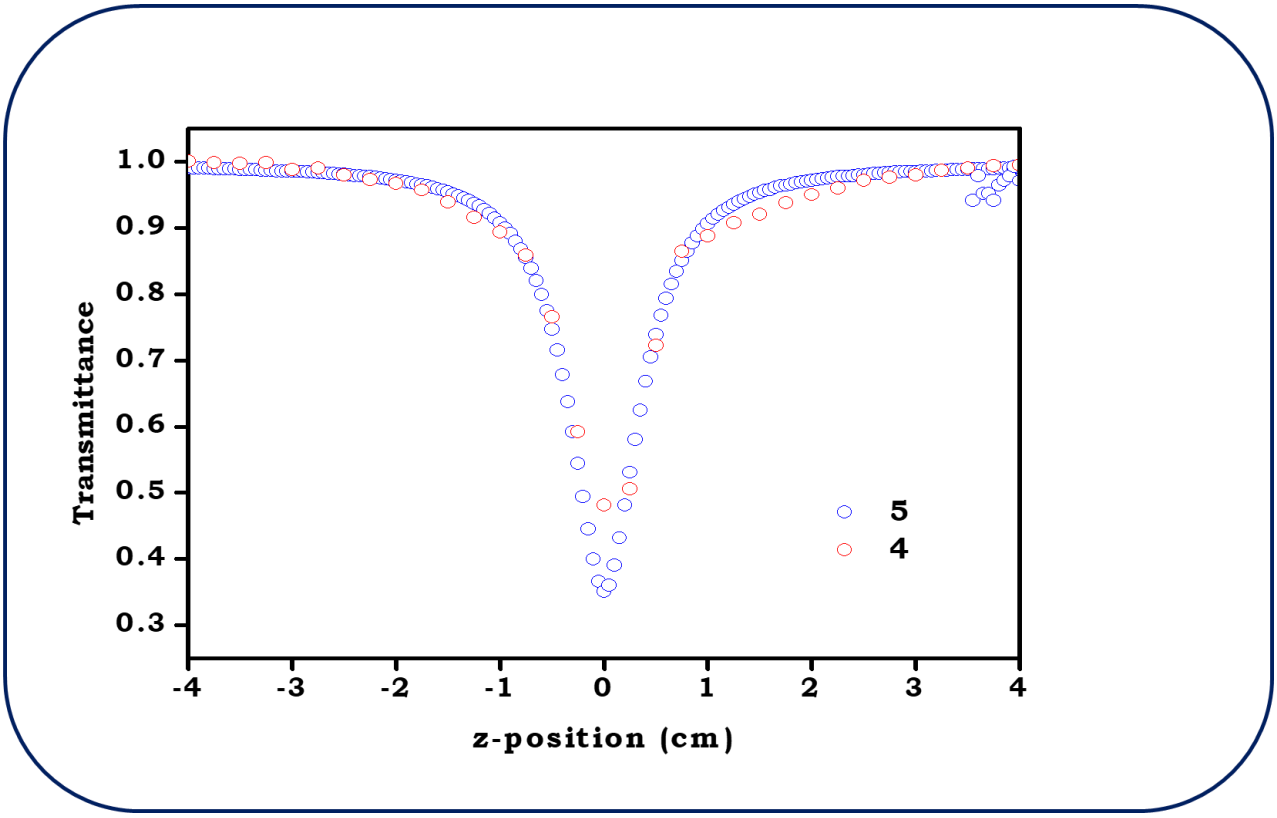

Fig. 5.4 *Z-scan profiles of complexes* ***4*** *and* ***5*** *in DMSO at λ=532 nm*

5.4 Phthalocyanine-Quantum Dots NLO parameters

Comparing NLO response of conjugates of core/shell and core/shell/shell, shows that the latter (except for conjugates of complexes **2** and **3**), generally give larger β_{eff} and $I_m[\chi^{(3)}]$ values even though the Φ_T values and reduction in transmittance are about the same in most cases. The increased β_{eff} and $I_m[\chi^{(3)}]$ values correspond with increase in Φ_T values. SQDs contribute to NLO behaviour of Pcs due to free carrier absorption (FCA) mechanism which occurs when there is linear absorption at excitation wavelength **[43]**. The SQDs alone showed good NLO behaviour with the core/shell/shell showing better activity as compared to the core/shell but their conjugates with the low symmetry Pc complexes afforded the best NLO features (**Fig. 5.5**), using complex **4**-SQDs as an example. This is judged by the lower dip in transmittance for the conjugates. SQDs with ZnS shell (SQD2) afforded better NLO responses on Z-scan than ZnSe shell (SQD1) (**Fig. 5.4**), hence generally higher β_{eff}, $I_m[\chi^{(3)}]$, and k values for the conjugates of the former (**Table 5.1**). This could be attributed to stronger absorption of SQD2 with ZnS at 532 nm hence more free carrier absoption. I_{lim} values improve (decrease) in the presence of SQDs. Again, complex **5**, **4** and their conjugates showed the best OL behaviour with the lowest I_{lim} values.

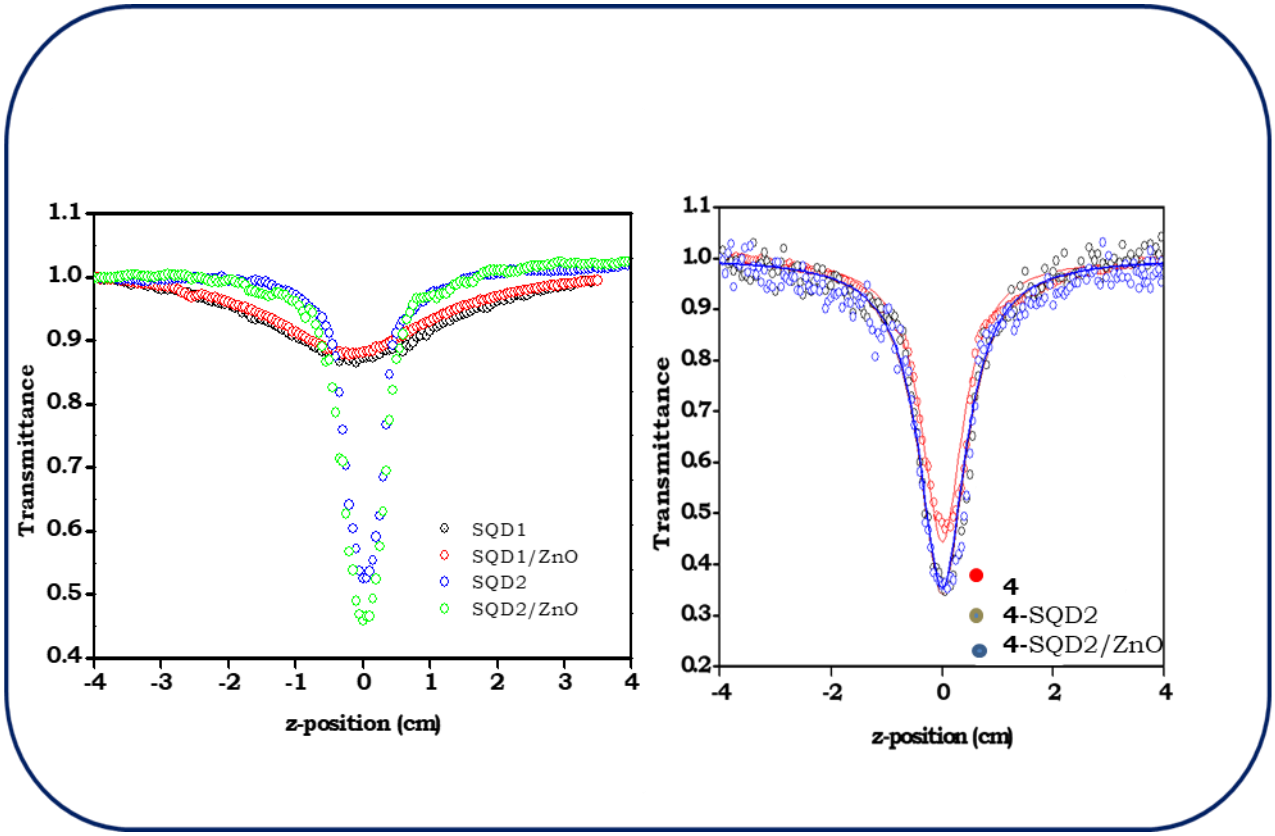

Fig. 5.5: *Z-scan signature of SQDs and Pcs-SQDs, using complex* ***4*** *as an example.*

Conclusion

Nonlinear optical studies of asymmetrical MPcs alone and when conjugated to SQDs were investigated using open aperture Z-scan technique. Complexes **4** and **5** alone showed better NLO response in terms of third order nonlinear susceptibility $I_m[\chi^{(3)}]$, nonlinear absorption coefficient (β_{eff}) and limiting threshold (I_{lim}) compared to the rest of the Pcs studied. Enhanced NLO behaviour of MPcs when linked to SQDs was observed compared to Pc complexes alone.

Chapter 6 : Conclusion and Future prospect

This chapter summarizes the syntheses, photophysical and nonlinear optical response of asymmetrical phthalocynines with zinc central metal and their nanoconjugates.

Chapter 6 Conclusion

6.1 Conclusion and future prospect

The synthesis of asymmetrical phthalocyanines with zinc central atom was achieved and characterized using various techniques. Evaluation of the photophysical properties of asymmetrical phthalocyanines showed high triplet quantum yields due to increased dipole moment.

Improved photophysical properties of asymmetric Pcs were achieved by covalently linking phthalocyanines to semiconductor quantum dots. Föster resonance energy transfer revealed positive changes in photophysical properties of asymmetric phthalocyanines.

Nonlinear optical response of asymmetrical phthalocyanine alone and conjugates is investigated in solution using Z-scan. Phthalocyanines show reverse saturable absorption behaviour. Complexes **4** and **5** exhibit higher third order nonlinear susceptibility, nonlinear absorption coefficient and lower limiting threshold (I_{lim}), hence better optical limiting behaviour. The complexes and nanoconjugates show great promise as optical limiter.

6.2 Future prospect

Nonlinear optical response of studied phthalocyanines incorporated to heavier central metal can be explored. It would be of interest to see changes in optical limiting behaviour of phthalocyanine-semiconductor quantum dots embedded in thin film.

Reference

1. X.L. Zhang, X. Zhao, Z.B. Liu, S. Shi, W.-Y. Zhou, J.G. Tian, Y.F. Xu, Y.S. Chen, Transient thermal effect, nonlinear refraction and nonlinear absorption properties of graphene oxide sheets in dispersion J. Opt. 21 (2013) 7511.
2. B. K. Periyasamy, R. S. Jebas, B. Thailampillai, Synthesis and spectral studies of 2-aminopyridiniumpara-nitrobenzoate: a novel optoelectronic crystal, Mater. Lett. 61 (2007) 1489.
3. J. Bardan, R. Hierle, A. Perigaud, J. Zyss, D. J. Williams, Nonlinear Optical Properties of Organic Molecules and Polymeric Materials, American Chem. Soc. Washington, 223 (1993).
4. R. W. Munn and C. N. Ironside, Principles and Applications of Nonlinear Optical Materials, Chapman and Hall, London (1993).
5. T. Strudley, R. Bruck, B. Mills, O.L. Muskens, An ultrafast reconfigurable nanophotonic switch using wavefront shaping of light in a nonlinear nano- material, Light Sci. App. 3 (2014) 207.
6. R.L. Sutherland, Handbook of Nonlinear Optics, Marcel Dekker, New York, NY, 2nd edn, (2003)
7. J. Wang, W.J. Blau, Numerical Approach for Optically Limited Pulse Transmission in Polymer-Phthalocyanine Composite Systems: Nonlinear optical propagation in a tandem structure comprising nonlinear absorption and scattering materials, Chem. Phys. Lett. 465 (2008) 265.

8. P.A . Angelimary, S. Dhanuskodi, Growth and characterization of a new nonlinear optic Bisthiourea zinc chloride, Cryst. Res. Technol. 36 (2001) 1231.
9. Y. Liu, Y. Chen, L. Cai, J. Wang, Y. Lin, J.J. Doyle, W.J. Blau, Optical limiting properties of axially substituted indium phthalocyanines in the solid PMMA composite films, Mater. Chem. Phys. 107 (2008) 189.
10. B.N. Moolya, S.M. Dharmaprakash, Synthesis, growth and characterization of nonlinear optical crystal: L-tyrosine hydrobromide, J. Cryst. Growth. 290 (2006) 498.
11. S.S. Hussaini, N. R. Dhumane, V. G. Dongre, M. D. Shirsat, Growth and characterization of an NLO material - crystal of triglycine acetate, J. Mater. Sci. Poland 27 (2009) 365.
12. Y. X. Fan, R.C. Eckardt, R.L. Byer, R.K. Rout, R.S. Feigelson, AgGaS2 infrared parametric oscillator, App. Phys. Lett. 45(1984) 313.
13. T.H. Wei, D.J. Hagan, M.J. Sence, E.W. Van Stryland, J. W. Perry, D. R. Coulter, Direct Measurements of Nonlinear Absorption and Refraction in Solutions of Phthalocyanines, App. Phys. 54 (1992) 46.
14. E.M. Maya, A.W. Snow, J.S. Shirk, G.S Richard, R.S. Pong, G.L. Flom, J. Robert, Synthesis, aggregation behaviour and nonlinear absorption properties of lead phthalocyanines substituted with siloxane chains, J. Mater. Chem. 13 (2003) 1603.
15. Y. Li, T.M. Pritchett, J. Huang, M. Ke, P. Shao, W. Sun, Photophysics and nonlinear absorption of peripheral-substituted zinc phthalocyanines, J. Phys. Chem. 112 (2008) 7200.

16. C.G. Claessens, W.J. Blau, M. Cook, M. Hanack, R.J.M. Nolte, T. Torres, D. Wohrle, Monatshefte, Phthalocyanines and Phthalocyanine Analogues: The Quest for Applicable Optical Properties, Monats. Chem. 132 (2001) 3.
17. M. Gouterman, In The Porphyrins, Part A. Physical chemistry, D. Dolphin (Ed), Academic Press, New York 3 (1978).
18. A. Zawadzka, P. Plociennik, J. Strzelecki, M. Pranaitis, S. Dabos-Seignon, B. Sahraoui, Structural and nonlinear optical properties of as-grown and annealed metallophthalocyanine thin films, Thin Sol. Films 545 (2013) 429.
19. R. Bonnett, In Chemical Aspects of Photodynamic Therapy, Gordon and Breach Science Publishers: Amsterdam (2000) 248.
20. M. Li, B. Mai, A. Wang, Y. Gao, X. Wang, X. Liu, S. Songa Q. Liu, S. Wei, P. Wang, Photodynamic antimicrobial chemotherapy with cationic phthalocyanines against Escherichia coli planktonic and biofilm cultures. RSC Adv. 7 (2017) 40734.
21. A.B. Sorokin, Phthalocyanine metal complex for catalysis. Chem. Rev. 113 (2013) 8152.
22. J.A. de Saja, M. L. Rodriguez-Mendez, Sensors based on double-decker rare earth phthalocyanines, Adv. Colloid. Interfac. 116 (2005) 1.
23. A. Hagfeld. G. Boschloo, L. Sun, L. Kloo, H. Pettersson. Dye-Sensitized Solar Cell. Chem. Rev. 110 (2010) 6595.
24. P.R. Somani, S. Radhakrishnan, Electrochromic materials and devices: present and future, Mater. Chem. Phy. 77 (2002) 117.

25. A.K. Kempa, J. Dobrowolski, Palladium phthalocyanine and its polymorphic forms, Canadian J. Chem. 66 (1988) 2553.

26. Y. Chen, Y. Lin, M.E. Ei-Khouly, X. Zhuang, Y. Araki, O. Ito, W. Zhang, Supramolecular Zinc Phthalocyanine-Perylene Bisimide Triad: Synthesis and Photophysical Properties, J. Phy. Chem. 111 (2007) 16096.

27. M. Quintilian, E.M Garcia-Frutos, P.Vazquez, T. Torres, Synthesis of diiodo butadiynyl-bridged bisphthalocyaninatozinc(II) complexes, J. Inorg. Biochem. 102 (2008) 388.

28. M.S. Rodriguez-Morgade, G. de la Torre, T. Torres, in The Porphyrin Handbook, eds. K. M. Kadish, K. M. Smith, R. Guilard, Academic Press, San Diego 15 (2003) 125.

29. Y. Lui, Y. X u, D. Zhu, T. Wada, H. Sasabe, L. Lui, W. Wag, Langmuir-Blodgett films of an asymmetrically substituted metal-free phthalocyanine and the second-order non-linear optical properties, Thin Sol. Films 244(1994) 943.

30. Y. Lui, Y. X u, D. Zhu, T. Wada, H. Sasabe, Synthesis and characterization of a novel unsymmetrical metal - free phthalocyanine with donor - acceptor substituents, Heterocyc. Chem. 31 (1994) 1017 .

31. C.V. van Nostrum, R.J.M. Nolte, Functional supramolecular materials: self-assembly of phthalocyanines and porphyrazines, Chem. Comm. 21 (1996) 2385.

32. V.N. Nemykin, S.V. Dudkin, F. Dumoulin, C. Hirel, A.G. Gürek, V. Ahsen, Synthetic approaches to asymmetric phthalocyanines and their analogues, Arkivoc (2014) 142.

33. N. Kobayashi, R. Kondo, S.I. Nakajima, T. Osa, New route to unsymmetrical phthalocyanine analogs by the use of structurally distorted subphthalocyanines, J. Am. Soc. 112 (1990) 9640.

34. T. Yonekura, T. Ohsaka, F. Kitamura, K. Tokuda, Synthesis and electrochemical properties of bis(octacyanophthalocyaninato)neodymium(III) complex, J. Porphyr. Phthalocy. 9 (2005) 54.

35. B. Simic-Glavaski, Phthalocyanine: Properties and Applications, (Eds) A.B.P. Lever, C.C. Leznoff, VCH Publishers, New York, Vol.3 (1993).

36. J.M. Fox, T.J. Katz, S. Van Elshocht, T. Verbiest, M. Kauranen, A. Persoons, T. Thongpanchang, T. Krauss; L. Brus, Synthesis, Self-Assembly, and Nonlinear Optical Properties of Conjugated Helical Metal Phthalocyanine Derivatives, J. Am. Chem. Soc. 121 (1999) 3453.

37. N. Nwaji, D.O. Oluwole, J. Mack, M. Louzada, S. Khene, J. Britton, T. Nyokong, Improved nonlinear optical behaviour of ball type indium(III) phthalocyanine linked to glutathione capped nanoparticles, Dyes Pigm. 140 (2017) 417.

38. G. Torre, P. Vazquez, F. Agullo-Lopez, T. Torres, Phthalocyanines and related compounds: organic targets for nonlinear optical applications, J. Mater. Chem. 8(1998) 1671.

39. D. Dini, Synthesis of axially substituted gallium, indium and thallium phthalocyanines with nonlinear optical properties, Arkivoc 2006 (2005) 77.

40. G. Torre, P. Vazquez, F. Agullo-lopez, T. Torres, Role of Structural Factors in the Nonlinear Optical Properties of Phthalocyanines and Related Compounds, Chem. Rev. 104 (2004) 3723.
41. T. Chervy, J. Xu, Y. Duan, C. Wang, L. Mager, M. Frerejean, J.A.W. Münninghoff, P. Tinnemans, J.A. Hutchison, C. Genet, A.E. Rowan, T. Rasing, W. Ebbesen, High-Efficiency second-harmonic generation from hybrid light-matter states, Nano Lett. 16 (2016) 7352.
42. J. Britton, M. Durmus, S. Khene, V. Chaukea, T. Nyokong, Third order nonlinear optical properties of phthalocyanines in the presence nanomaterials and in polymer thin films, J. Porphyr. Phthalocy. 17, (2013) 691.
43. K. Sanusi, S. Khene, T. Nyokong. Enhanced optical limiting performance in phthalocyanine-quantum dot nanocomposites by free-carrier absorption mechanism, Opt. Mater. 37 (2014) 572.
44. D.O. Oluwole, A.V. Yagodin, N.C Mhkize, K.E. Sekhosana, A.G. Martynov. Y.G. Gorbunova, A.Y. Tsivadze, T. Nyokong, First example of nonlinear optical materials based on nanoconjugates of sandwich phthalocyanines with quantum dots, Chem. Euro. J. 23 (2017) 2820.
45. K. Sanusi, E. Antunes, T. Nyokong, Optical nonlinearities in non–peripherally substituted pyridyloxyphthalocyanines: a combined effect of symmetry, ring-strain and demetalation, Dalt. Trans. 43 (2014) 999.
46. N. Njemuwa, O.M. Bankole, J. Britton, T. Nyokong, phthalocyanine and nonlinear optical study of benzothiazole substituted phthalocyanine in solution and thin films, J. Porphyr. Phthalocy. 21 (2017) 263.

47. T. Nyokong, In Structure and Bonding: Functional Phthalocyanine Molecular Materials, Jiang J. Mingos DMP. (Eds.) Spri. 135 (2010) 45.

48. J. Mack, N. Kobayashi, Low Symmetry Phthalocyanines and Their Analogues, Chem. Rev. 111 (2011) 281.

49. J. Britton, A.G. Martynov, D.O. Oluwole , Y.G. Gorbunova, A. Yu. Tsivadze, T. Nyokong, Improvement of nonlinear optical properties of phthalocyanine bearing diethylene glycol chains: Influence of symmetry lowering vs. heavy atom effect, J. Porphyr. Phthalocy. 20 (2016) 1296

50. S.V. Rao, P.T. Anusha, L. Giribabu, S.P. Tewari, Picosecond optical nonlinearities in symmetrical and unsymmetrical phthalocyanines studied using the Z-scan technique, Pramana. 75 (2010) 1017.

51. Y. Li, T.M. Pritchett, J. Huang, M. Ke, P. Shao, W. Sun, Photophysics and Nonlinear Absorption of Peripheral-Substituted Zinc Phthalocyanines, J. Phys. Chem. A. 112 (2008) 7200.

52. J. Fu, X.Y. Li, K.P. Ng, C. Wu, Encapsulation of phthalocyanines in biodegradable poly(sebacic anhydride) nanoparticles, Langmuir. 18 (2002) 3843.

53. J. Fu, X.-you Li, D.K.P, Ng, C.Wu, Encapsulation of Phthalocyanines in Biodegradable Poly(sebacic anhydride) Nanoparticles, Langmuir 18 (2002) 3843.

54. T.W.J. Gadella Jr, R.M. Clegge, T.M. Jovin, 'Fluorescence lifetime imaging microscopy: pixel-by-pixel analysis of phase modulated data, Bioimag. 2 (1994) 139.

55. N.J. Turro, In Modern Molecular Photochemetry the Benjamin/ Cummings Publishing Co. Inc. New York (1978)

56. S. Fery-Forgues, D. Lavabre, Are Fluorescence quantum yields so tricky to measure? a demonstration using familiar stationery products. J. Chem. Educ. 76 (1999) 1260.

57. A. Ogunsipe, J. Chen, T. Nyokong, Photophysical and photochemical studies of zinc(II) phtalocyanine derivatives-effects of substituents and solvents. New J. Chem. 28 (2004) 822.

58. S. Dhami, A.J. de Mello, G. Rumbles, S.M. Bishop, D. Philips, A. Beeby, Phthalocyanine fluorescence at high concentration: dimers or reabsorption effect? Photochem. Photobiol. 61 (1995) 341.

59. A.M. Brouwer, A.M. Standards for photoluminescence quantum yield measurements in solution. Pure App. Chem. 83 (2011) 2213–2228.

60. M. Idowu, J.Y. Chenab, T. Nyokong, Photoinduced energy transfer between water-soluble CdTe quantum dots and aluminium tetrasulfonated phthalocyanine, New J. Chem. 32 (2008) 290.

61. M.M. Barroso, Quantum dots in cell biology, J. Histochem. Cystchem. 59 (2011) 237.

62. L. Stryer, Fluorescence energy transfer as a spectroscopic ruler, Annu. Rev. Biochem. 47 (1978) 819.

63. E.Z. Chong, D.R. Matthews, H.D Summers, K.L. Njoh, R.J. Erringsto, P.J. Smith, Development of FRET-Based Assays in the Far-Red Using CdTe Quantum Dots, J. Biomed. Biotechnol. 2007 (2007) 1.

64. A.H. Clayton, K. Nectarios, H.C. Stephen, C.N. Edouard, Dual-channel photobleaching FRET microscopy for improved resolution of protein association states in living cells, Eur. Biophy. J. 34 (2005) 82

65. H. Du, R.C.A Fuh, J. Li, L.A. Corkan, J.S. Lindsey, PhotochemCAD: A Computer-Aided Design and Research Tool in Photochemistry and Photobiology, Photochem. Photobiol. 68 (1998)141.

66. J.S. Hsioao, B.P. Krueger, R.W Wagner, T.E. Johnson, J.K. Delaney, D.C. Mauzerall, G.R. Fleming, J.S. Lindsey, D. F. Bocian, R.J. Donohoe, Soluble Synthetic Multiporphyrin Arrays: Modular Design and Synthesis, J. Am. Chem. Soc. 118 (1996) 11181.

67. T.H. Tran-Thi, C. Desforge, C. Thiec, S. Gaspard, Singlet-singlet and triplet-triplet intramolecular transfer processes in a covalently linked porphyrin-phthalocyanine heterodimer. J. Phys. Chem. 93 (1989) 1226

68. T. Fukuda, K. Ono, S. Homma, N. Kobayashi, Phthalocyanine producing green, ocher, and red colors depending on the central metal, Chem. Lett. 32 (2003) 736.

69. T. Nyokong, E. Antunes, In Eds. K.M. Kadish, K.M Smith, R. Guilard, The Handbook of Porphyrin Science. Chapter title: Photochemical and photophysical properties of metallophthalocyanine, Singapore: World Scientific pp. 247 (2010).

70. P. Kubat, J. Mosinger, Photophysical properties of metal complexes of meso-tetrakis (4- sulphonatophenyl) porphyrin, J. Photochem. Photobiol. 96 (1996) 93.

71. S.S.M. Rodrigues, D.S.M. Ribeiro, J.X. Soares, M.L.C. Passos, M.L.M.F.S. Saraiva, J.L.M. Santos, Application of nanocrystalline CdTe quantum dots in chemical analysis: implementation of chemo-sensing schemes based on analyte-triggered phototluminescence modulation, Coordin. Chem. Rev. 330 (2017) 127.

72. S.L. Murov, Carmichael, G.L. Hug, Handbook of photochemistry (2nd edn) M. Decker, New York (1993)

73. N. Sozer, J.L. Kokini, Use of quantum nanodot crystals as imaging probes for cereal proteins, Food Res. Int. 57 (2014) 142.

74. Y.B. Monakhova, I. Yu Goryacheva, Chemometric analysis of luminescent quantum dots systems: long way to go but first steps taken, Trends. Anal. Chem. 82 (2016) 164.

75. G. Schmid in nanoparticles: from theory to application, 2nd ed. Willey-VCH, Weinheim (2010).

76. P. Juzenas, W. Chen, Y.P. Sun, M.A.N. Coelho , R. Generalov, N. Generalova, I.L. Christensen, Quantum dots and nanoparticles for photodynamic and radiation therapies of cancer, Adv. Drug Delivery Reviews 60 (2008) 1600.

77. H. He, X. Sun, X. Wang, H. Xu, Synthesis of highly luminescent and biocompatible CdTe/CdS/ZnS quantum dots using microwave irradiation: a comparative study of different ligands, J. Lumin. 29 (2014) 837.

78. Z.A. Peng, X.G. Peng, Formation of high-quality CdTe, CdSe, and CdS nanocrys- tals using CdO as precursor, J. Am. Chem. Soc. 123 (2001) 183.

79. Z.Y. Gu, L. Zou, Z. Fang, W.H. Zhu, X.H. Zhong, One-pot synthesis of highly lumi- nescent CdTe/CdS core/shell nanocrystals in aqueous phase, Nanotech. 19 (2008) 135604.

80. M.H. Majles Ara, Z. Moslemi, H. Naderi, A. Mihandoost, A. Daneshfar, R. Sahraei, Nonlinear optical properties of CdTe nanocrystals synthesized by a green room temperature solution method, App. Phys. 118 (2015) 567.

81. Y. Jiao, D. Yu, Z. Wang, K. Tang, X. Sun, Synthesis, nonlinear optical properties and photoluminescence of ZnSe quantum dots in stable solutions, Mater. Lett. 61 (2007) 1541.

82. H. Jorkaala, H. Stennenen, Nonlinear optical properties of ZnSe nanocrystals incorporated within polyvinyl alcohol photopolymer matrices, J. Opt. A, Pure App. Opt. 4 (2002) 366.

83. J. Ma, J.Y. Chen, M. Idowu, T. Nyokong, Generation of Singlet Oxygen via the Composites of Water-Soluble Thiol-Capped CdTe Quantum Dots Sulfonated Aluminum Phthalocyanine, J. Phys. Chem. 112 (2008) 4465.

84. F. Erogbogbo, Ching-Wen Chang, J. May, P. N. Prasad, M. T. Swihart, Energy transfer from a dye donor to enhance the luminescence of silicon quantum dots, Nanoscale 4 (2012) 5163

85. S. D' Souza, E. Antunes, T.Nyokong , Synthesis and photophysical studies of CdTe quantum dot-monosubstituted zinc phthalocyanine conjugates, Inorg. Chimi. Acta 367 (2011) 173.

86. Z. Hooshyar, G.R. Bardajee, Fluorescence enhancement of glutathione capped CdTe/ZnS quantum dots by embedding into cationic starch for sensitive detection of rifampicin, Mol. Biomol. Spectr. 173 (2017) 144.

87. D. O. Oluwole, C.M. Tilbury, E. Prinsloo, J. Limson, Tebello Nyokong, Photophysicochemical properties and in vitro cytotoxicity of zinc tetracarboxyphenoxy phthalocyanine – quantum dot nanocomposites, Polyhedron 106 (2016) 92.

88. K.E. Sekhosana, E. Antunes, S. Khene, S. D'Souza, T. Nyokong Fluorescence behaviour of glutathione capped CdTe/ZnS quantum dots chemically coordinated to zinc octacarboxy phthalocyanines, J. Lumin. 136 (2013) 255.

89. O. Adegoke, T. Nyokong, Probing the sensitive and selective luminescent detection of peroxynitrite using thiol-capped CdTe and CdTe@ZnS quantum dots, J. Lumin. 134 (2013) 448.

90. O. Osifeko, T. Nyokong, Synthesis and physicochemical properties of zinc and indium phthalocyanines conjugated to quantum dots, gold and magnetic nanoparticles, Dyes Pigm. 131 (2016) 186.

91. D.O. Oluwole, T. Nyokong, Comparative photophysicochemicalbehaviour of nanoconjugates of indium tetracarboxyphenoxyphthalocyanines covalently linked to GSH-CdTe/ZnSe/ZnO, J. Photochem. Photobiol. 312 (2015) 34.

92. C. Tshangana, T. Nyokong,Photophysical properties gallium octacarboxy phthalocyanines conjugated to CdSe@ZnS quantum dots, Spectrochim. Acta 151 (2015) 397.

93. J. Britton, A.G. Martynov, D.O Oluwole, Y.G. Gorbunova, A. Y. Tsivadze, T. Nyokong, Improvement of nonlinear optical properties of phthalocyanine bearing diethyleneglycole chains: Influence of symmetry lowering vs. heavy atom effect, J. Porphyr. Phthalocy. 20 (2016) 1296.

94. D.O. Oluwole, A.V. Yagodin, J. Britton, A.G. Martynov, Y. G. Gorbunova, A.Y. Tsivadzec, T. Nyokong, Optical limiters with improved performance based on nanoconjugates of thiol substituted phthalocyanine with CdSe quantum dots and Ag nanoparticles, Dalton. Trans. 46 (2017) 16190.

95. N. Nwaji, S. Dingiswayo, J. Mack, T. Nyokong, Photophysical and enhanced nonlinear optical response in asymmetric benzothiazole substituted phthalocyanine covalently linked to semiconductor quantum dots, Spectrochim. Acta 204 (2018) 629.

96. N. Nwaji, J. Mack, T. Nyokong, An optical limiting study in aminophenoxy substituted phthalocyanine in the presence of semiconductor quantum dots, J. Lumin. 203 (2018) 247.

97. J. Britton, M. Durmus, V. Chauke, T. Nyokong. Poly methyl methacrylate films containing metallophthalocyanines in the presence of CdTe quantum dots: Non-linear optical behaviour and triplet state lifetimes, J. Mol. Stru. 209 (2013) 1054.

98. E. Dube, N. Nwaji, D.O Oluwole, J. Mack, T. Nyokong, Investigation of photophysiochemical properties of zinc phthalocyanines conjugated to metallic nanoparticles, J. Photochem. Photobiol. 349 (2017) 148.

99. Y. Li, T.M. Pritchett, J. Huang, M. Ke, P. Shao, W. Sun, Photophysics and Nonlinear Absorption of Peripheral-Substituted Zinc Phthalocyanines, J. Phys. Chem. A. 112 (2008) 7200.

100. D.O. Oluwole, E. Prinsloo, T. Nyokong, Photophysicochemical properties of nanoconjugates of zinc(II) 2(3)–mono–2–(4–oxy)phenoxy)acetic acid phthalocyanine with capped silver and silver–gold nanoparticles, Polyhedron 119 (2016)434.

101. S. Anandan, S. Vetrivela, S. Karthikeyan, R. Jayavel, G. RAVI, Crystal growth, spectral and thermal analyses of a semi organic nonlinear optical single crystal: L-tyrosine hydrochloride, Optoelectron. Adv. Mater. Rapid Commun. 6 (2012) 1128.

102. S. Anandan, T. Saravanan, S. Vasudevan, R. Mohan, Kumar, R. Jayavel, Crystal growth and characterization of L-tyrosinebromide (LTB) nonlinear optical single crystals, J. Cryst. Growth. 312 (2010) 837.

103. K.N. Solov'ev, E.A. Borisevich, Intramolecular heavy-atom effect in the photophysics of organic molecule, J. Phys. Chem. 48 (2005) 231.

104. K. Hayashi, M. Nakamura, H. Miki, S. Ozaki, Photostable iodinated silica/porphyrin hybrid nanoparticles with heavy-atom effect for wide-field photodynamic/photothermal therapy using single light source, Adv Funct. Mater. 24 (2014) 503.

105. K. Gawarecki, Spin-orbit coupling and magnetic-field dependence of carrier states in a self-assembled quantum dot, Phys. Rev. B 97 (2018) 235408.

106. W. Jia, E.P. Douglas, F. Guo, W. Sun, Optical limiting of semiconductor nanoparticles for nanosecond laser pulses, App. Phys. Lett. 85 (2004) 6326.

107. M. Sheik-Bahae, A.A. Said, E.W. Van Stryland, 1989) 'High-sensitivity, single-beam n_2 measurements, Opt. lett. 14 (1989) 955.

108. Y. Liu, Y. Chen, L. Cai, J. Wang, Y. Lin, J.J. Doyle, W.J. Blau, Optical limiting properties of axially substituted indium phthalocyanines in the solid PMMA composite films, Mater. Chem. Phys. 107 (2008) 189.

109. T. H. Wei, D.J. Hagan, M.J. Sence, E. W. Van Stryland , J. W. Perry, D. R. Coulter, Direct Measurements of Nonlinear Absorption and Refraction in Solutions of Phthalocyanines, App. Phys. 54 (1992) 46.

110. T. Pritchett, In Models for Saturable and Reverse Saturable Absorption in Materials for Optical Limiting; Sensors and Electron Devices Directorate. Arm. Res. Lab. (2002) 20783.

111. Y. Chen, M. Hanack, W. J Blau, D. Dini, Y. Liu, Y. Lin, J. Bai, Soluble axially substituted phthalocyanines: Synthesis and nonlinear optical response, J. Mater. Sci. 41 (2006) 2169.

112. A. Fashina, E. Antunes, T. Nyokong, Characterization and photophysical behavior of phthalocyanines when grafted onto silica nanoparticles, Polyhedron 53 (2013) 278.

113. J. Huang, M. Ke, Synthesis of peripheral and non-peripheral substituted metallophthalocyanines, Chinese Patent Application No. 200710200223 (2007).

114. J. J. Weiwei, S. D Dongping, Tyrosine phthalocyanines derivates, preparation thereof and applications in preparation of photodynamic drugs, Chinese patent CN101289450B (2008).

115. M. Panigrahi, S. Dash, S. Patel, P.K. Behera, B.K. Mishra, Reversal in sol- vatochromism in some novel styrylpyridinium dyes having a hydrophobic cleft. Spectrochim Acta 68 (2007) 62.

116. L. Li, J. F. Zhao, N. Won, H. Jin, S. Kim, J. Y. Chen, Quantum dot-aluminum phthalocyanine conjugates perform photodynamic reactions to kill cancer cells via fluorescence resonance energy transfer, Nanoscale Res. Lett. 7 (2012) 386.

117. P.R. Prabakaran, R. Kesavamoorthy, G.L.N. Reddy, F.P. Xavier, Structural Investigation of Copper Phthalocyanine Thin Films Using X-Ray Diffraction, Raman Scattering and Optical Absorption Measurements, Phys. Status Solid, 220 (2002) 1175.

118. A.W. Snow, J.R. Griffith, N.P. Marullo, Syntheses and characterization of heteroatom-bridged metal-free phthalocyaninenetwork polymers and model compounds, Macromolecules 17 (1984) 1614.

119. R. Jenkins, R.L. Synder, Introduction to X-ray diffractometry. New York: Wiley Sons 138 (1996) 47.

120. M.J. Stillman, T. Nyokong, in: C.C. Leznoff, A.B.P. Lever (Eds.), Phthalocyanines: Properties and Applications, vol. 1, VCH Publishers, New York, NY, (1989) (Chapter 3).

121. C.M. Donega, Synthesis and properties of colloidal heteronanocrystals, Chem. Soc. Rev. 40 (2011) 1512.

122. X.-F. Zhang, X. Li, L. Niu, L. Sun, L. Liu, Charge Transfer Photophysics of Tetra(α-amino) Zinc Phthalocyanine, J. Fluoresc. 19 (2009) 947.

123. F.X. Sauvage, A Laser Photolysis Study of Triplet Lifetimes and of Triplet-Triplet Annihilation Reactions of Phthalocyanins in DMSO Solutions, Laser Chem. 8 (1988) 1.

124. M. Van Leeuwen, A. S. Beeby, H. Ashworth, The photochemistry and photophysics of a series of non-peripherally substituted zinc phthalocyanines, Photochem. Photobiol. Sci. 9 (2010) 370.

125. J.R. Darwent, P. Douglas, A. Harriman, G. Porter, M.C. Richoux, Metal phthalocyanines and porphyrins as photosensitizers for reduction of water to hydrogen, Coord. Chem. Rev. 44 (1982) 83.

126. Y. Chen, M. Hanack, W. J. Blau, D. Dini, Y. Liu, Y. Lin, J. Bai, Soluble axially substituted phthalocyanines: Synthesis and nonlinear optical response, J. Mater. Sci. 41 (2006) 2169.

127. D. Dini, M. Hanack, in: K.M. Kadish, K.M. Smith, R. Guilard (Eds.), The Porphyrin Handbook: Physical Properties of Phthalocyanine-based Materials, Academic Press, New York 17 (2003) 22.

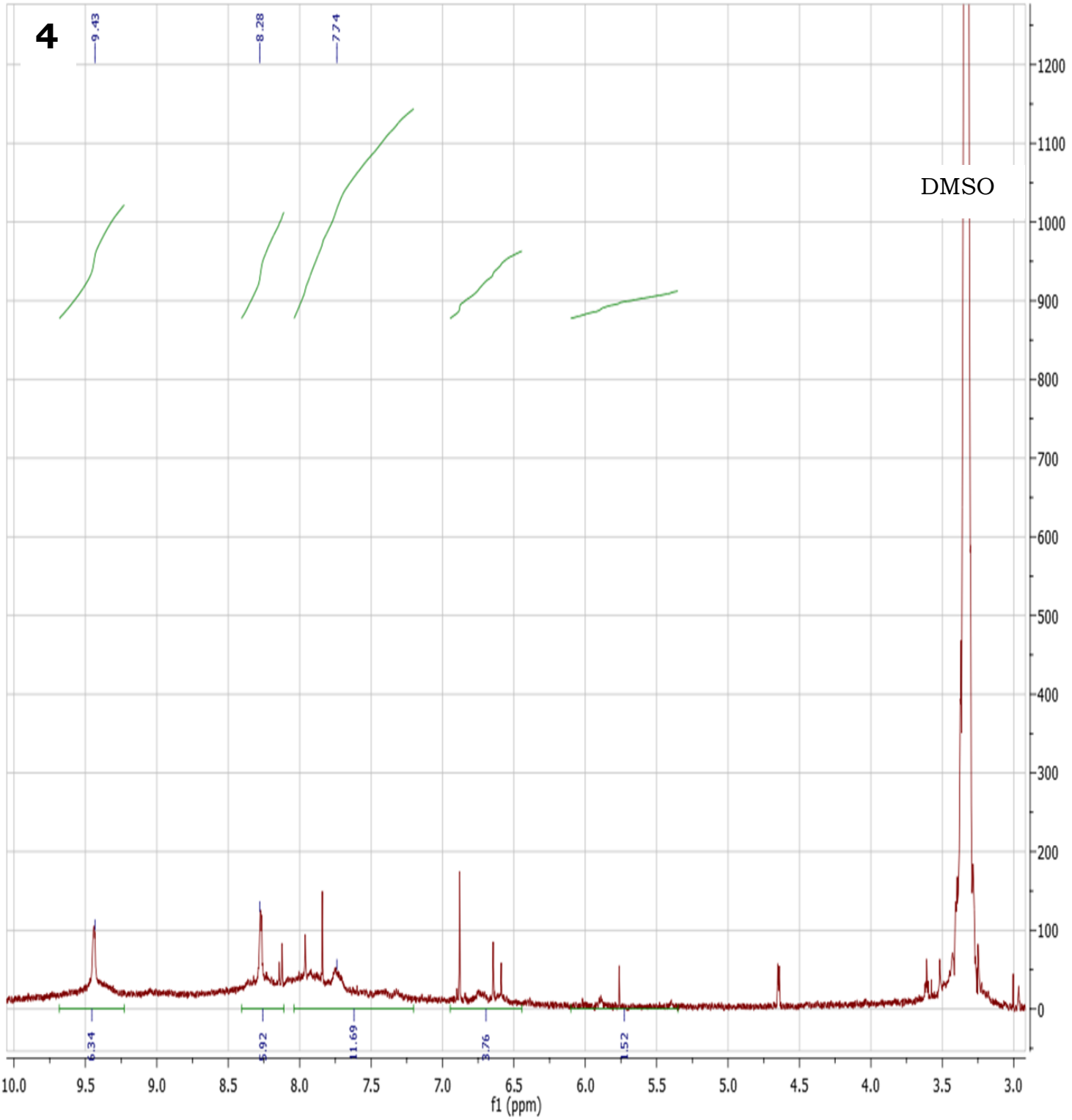

***Fig. A1**: [1]H-NMR spectrum of complex **4** in DMSO.*

5

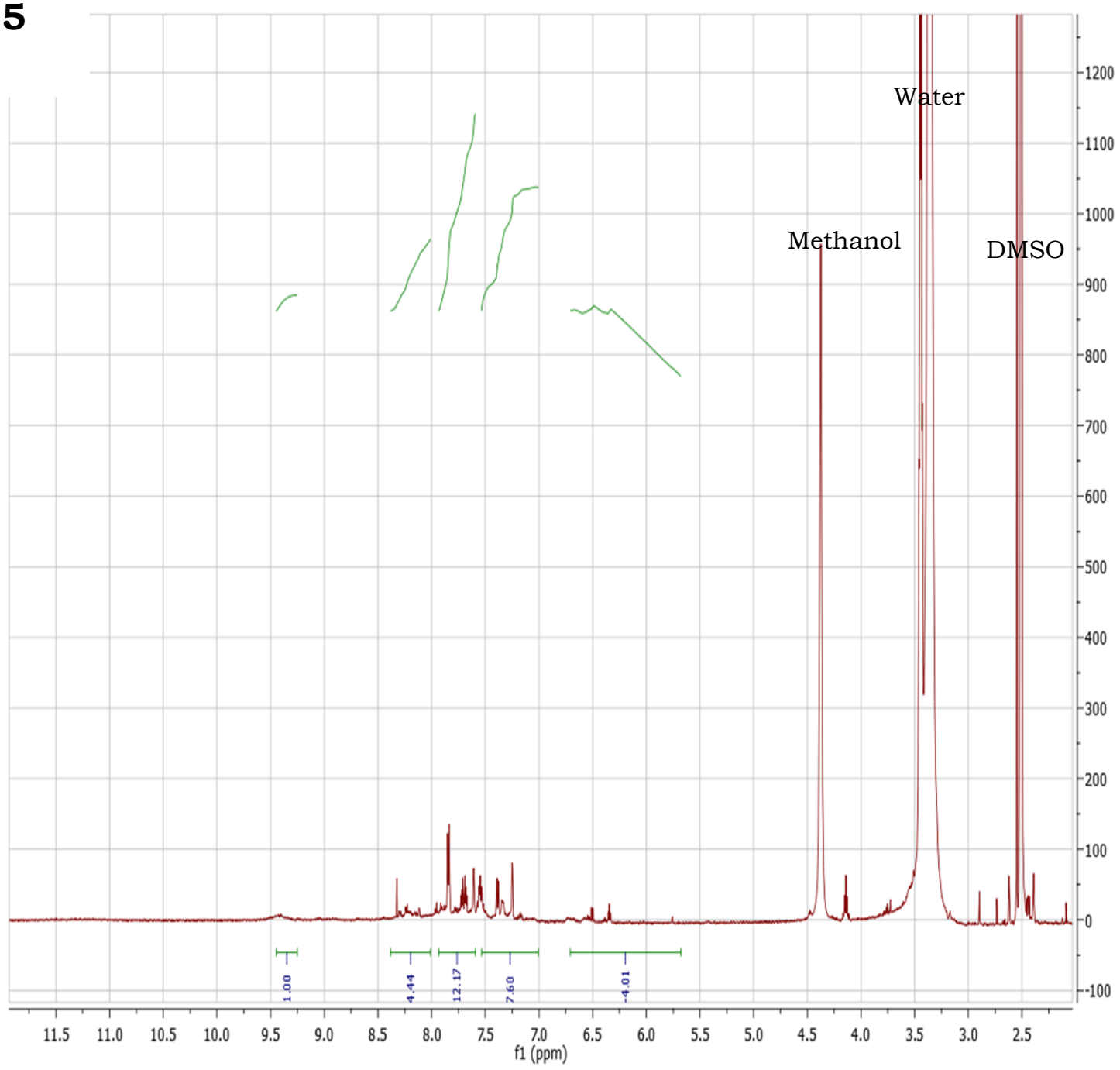

***Fig. A2**: [1]H-NMR spectrum of complex **5** in DMSO.*

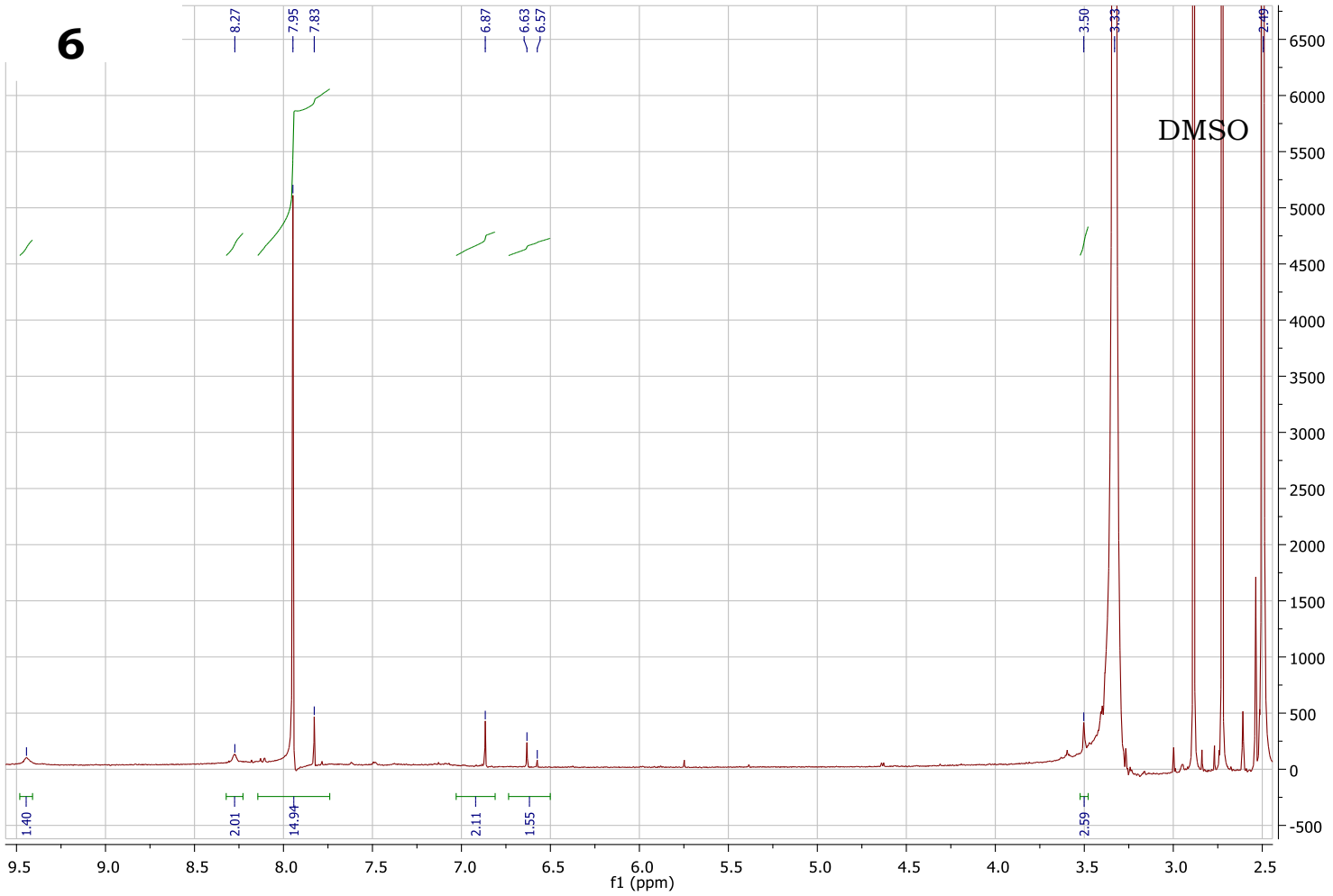

***Fig. A3**: [1]H-NMR spectrum of complex **6** in DMSO.*